Controlling intermolecular interactions at surfaces through chemical ligands: supramolecular aggregation, covalent coupling and chirality at reduced dimensions

Inauguraldissertation

zur

Erlangung der Würde eines Doktors der Philosophie

vorgelegt der

Philosophisch–Naturwissenschaftlichen Fakultät

der Universität Basel

von

Serpil Boz

aus Istanbul (Türkei)

Basel, 2010

Genehmigt von der Philosophisch-Naturwissenschaftlichen Fakultät auf Antrag von:

PD. Dr. Meike Stöhr
Prof. Dr. Thomas Jung
Prof. Dr. Marcel Mayor
Prof. Dr. Ernst Meyer

Basel, 30.03.2010

Prof. Dr. Eberhard Parlow, Dekan

Abstract

The development of scanning probe methods enabled the investigation of molecules adsorbed on surfaces with impressive resolution. A delicate balance between molecule-substrate and intermolecular interactions such as van der Waals interactions, H-bonding or dipolar coupling guides the arrangement of molecules in well-ordered patterns. A very appealing concept is to profit from the order of these pre-organized structures and to interlink the molecular building blocks to macromolecules, which is the main goal of the first part of this thesis.

By making use of a new concept, we are able to control both, the molecular self-assembly and the subsequent intermolecular coupling reactivity by protecting group chemistry. We describe heat induced formation of polymeric structures from biphenyl derivatives adsorbed on both Cu(111) and Ag(111) surfaces. Moreover, we studied how to control the arrangement and the size of the resulting polymeric structures by modification of the end groups of the biphenyl units.

For all biphenyl derivatives, well-ordered supramolecular networks are transformed into covalently bound dimers through annealing at elevated temperatures. Further annealing of such structures results in the formation of interlinked cross-like or trimeric structures and long chains.

In the second part, the effect of the chirality on the resulting surface assemblies is studied for the case of a helicene derivative deposited on a Cu(111) surface. The helicene derivative used in this work consists of a helicene core to which two opposed cyano side groups are attached. Herein, it is shown how the cyano groups influence the adsorption geometry of the molecules upon deposition on the surface and the formation of the self-assembled structures.

Adsorption of both racemic and enantiopure forms of the molecule are analyzed in detail and a chirality transfer of the molecular building blocks into the extended molecular domains is confirmed from the comparison of the experimental results of both cases. Finally, behaviour of the enantiopure form of the molecule at room temperature is studied, which reveals a metastable nanoporous network. In this section, a time induced phase transition of the nanoporous network into a stable dimeric arrangement is shown and possible reasons for this conversion are discussed.

Contents

Abstract 1

Contents 3

Abbreviations 5

1 Introduction 7

References 1 10

2 Fundamentals 11

2.1 Experimental Methods 11

2.1.1 STM 11

2.1.2 LEED 15

2.1.3 XPS 17

2.2 Molecular self-assembly 18

2.3 Polymerization 20

2.4 Chirality 21

2.5 Investigated molecules 22

2.5.1 Biphenyl derivatives 22

2.5.2 Cyano-helicene 23

2.6 Sample preparation 24

References 2 25

3 Controlling the organization and heat induced coupling of biphenyl derivatives on metal surfaces through protecting group chemistry 31

3.1 Heat induced coupling of a biphenyl derivative on metal surfaces 32

3.2 Heat induced coupling of a fluorinated biphenyl derivative on metal surfaces 49

3.2.1 Ag(111) 49

3.2.2 Cu (111): 54

3.3 Heat induced coupling of an asymmetric biphenyl derivative on metal surfaces 56

3.3.1 Ag(111) 56

3.3.2 Cu(111): 62

References 3 66

4 Control of chirality in 2D structures by the chirality of its building blocks: Cyano helicene on Cu(111) 69

4.1 Low temperature measurements 70

4.1.1 Enantiopure cyano helicene 70

4.1.2 Racemic cyano helicene 77

4.2 Room temperature measurements: Time-induced phase transition of a helicene porous network into a dimeric pattern 80

References 4 87

5 Conclusions and Outlook 91

References C&O 94

Appendix 1 95

References A1 100

Appendix 2 101

Appendix 3 107

References A3 114

Acknowledgements 115

Publications 117

Conferences 119

Curriculum Vitae 121

Abbreviations

SPM	Scanning Probe Microscopy
SAMs	Self-Assembled Monolayers
BOC	*tert*butoxycarbonyl
STM	Scanning Tunneling Microscopy
LDOS	Local Density of States
DOS	Density of States
LEED	Low Energy Electron Diffraction
XPS	X-Ray Photoelectron Spectroscopy
ESCA	Electron Spectroscopy for Chemical Analysis
QMB	Quartz Micro Balance
UHV	Ultra High Vacuum

1 Introduction

The implementation of top-down technologies with the aim of making miniaturized structures is about to reach certain limits. With reduced dimension, producing defect free device structures becomes increasingly difficult and expensive. The formation of 2D nanostructures by self-assembly on surfaces as a bottom-up approach is therefore a promising alternative for the fabrication of nanoscale devices. This bottom-up approach relies on two main pillars: 1) the reproducibility of chemical synthesis to make identical molecules with complex shapes and highly specific functions, and 2) the capability of such molecules to serve as building blocks for increasingly complex structures through self-assembly. The well established examples of Langmuir Blodgett films[1] and self-assembled monolayers (SAMs)[2] have been topped by the self-assembled architectures provided by supramolecular chemistry.[3] These structures with increasing complexity have so far mainly been studied in statistical ensembles, thereby being of very limited applicability in the context of practical organic devices with reproducible characteristics at miniaturized scale.

By the combination of surface/interface science, in particular the engineering of atomically clean substrate surfaces, and the decoration of self-assembled structures thereon, investigation can be achieved either on the nanometer scale by disk drives or down to the sub-angstrom scale by scanning probe microscopy (SPM). The intrinsic properties of addressable surface structures like e.g. mechanical bi-stability or non-linear opto-electronic behavior have lead to intensive research in recent years. Thereby, the term 'supramolecular architectonics'[4] for the engineering of supramolecular structures at surfaces has been introduced. Combining supramolecular chemistry and surface science, highly reproducible and individually adressable structures can be tailored at surfaces. For basic research, STM provides a 'microscopic' tool for the structural investigation of such layers. Moreover, individual molecules can be arranged into specific structures with the help of an STM tip, thereby providing a means to induce and study a wealth of device characteristics like switching events and non-linear properties.[5]

In the development of supramolecular architectures, it has to be noted that the majority of such structures are inherently fragile due to weak intermolecular interactions. For building supramolecular architectures it becomes therefore important to interconnect the molecules by covalent bonds.[6] A further interesting issue is the control of the chirality in a supramolecular architecture by the chirality of its building blocks.

In this thesis two main topics of supramolecular architectonics have been adressed:
1) Formation of covalent bonds from pre-organized molecular structures at surfaces;
2) Non-covalent supramolecular architectonics at surfaces.

In the first project, a new concept is used to interlink the pre-organized molecular building blocks by specific covalent bonds formed at the surface. Firstly, self-assembled monolayers are formed by Boc protected biphenyl derivatives which are adsorbed both on Cu(111) and Ag(111) surfaces. Subsequently, the formation of covalently bound structures from the pre-organized molecular building blocks is accomplished by making use of protecting group chemistry. This concept offers a fascinating control on the formation and the arrangement of the resulting interlinked structures by the modification of the end groups.

In the second project, the goal has been to design supramolecular networks with specifically programmed chirality. This, for example, would be an important pre-requisite to convert vibrational energy into rotational energy on the nanometer scale by using these chiral networks as host-guest systems. Helicenes, a class of molecules characterized by their spiral form with either positive or negative helicity, have been chosen and functionalized towards supramolecular aggregation with the cyano binding motif. These molecules provide a vehicle to control the chirality of the formed supramolecular architecture in dependence of the building blocks helicity or the degree of mixing of the two chiral components. A full control of chirality in supramolecular networks is aimed by this new approach.

The thesis is outlined as follows:

Chapter 1 gives an introduction into the concepts studied in this thesis.

Chapter 2 highlights the principles of the experimental methods used in this thesis. The theoretical principles of scanning tunneling microscopy are summarized together with a short introduction about the imaging of adsorbed molecules, low energy electron diffraction and X-ray photoelectron spectroscopy. It also gives an introduction into the concepts of self-assembly, polymerization and chirality on surfaces and describes the investigated molecules which were used within the framework of the two different projects presented in this thesis.

Chapter 3 presents the experimental results of Boc protected biphenyl derivatives on Ag(111) and Cu(111) surfaces showing that on-2D surface reactions can be induced by temperature and covalently bound structures are obtained from the pre-organized molecular building blocks. Based on the experimental results, the intermolecular interactions which stabilize different structures are discussed.

Chapter 4 comprises the STM results of cyano helicene molecule on Cu(111) substrate. The adsorption geometry of the molecule based on its 3D structure as well as the aspect of chirality based on its chiral configuration is discussed.

Chapter 5 summarizes the results and gives an outlook to the future experiments based on the investigated subjects. By using the concepts of protecting group chemistry it is

possible, first, to interconnect the molecules by self-assembly approach and second, to obtain covalently linked structures in a controlled way on surfaces. Additionally, chirality control in a supramolecular layer is achieved by using chiral helicene molecules.

The aim in the future will be on the formation of long-range-ordered and highly stable (covalently bound) surface structures as well as on the formation of more stable supramolecular architectures derived from different helicene derivatives.

References 1

[1] a) K. B. Blodgett, *Monomolecular films of fatty acids on glass,* J. Am. Chem. Soc. 56, 495 (**1934)**; b) K. B. Blodgett, *Films Built by Depositing Successive Monomolecular Layers on a Solid Surface***,** J. Am. Chem. Soc. 57, 1007–1022 (**1935**).

[2] J. C. Love, L. A. Estroff, J. K. Kriebel, R. G. Nuzzo, and G. M. Whitesides, *Self-Assembled Monolayers of Thiolates on Metals as a Form of Nanotechnology,* Chem. Rev. 105, 1103–1170 (**2005**).

[3] a) J. M. Lehn, *Supramolecular chemistry - receptors, catalysts, and carriers*, Science 227, 849 (1985); b) D. J. Cram, *The design of molecular hosts, guests and their complexes (Nobel Lecture),* Angew. Chem. Int. Ed. 27**,** 1009-1020 (**1988**).

[4] J. Barth, *Molecular Architectonic on Metal Surfaces,* Annual Rev. Phys. Chem. **58**, 375-407 (**2007**).

[5] N. Wintjes**,** D. Bonifazi, F. Y. Cheng, A. Kiebele, M. Stöhr, T. Jung, H. Spillmann, F. Diederich, *A supramolecular multiposition rotary device*, Angew. Chem. Int. Ed. 46**,** 4089-4092 (**2007).**

[6] A. Gourdon, *On-surface covalent coupling in ultrahigh vacuum*, Angew. Chem. Int. Ed. 47**,** 6950-6953 (**2008).**

2 Fundamentals

2.1 Experimental Methods

2.1.1 STM

The scanning tunneling microscope (STM) was invented in 1981 by Binnig and Rohrer[1], who were awarded the Nobel Prize in physics in 1986 for their invention. The STM is a powerful tool for obtaining atomic-scale images of surfaces in real space. In addition to the topographic information, also information on the electronic surface properties can be gained. Furthermore, the size and conformation of molecules and aggregates adsorbed on a surface can be studied as well as the manipulation of individual atoms or molecules are possible. Since STM is a real space method, the interpretation of the observed data is usually faster and more intuitive in comparison to techniques working in reciprocal space.

Considering the high resolution of the images obtained, there is substantial interest in imaging (molecular) adsorbates with an STM. However, there are some difficulties and uncertainties in obtaining reliable and easily interpretable images as many effects can influence the appearance of adsorbates in STM images[1] for the reason that the image is not the topographical map of the adsorbate but a representation of the local density of electronic states (LDOS) at the Fermi level.

For isolated adsorbates, the appearance in the STM images can depend on the applied bias voltage[3] as well as on the adsorption site.[4] However, in the case of larger adsorbates as organic molecules, the situation is more complicated. Even though most of the STM images reveal internal structures and details of the molecules, in some cases the appearance cannot be related directly to the molecular structure as the applied voltage[5], the adsorption site[6] and also the molecule-surface interactions[7] will influence the appearance. Moreover, the appearance of isolated molecules might be different to the ones which are positioned in a periodic network (compare the STM images of a helicene derivative in different surface structures in A3). In addition, if a molecule diffuses or rotates much faster than the characteristic scanning speed of the STM, identifying the molecule might be impossible.[8] In addition, molecular conformations can lead to different appearances on the substrate.[9]

In contrast to the Tersoff and Hamann model, which will be introduced in the following section, the tip has an influence in STM imaging. Alterations of the tip by

[1] A review by P.Sautet discusses these effects extensively.[2]

voltage pulses and/or even contaminations that move to the tip from the surface during an STM experiment can affect the tunneling current and the resulting STM image (see figure 2.1).

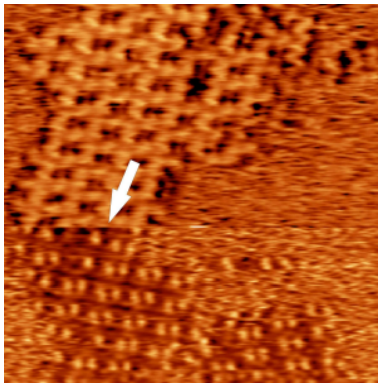

Figure 2.1. STM image showing the different appearance of the imaged molecules induced by a spontaneous change of the tip. The position of the tip change is shown with an arrow. Biphenyl **3** on Ag(111) (21.4x21.6 nm^2, 20 pA, -1.9 V, RT).

Basic principle

In STM, a sharp metallic tip is brought into close proximity (in the order of a few angstroms) to a (semi-) conducting surface and slowly scans across the surface at this distance of only a few angstrom units (see the schematic representation in figure 2.2). A bias voltage is applied to the system (usually in the range of 0.01 to 3V) and a tunneling current is measured between the tip and the sample. The tunneling current has an exponential dependence on the distance between tip and sample. Therefore, as the tip passes over the surface by means of piezo-electric drivers (x- and y- piezos) to obtain a 2D map of the surface, even the smallest details such as depressions and protrusions on the surface lead to changes in the measured tunneling current. During acquisition of the image, a feedback system monitors the tunneling current and adjusts the tip-sample separation by means of a piezoelectric element (z-piezo) to maintain a constant tunneling current. These adjustments are recorded by a computer and presented as an image in the STM software. This operation mode is called constant current mode (figure 2.3a) and is usually used on rough or large scale images so that the tip does not crash into the surface. It gives high resolution images at low scan speeds. In the constant height mode (figure 2.3b), the tip is moved at constant height and variations in the tunneling current are translated into an image. This mode allows faster scanning and is usually used on very flat surfaces. In this thesis, all images were taken in the constant current mode. The data is displayed in colors which were chosen in such a way that bright spots represent protrusions and dark spots represent valleys or depressions.

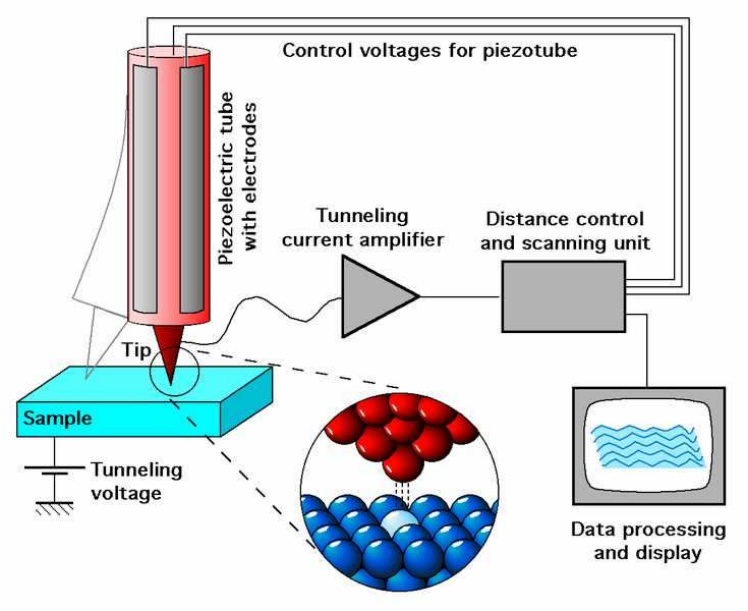

Figure 2.2. Schematic diagram[2] demonstrating the operation of a scanning tunneling microscope.

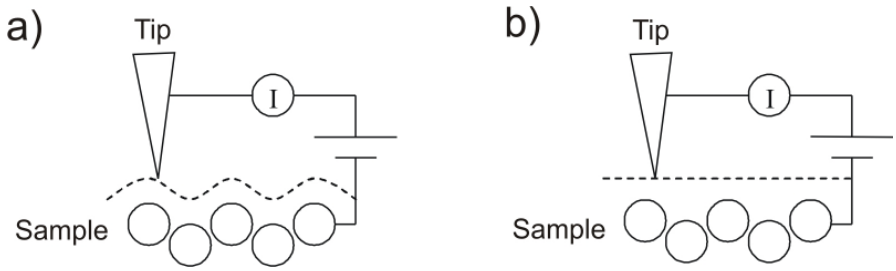

Figure 2.3. Schematic illustration of two different operation modes of STM : the constant current mode (left) and the constant height mode (right). Dashed lines show paths of tip.

STM can be performed in various environments such as vacuum, air, at the solid-liquid interface and at low or high temperatures. In most cases, special techniques for sample preparation are not required and samples remain free of damage. In view of such advantages, STM can also be a very suitable technique for biological and electrochemical studies.

In STM, a precise theoretical description of the tunneling current is not straightforward due to the unknown geometrical and chemical structure of the tunneling probe tip. However, under some assumptions and simplifications such as low temperature, small bias and assuming an arbitrary geometry for the tip most of the

[2] Michael Schmid, TU Wien; adapted from the IAP/TU Wien STM Gallery.

aspects of the tunneling mechanism can be understood. There are many different approaches that explicate the behaviour of the tunnelling phenomenon[3]. The most widely used one is the Bardeen`s perturbation theory[11] which is the pioneered one among the others.

In classical mechanics an electron cannot penetrate into or across a potential barrier if its energy E is smaller than the potential barrier (E_{bar}). On the other hand, according to quantum mechanics the probability for an electron to tunnel through a barrier is given by

$$Q = \exp\left(\frac{-2d}{\hbar}\sqrt{2m(E_{bar} - E)}\right) \qquad 2.1$$

where m is the mass of the electron and d is the width of the potential barrier.

Bardeen, in his approach, studied tunneling current flowing between two metals which are seperated by an insulator (metal-insulator-metal junction). Instead of solving the Schrödinger equation for the whole system, he divided it into two independent subsystems for each side of the junction. In this simple theory, the specific geometry of the gap is neglected and the tunneling gap is modeled as a one-dimensional system. The formula which is commonly used to describe electron transitions in perturbation theories is Fermi's Golden Rule, which gives the transition rate between two quantum states. Applying this to the tunneling transitions in STM by assuming the two electrodes to be the tip and the sample, Fermi`s Golden rule then gives the probability of an electron to tunnel between a sample state and a tip state. The tunneling current I between tip and sample measured while applying a small bias voltage U (with respect to the tip) is given by (with $E_F = 0$)

$$I = \frac{4\pi e}{\hbar}\int_0^{eU} dE\rho_t(E - eU)\rho_s(E)T(E, eU, d) \qquad 2.2$$

Hence the current is given by a combination of the local densities of states of the sample ρs and of the tip ρt. T(E, eU, d) is the transmission coeffient for electrons with energy E tunneling from the tip into the sample and given by

$$T(E, eU, d) = \exp\left(\frac{-2d}{\hbar}\sqrt{2m(\frac{\phi_s + \phi_t - eU}{2} - E)}\right) \qquad 2.3$$

where ϕ_t and ϕ_s are the work functions of the tip and the sample, respectively.

According to equation 2.2, the tunneling current is simply an integral of the transmission coefficient multiplied with the density of states (DOS) of the tip and the sample. However, in this simple model, the geometry of the tip is not considered and tip

[3] A review by D. Drakova discusses some of these approaches.[10]

and sample have a perfectly symmetric role. This means, the DOS of tip and sample are exchangeable. The first theoretical model in this respect is the s-wave-tip model of J. Tersoff and D. R. Hamann.[12] They modeled the tip apex as a little sphere, implying that only the s-wave solutions of the spherical potential well are important. Using Bardeen`s formalism they find that at low biases the tunneling current is proportional to the surface local density of states (LDOS) at the Fermi level at the center of the sphere with radius r_0

$$I \propto eU\rho_s(E_{F,s})\rho_t(E_{F,t}, r_0)\exp\left(-\frac{2d}{\hbar}\sqrt{m\frac{\phi_s+\phi_t}{2}}\right) \qquad 2.4$$

The Tersoff-Hamann model fails to explain the reason for atomic resolution in STM. The reason is that only the properties of the sample contribute to the STM image while the detailed structure of the tip wavefunctions are neglected. As expressed in equation 2.4 the dependence of the current on the density of states of the tip is expressed just by a constant. Therefore, by detecting the tunneling current, only the local density of states of the sample is recorded, not of the tip.

Chen, in 1990, introduced an extension of the Tersoff-Hamann theory that takes into account a more detailed model of the tip structure.[13] This model allowed the interpretation of high resolution features in STM. Chen took into account the d_z^2 like states of the tip which are close to the Fermi edge and thus contribute to the tunneling current.

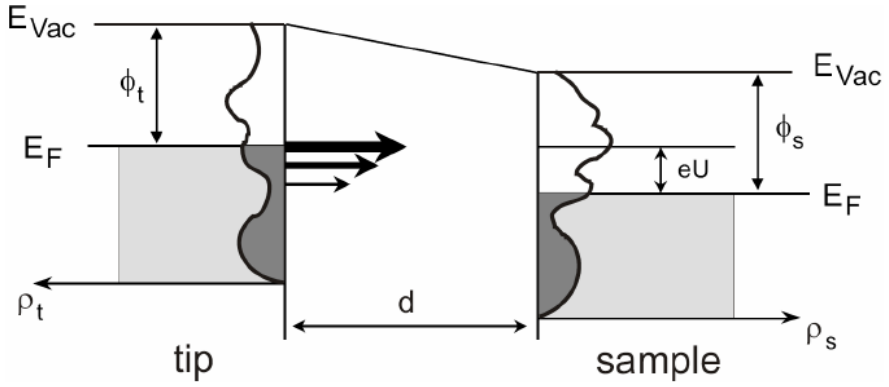

Figure 2.4. Schematic energy level diagram of a tip-sample junction. A positive bias U is applied to the sample. The probability of tunneling is larger for electrons which are close to the Fermi energy as indicated with the different sizes of the arrows. $\rho_{t,s}$ indicate the density of states and $\phi_{t,s}$ the work function for the tip and the sample, respectively.

2.1.2 LEED

Low energy electron diffraction (LEED) is another important experimental method used in this thesis to characterize the structural features of our samples.

After the proposal of the wavelike nature of particles by Louis de Broglie in 1924, the possibility of the occurrence of electron diffraction was proposed. In his work, he suggested that the wavelength of a particle with linear momentum p is given by h/p, where h is Planck's constant. The de Broglie hypothesis was experimentally confirmed at Bell labs by Davisson and Germer[14] in 1927 when they observed a diffraction pattern of low energy electrons which are backscattered from a crystalline nickel target.

In this technique, a beam of low energy electrons (from few to some hundreds eV) is used for bombardment of the sample surface and the diffracted electrons are observed as spots on a fluorescent screen. The sample must be a single crystal in order to generate a back-scattered electron diffraction pattern. By analyzing the position of the spots it is possible to obtain information on the symmetry and size of the surface structure. Moreover, in the presence of adsorbates analysis of the spot positions provides information about the size and rotational alignment of the adsorbate unit cell with respect to the substrate unit cell. Surface sensitivity of LEED comes from the two following reasons: First, at low energies, the mean free path of the electrons in the surface is very short (just a few nanometers, or 2-3 atomic layers), thus most collisions occur in the very top layers of a sample. Second, the de Broglie wavelength of an electron $\lambda = h/p = h/\sqrt{2mE}$ (p: electron momentum) is comparable to the interatomic distances which satisfies the atomic diffraction condition.

The diffraction pattern observed on LEED experiments is the Fourier transform of the real space lattice. In three dimensions, for an incident electron with wave vector k_i and scattered wave vector k_f, the condition for constructive interference and thus diffraction of scattered electron waves are given by the Laue condition

$$k_f - k_i = G_{hkl} \tag{2.5}$$

where G_{hkl} is a vector of the reciprocal space and given by

$$G_{hkl} = ha^* + kb^* + lc^* \tag{2.6}$$

where (h,k,l) is a set of integers and a^*, b^* and c^* are the primitive reciprocal space vectors. Since only elastic scattering is considered, the magnitudes of the wave vectors are unchanged which means $|k_f| = |k_i|$. Since, as mentioned above, for low energy electrons only the topmost atomic layers are involved in scattering, for the component perpendicular to the surface no diffraction occurs. As a result, the reciprocal lattice of a surface is a 2D lattice with rods extending perpendicular from each lattice point and in 2D form equation (2.5) reduces to

$$k_f^{\parallel} - k_i^{\parallel} = G_{hk} = ha^* + kb^* \tag{2.7}$$

In this 2D case, the possible elastically scattered beams (k_f) can be obtained by using the Ewald`s sphere construction. The wave vector k_i of primary beam is positioned with

its end at the (0,0) reciprocal lattice point and a sphere is constructed around its starting point. As seen from figure 2.5, the Laue condition is satisfied for every point at which the sphere crosses a “reciprocal lattice rod”.

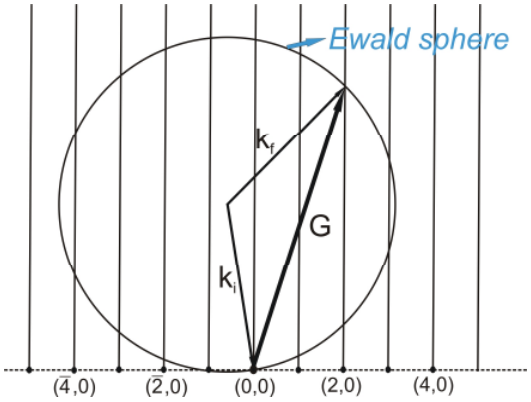

Figure 2.5. Ewald construction for elastic scattering on a 2D surface lattice. The intersections between Ewald`s sphere and reciprocal lattice rods identify the allowed diffracted beams.

In LEED experiments, the diffraction transforms a lattice in real space into a reciprocal space lattice. Therefore, in order to interpret a LEED pattern, the lattice in reciprocal space has to be transformed into real space. However, this procedure is quite difficult for complex diffraction patterns. To overcome this problem, numerous software tools have been developed to simulate the LEED patterns. In this thesis the LEEDpat 2.1 software developed by K. Hermann and M. A. van Hove[15] has been used to simulate the LEED patterns.

2.1.3 XPS

X-ray photoelectron spectroscopy (XPS) is based on the photoelectric effect discovered by Heinrich Rudolf Hertz in 1887. Later, in 1964, Kai Siegbahn[4] and his group in Uppsala in Sweden recorded the first high energy resolution XPS spectrum of cleaved sodium chloride (NaCl).

In XPS, photons of fixed energy are irradiated onto a sample which leads to the emission of electrons from the sample. The kinetic energy of the electron that is emitted from the surface can be measured as

$$E_{kin}=\hbar\omega-E_{bin}-\Phi \qquad 2.8$$

[4] Nobel Prize in 1981

where E_{bin} is the binding energy of the electron in its initial state, ħw is the photon energy and Φ is the work function of the sample. In figure 2.6, a schematic representation of the photoemission process on a metal surface is illustrated.

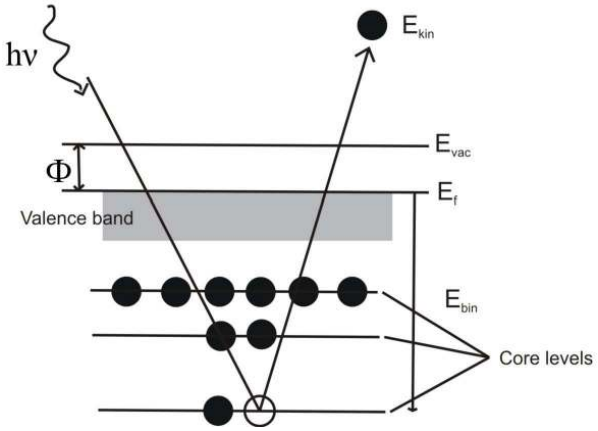

Figure 2.6. Schematic representation of the photoemission process on a metal surface.

Most commonly, Al K-alpha (1486.6eV) or Mg K-alpha (1253.6eV) X-ray sources are employed in commercially or privately built XPS systems. When XPS is done at a synchrotron all energies are available. Similar to LEED explained above, the XPS technique is highly surface sensitive due to the short range of the photoelectrons that are excited from the solid. Each photoelectron leaving the sample produces a characteristic XPS peak in the photoelectron spectrum at characteristic binding energy values which are associated with each core atomic orbital (1s, 2s, 2p…). Therefore, the presence of a peak at a particular energy indicates the presence of a specific element in the sample. Moreover, the intensity of the peaks indicates the concentration of the elements. Thus, the technique provides a quantitative analysis of the surface composition, for which the term ESCA (Electron Spectroscopy for Chemical Analysis) is used.

Though XPS is insensitive to hydrogen and helium, every other element is detectable by this technique.

2.2 Molecular self-assembly

The term self-assembly[16] can be defined as a process in which components having sizes from the molecular (e. g. crystals) to the planetary (e. g. galaxies) scale organize spontaneously and reversibly into ordered patterns or structures without human intervention. However, most of the work in self-assembly focuses on the molecular level since imitating nature and creating molecules for the formation of supramolecular structures may help to develop methods for the construction of molecule-based devices which has become a central challenge in nanosciences.

Molecular self-assembly is the spontaneous association of molecules under equilibrium conditions into stable, structurally well-defined aggregates held together by non-covalent bonds.[16a] A simple example is a lipid bilayer which makes up the

membranes of cells. Each lipid is a molecule with a charged hydrophilic head and a neutral hydrophobic tail (figure 2.7). Since the cellular environment consists mainly of water, the lipids arrange themselves in a bilayer with the heads pointing towards the watery environment and with the tails facing towards each other.

Molecular self-assembly can be subdivided into intramolecular self-assembly and intermolecular self-assembly. Intramolecular self-assembly is usually called folding: a molecule changes its shape from a random conformation into a well-defined stable structure through non-covalent interactions. On the other hand, most often the term molecular self-assembly refers to intermolecular self-assembly by which supramolecular structures are formed. For the formation of supramolecular structures the concepts of supramolecular chemistry[17][5] are used, which examines non-covalent interactions between the molecules. These interactions include hydrogen bonding, л-л interactions, metal coordination, van der Waals, hydrophobic and electrostatic forces. Through these interactions perfect ordering of the molecules into stable, well-defined and relatively defect-free aggregates over large areas is achieved. Moreover, the components remain unchanged throughout the process.

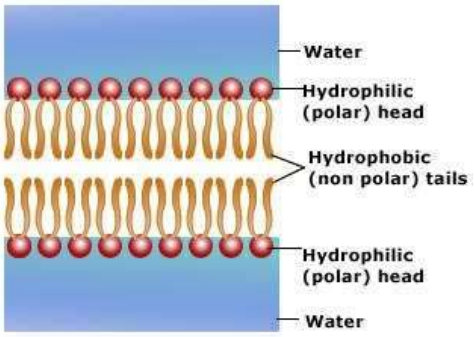

Figure 2.7. Schematic representation[6] of a lipid bilayer in an aqueous medium. The tails are facing towards each other while the heads interact with the watery environment.

Molecular self-assembly is a "bottom-up" approach, which stands for building functional devices out of prefabricated molecular building blocks. This stands in contrast to "top-down" techniques like lithography where a bulk material is etched down to the desired final structure. However, material wastage, high fabrication costs and defective structures are unavoidable with "top-down" techniques.

By making use of the bottom-up approach, numerous studies have been performed to be able to produce structures, for instance, DNA complexes with useful properties.[18]

The investigation of organic materials on surfaces provides the possibility of addressing the molecular components directly and controlling the outcome of the self-assembly process itself. STM enables the characterization of these molecular structures

[5] Donald J. Cram, Jean-Marie Lehn and Charles J. Pedersen were awarded the Nobel Prize in chemistry in 1987 for recognition of their work in the area of supramolecular chemistry.
[6] http://www.tutorvista.com/content/biology/biology-iii/cellular-micromolecules/lipids.php

on metal surfaces in real space. In this way, a detailed understanding of the interactions which stabilize the molecules forming the self-assembled structures, in particular molecule-substrate and molecule-molecule interactions, can be obtained. Numerous works have been published on the organization of molecules on metal surfaces up to date.[19]

2.3 Polymerization

The chemical reaction in which monomers are covalently linked to form a polymer (macromolecule) is called polymerization. Polymers can be naturally found in everyday life from rubber and cellulose to natural biopolymers such as DNA and proteins. Due to the astonishing range of properties accessible in polymeric materials, synthetic analogs have been created which are applied to everyday life as fibers, flexible films, adhesives, resistant paints etc.

Polymers are fascinating research targets in chemistry and molecular science since they are expected to have many applications in future technology. Therefore, many laboratories are devoted to do research and develop novel polymeric materials with unique functional properties for future technological applications. Some examples include the investigation of organic solar cells, organic light emitting devices, etc. Additionally, creating a covalently bonded 2D material with a periodic structure would have many applied aspects of the natural and engineering sciences.

Such covalently bonded 2D materials can be fabricated by traditional organic chemistry methods. However, creating such large macromolecules needs a lot of synthetic steps, and therefore requires a considerable effort. Moreover, since after every synthetic step some of the products necessary for the next step will diminish, obtaining large and complex structures will be impossible. Another point is that a 2D polymer in solution can have different conformations. For example, such polymers may spontaneously roll up or even form tubes under certain conditions. Supposed a 2D structure is obtained in spite of all these problems, there is no possibility to have it intact upon deposition on a surface.

A promising alternative to overcome the problems mentioned above could be to confine the reactions on plane surfaces and to use the supramolecular approach to pre-assemble the monomeric components into well-defined structures. In such an approach, first, the emphasis is placed on the molecular structure. Particularly, the functional groups of the molecules need to be chosen such that an interaction between them is possible and the molecules can aggregate on the surface by non-covalent bonds. Subsequently, the covalent connection is achieved by an external trigger such as thermal activation, UV radiation or manipulation. STM is a promising technique not only for imaging these structures but also for creating covalent bonding between the molecules directly on a surface by using the STM tip. However, while self-assembly properties of numerous molecules have been studied on surfaces in detail, studies of chemical reactions investigated by scanning probe methods have just emerged. The first approach in this area was reported by Takami et al. who irradiated 1,15,17,31-dotriacontatetrayne

monolayers with UV light.[20] With a similar approach, Barner et al. connected two dendronized polymers.[21] In a different approach, two phenyls were interlinked by excitation with electrons from an STM tip[22] or diacetylene compounds were polymerized to polydiacetlyenes.[23]

Recently, a new method has been developed by Grill and Hecht who polymerized a porphyrin derivative by thermally activating the compounds either directly on the surface by annealing the sample after deposition of the molecules or already during deposition.[24] Parallel to their work, providing larger macromolecular structures with similar approaches has drawn considerable attention and is studied by many other research groups.[25-28]

In chapter 3, a new strategy for a thermally induced formation of polymeric nanostructures from pre-organized molecular building blocks using protecting group chemistry is presented. Through this concept, interlinking of individual monomers can be obtained by thermally releasing the protecting groups and the resulting structures can be controlled by modifying the functional groups as well as the molecular core.

2.4 Chirality

Chirality comes from the Greek word for hand (*χειρ*, *kheir*). The term "chiral" describes all objects that can not be superimposed on their mirror image. Numerous chiral objects can be found both in the macroscopic and in the microscopic world: the best example is our hands. Further well-known examples are helically formed snails (see figure 2.8) and molecules like DNA and lactic acids. They exist in two enantiomeric forms denoted as **L** and **R** for the left-handed and right-handed form, respectively. A mixture of equal amounts of the two enantiomers is called a racemic mixture (**RL** or **LR**). When two enantiomers are separated, the outcome is called "homochiral (**LL** or **RR**)".

The evidence of chirality in nature was first discovered by Louis Pasteur in his famous experiment[7] in 1848. While he was examining crystals of sodium ammonium tartrate, he discovered the existence of two types of crystals which were mirror images of each other. He managed to separate them and deduced from the experimental results that the asymmetry of the crystals was originating from the asymmetry of the molecular compounds.

Left and right handed molecules have the same physical and chemical properties. However, nature does not treat the two chiralities in the same way, for the reason that when they interact with another chiral species or environment, the response differs. Therefore, their chiral separation is of importance. For example, in the pharmaceutical industry, the wrong chirality of a molecule can be inactive or even harmful for the body, as happened in the case of drug thalidomide.[30] Moreover, many of the basic molecular building blocks of life are chiral and occur with either the one or the other handedness.

[7] The description of Pasteur`s chemical and crystallographic work can be found in a recent publication by H.D.Flack.[29]

For example, all amino acids forming proteins exist only in the left handed enantiomer while the double helix structure of DNA is right handed. To understand this homochirality, a large number of investigations have been carried out. However, the difficulty in understanding the chirality transfer of the molecules into mesoscopic 3D structures has led to study chiral molecules on surfaces, especially after the recent development of heteregenous catalysis[31] which uses a chiral modifier on a metal surface to induce an enantioselective synthesis.

Studying the interaction of chiral molecules with single crystal surfaces provides a framework for understanding the nature of chirality. By making use of the STM, 2D chiral assembly and recognition processes have been observed on surfaces with molecular resolution.[32-38] Nevertheless, the mechanism behind chirality on surfaces has many open questions since molecule-substrate interactions may influence the geometric conformations and electronic characteristics of the molecules.

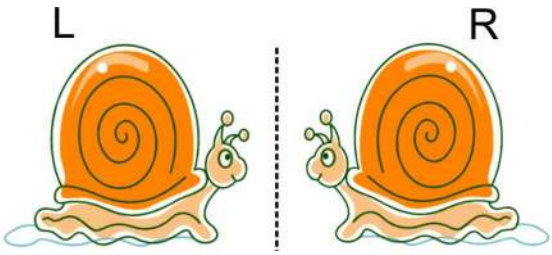

Figure 2.8. The snail shell is a good representative for a chiral object. Mirror image **L** and **R**-snails can not be superimposed by any rotation.

2.5 Investigated molecules

2.5.1 Biphenyl derivatives

In chapter 3, the investigations of organic molecules on metal surfaces are focused on *tert*.butoxycarbonyl (Boc) protected 4,4'-diaminophenyls on Ag(111) and Cu(111) substrates.

The protecting groups are introduced into a molecule by a chemical modification of a functional group which would not survive a subsequent chemical reaction. In other words, they protect the functional group. The modified functional group is then called the protecting group for the original functional group. After the desired chemical reaction is completed, the protecting group is removed giving back the original functional group. This process is called deprotection.

Boc protecting groups are used to protect amines in chemical reactions. In this thesis, they are explored as intermolecular organizers on surfaces since Boc protected amine exhibits both hydrogen bond donor and acceptor functionalities which may

provide lateral ordering for the compounds on surfaces. Furthermore, the protecting groups can easily be cleaved by heat or pressure. Such chemical reactions of the intermediates generated after deprotection could be favoured.

The investigated organic compounds featuring end groups with different functionalities or positions are shown in figure 2.9. All molecules consist of a biphenyl core as the molecular backbone and two amine protecting groups attached to it. In biphenyl **1** and **2**, both end groups are placed in para positions to the backbone while biphenyl **3** exhibits an asymmetric shape as one of the end groups is placed in meta position. On the other hand, biphenyl **2** has the same symmetry as biphenyl **1** but contains 3 fluorine atoms at one of the end groups which make this part more reactive.

The molecules were synthesized by Umut Soydaner in the group of Prof. Marcel Mayor (Chemistry Department, University of Basel).

The experimental results and further discussion on the Boc protected biphenyl compounds adsorbed on Ag and Cu(111) will be given in detail in chapter 3.

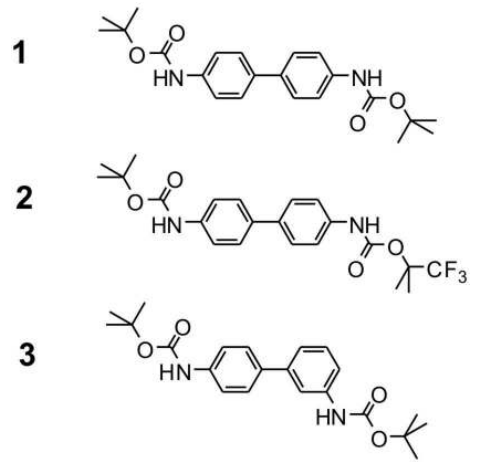

Figure 2.9. Molecular structures of the three biphenyl derivatives: **1:** 4,4'-di(*tert*.butoxycarbonyl-amino)biphenyl, **2:** 4-(*tert*.butoxycarbonyl-amino)-4'(1''-methyl-1''trifluoromethyl- ethoxycarbonyl-amino) biphenyl, and **3:** 3,4'-di(*tert*.butoxycarbonyl-amino) biphenyl.

2.5.2 Cyano-helicene

Helicenes are polycyclic aromatic hydrocarbons in which aromatic rings are angularly annulated forming a helical π-conjugated system. Two enantiomeric forms, namely, clockwise and anticlockwise helicenes exist and they are non-superimposible.

The first enantiomeric resolution of a helicene composed of 6 benzene rings was achieved[39] by M. S. Newman and D. Lednicer in 1956. Today, the synthesis of helicenes with different lengths and components is possible.[40-42]

Their rigid helical structure as well as spectral and optical features make them good candidates for applications in enantioselective catalysis[43,44] and chiral recognition.[42,45] Additionaly, their sublimation properties -high thermal stability and low sublimation temperatures- allow potential surface studies. Their van der Waals self-assembly has been studied in pioneering papers.[46-52]

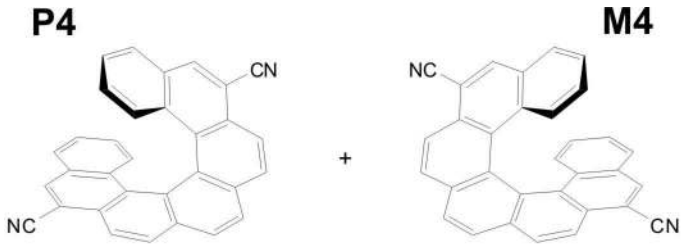

Figure 2.10. Molecular structure of the two enantiomeric forms of 6,13-dicyano-[7]-helicene, M and P .

The helicene derivative, 6,13-dicyano-[7] helicene, investigated in this thesis was synthesized by Michael Schär in the group of Prof. Francois Diederich at the ETH Zürich. The structure of the molecule (with two opposite enantiomers M and P) is shown in figure 2.10. The molecule has a helicene core composed of 7 benzene rings to which two opposed cyano side groups to direct supramolecular aggregation are attached at positions 6 and 13. Such cyano interactions had been previously established in 3D crystals by Desiraju[53] and for surface architectonics first by Yokoyama[54] and then further developed in collaboration of F. Diederich and T. Jung.[55-58]

As the fourth molecule studied in this thesis, the two enantiomers of helicene will be called as **P4** and **M4** and the detailed investigation of the adsorption structures of the racemic and the enantiopure forms of the molecule on Cu(111) will be given in chapter 4.

2.6 Sample preparation

The experiments have been performed with a low temperature-UHV system (base pressure of $1x10^{-10}$ mbar) as well as a homebuilt room temperature-UHV system. The substrates used in this study are Cu and Ag single crystals cut along (111) crystallographic directions, which were cleaned by repeated cycles of sputtering with Ar+ ions and thermal annealing. This procedure provides well defined, flat terraces of about 100nm in width. The organic molecules were deposited onto the substrates by sublimation from a Knudsen-cell type evaporator [www.kentax.com]. During molecule deposition, the substrates were held at room temperature. The deposition rate was controlled by a quartz micro balance (QMB). STM measurements were performed both at room temperature and 77K.

References 2

[1] (a) G. Binnig, H. Rohrer, *Scanning tunneling microscopy,* Helvetica Physica Acta 55**,** 726-735 (**1982)** (b) G. Binnig, H.Rohrer, C. Gerber, E. Weibel, *Tunneling through a controllable vacuum gap*, Appl. Phys. Lett. 40, 178-180 (**1982**).

[2] P. Sautet, *Images of adsorbates with the scanning tunneling microscope: Theoretical approaches to the contrast mechanism,* Chem. Rev. 97, 1097-1116 (**1997).**

[3] R. Berndt, J. K. Gimzewski, R. R. Schlittler, *Bias-dependent STM images of oxygen-induced structures on Ti(0001) facets,* Surf. Science, 310, 85-88 (**1994**).

[4] M. L. Bocquet, P. Sautet, *STM and chemistry: a qualitative molecular orbital understanding of the image of CO oil a Pt surface,* Surf. Science 360, 128-136 (**1996**).

[5] L. Ramoino, *Adsorption and self-organization of CuOEP on heterogeneous surfaces : Tuning the molecule-substrate interaction*, Thesis (2005).

[6] J. Kröger, H. Jensen, R. Berndt et al., *Molecular orbital shift of perylenetetracarboxylic-dianhydride on gold,* Chem. Phy. Let. 438, 249-253 (**2007**).

[7] T. A. Jung, R. R. Schlittler, J. K. Gimzewski, *Conformational identification of individual adsorbed molecules with the STM,* Nature 386 (1997).

[8] J. K. Gimzewski, C. Joachim, R. R. Schlittler et al., *Rotation of a single molecule within a supramolecular bearing*, Science 281, 531-533 **(1998).**

[9] F. Moresco, G. Meyer, K. H. Rieder et al., *TBPP molecules on copper surfaces: a low temperature scanning tunneling microscope investigation,* Surf. Science 499**,** 94-102 **(2002).**

[10] D. Drakova, *Theoretical modelling of scanning tunnelling microscopy, scanning tunnelling spectroscopy and atomic force microscopy*, Rep. Prog. Phys**.** 64, 205-290 (**2001**).

[11] J. Bardeen, *Tunnelling from a many-particle point of view*, Phy. Rev. Let. 6**,** 57-& (**1961).**

[12] J. Tersoff, D. R. Hamann, *Theory and application for the scanning tunneling microscope,* Phy. Rev. Let. 50, 1998-2001 (**1983).**

[13] a) C. J. Chen, *Origin of atomic resolution on metal-surfaces in scanning tunneling microscopy***,** Phy. Rev. Let. 65**,** 448-451 (1990) b) C. J. Chen**,** *Microscopic view of scanning tunneling microscopy,* J. Vac. Science & Tech. A 9, 44-50 (**1991**).

[14] C. Davisson, L. H. Germer, *Diffraction of electrons by a crystal of nickel*, Phy. Rev. 30**,** 705-740 **(1927).**

[15] K. Hermann, M. A. van Hove, *LEED pattern simulator LEEDpat Version 2.1* (**2006**).

[16] (a) G. M. Whitesides, J. P. Mathias, C. T. Seto, *Molecular self-assembly and nanochemistry - a chemical strategy for the synthesis of nanostructures,* Science 254, 1312-1319 (**1991**); (b) G. M. Whitesides, M. Boncheva, *Beyond molecules: Self-assembly of mesoscopic and macroscopic components*, Proc. Natl. Acad. Sci. U.S.A. 99, 4769-4774 (**2002**).

[17] a) J. M. Lehn, *Supramolecular chemistry - receptors, catalysts, and carriers,* Science 227, 849-856 (1985); b) D. J. Cram, *The design of molecular hosts, guests, and their complexes (nobel lecture),* Angew. Chem. Int. Ed. 27**,** 1009-1020 **(1988).**

[18] N. C. Seeman, *DNA in a material world,* Nature 421, 427–431 (**2003**).

[19] a) J. Barth, *Molecular Architectonic on Metal Surfaces,* Annual Rev. Phys. Chem. 58, 375-407 (**2007**); b) J.A.A.W. Elemans, S. B. Lei, S. De Feyter, *Molecular and Supramolecular Networks on Surfaces: From Two-Dimensional Crystal Engineering to Reactivity*, Angew. Chem. Int. Ed. 48, 7298-7332, (**2009**); c) Y. Yang, C. Wang, *Hierarchical construction of self-assembled low-dimensional molecular architectures observed by using scanning tunneling microscopy***,** Chem. Soc. Rev. 38, 2576-2589 (**2009**).

[20] T. Takami, H. Ozaki, M. Kasuga et al., *Periodic structure of a single sheet of a clothlike macromolecule (atomic cloth) studied by scanning tunneling microscopy*, Angew. Chem. Int. Ed. 36, 2755-2757 (**1997).**

[21] J. Barner, F. Mallwitz, L. J. Shu et al., *Covalent connection of two individual polymer chains on a surface: An elementary step towards molecular nanoconstructions,* Angew. Chem. Int. Ed. 42**,** 1932-1935 **(2003).**

[22] S. W. Hla, L. Bartels, G. Meyer et al., *Inducing all steps of a chemical reaction with the scanning tunneling microscope tip: Towards single molecule engineering***,** Phy. Rev. Let. 85**,** 2777-2780 **(2000).**

[23] a) Y. Okawa, M. Aono, *Materials science - Nanoscale control of chain polymerization*, Nature 409, 683-684 (**2001);** b) Y. Okawa, M. Aono, *Linear chain polymerization initiated by a scanning tunneling microscope tip at designated positions,* J. Chem. Phy. 115, 2317-2322 **(2001).**

[24] L. Grill, M. Dyer, L. Lafferentz et al., *Nano-architectures by covalent assembly of molecular building blocks,* Nature Nanotech. 2, 687-691 (**2007).**

[25] a) M. Treier, N. V. Richardson, R. Fasel, *Fabrication of Surface-Supported Low-Dimensional Polyimide Networks*, J. Am. Chem. Soc. 130**,** 14054 **(2008);** b) M. Treier, R. Fasel, N. R. Champness et al., *Molecular imaging of polyimide formation,* PhyChemChemPhys 11**,** 1209-1214 (**2009).**

[26] M. Matena, T. Riehm, M. Stöhr et al., *Transforming surface coordination polymers into covalent surface polymers: Linked polycondensed aromatics through oligomerization of N-heterocyclic carbene intermediates,* Angew. Chem. Int. Ed. 47 2414-2417 (**2008).**

[27] a) S. Weigelt, C. Busse, C. Bombis et al*., Covalent interlinking of an aldehyde and an amine on a Au(111) surface in ultrahigh vacuum,* Angew. Chem. Int. Ed. 46, 9227-9230 (**2007)**; b) S. Weigelt, C. Busse, C. Bombis et al., *Surface synthesis of 2D branched polymer nanostructures,* Angew. Chem. Int. Ed**.** 47, 4406-4410 (**2008).**

[28] M. I. Veld, P. Iavicoli, S. Haq et al., *Unique intermolecular reaction of simple porphyrins at a metal surface gives covalent nanostructures*, Chem. Com. 13, 1536-1538 (**2008).**

[29] H. D. Flack, *Louis Pasteur's discovery of molecular chirality and spontaneous resolution in 1848, together with a complete review of his crystallographic and chemical work***,** Acta Crystal. A 65**,** 371-389 **(2009).**

[30] E. G. Brown, D. Davies, *Chemical Asymmetric-Synthesis,* Nature 342**,** 631-636 **(1989**).

[31] H. U. Blaser, *Enantioselective synthesis using chiral heterogeneous catalysts,* Tetrahedron-Asymmetry 2, 843-866 (**1991).**

[32] K. H. Ernst, *Supramolecular Chirality*, Top. Cur. Chem. 265**,** 209-252 (**2006).**

[33] R. Cortes, A. Mascaraque, P. Schmidt-Weber et al., *Coexistence of Racemic and Homochiral Two-Dimensional Lattices Formed by a Prochiral Molecule: Dicarboxystilbene, on Cu(110),* Nano Let. 8**,** 4162-4167 **(2008).**

[34] C. Busse, S. Weigelt, L. Petersen et al., *Chiral ordering and conformational dynamics for a class of oligo-phenylene-ethynylenes on Au(111),* J. Phys. Chem. B 111**,** 5850-5860 **(2007).**

[35] W. Chen, H. Li, H. Huang et al., *Two-dimensional pentacene : 3,4,9,10-perylenetetracarboxylic dianhydride supramolecular chiral networks on Ag(111)*, J. Am. Chem. Soc. 130**,** 12285-12289 **(2008).**

[36] F. Vidal, E. Delvigne, S. Stepanow et al., *Chiral phase transition in two-dimensional supramolecular assemblies of prochiral molecules,* J. Am. Chem. Soc. 127**,** 10101-10106 (**2005).**

[37] S. M. Barlow, S. Louafi, D. Le Roux, J. Williams, C. Muryn, S. Haq, R. Raval, *Polymorphism in supramolecular chiral structures of R- and S-alanine on Cu(110*), Surf. Sci. 590, 243–263 **(2005).**

[38] M. Lingenfelder, G. Tomba, G. Costantini et al., *Tracking the chiral recognition of adsorbed dipeptides at the single-molecule level,* Angew. Chem. Int. Ed. 46**,** 4492-4495 (**2007).**

[39] M. S. Newman, D. Lednicer, *The synthesis and resolution of hexahelicene,* J. Am. Chem. Soc. 78**,** 4765-4770 (**1956).**

[40] P. Sehnal, I. G. Stara, D. Saman et al., *An organometallic route to long helicenes,* Proc. Nat. Ac. Sci. USA 106**,** 17605-17605 **(2009).**

[41] M. Miyasaka, A. Rajca, M. Pink, et al., *Cross-conjugated oligothiophenes derived from the (C2S)(n) helix: Asymmetric synthesis and structure of carbon-sulfur [11]helicene,* J. Am. Chem. Soc. 127**,** 13806-13807 **(2005).**

[42] E. Murguly, R. McDonald, N. R. Branda, *Chiral Discrimination in Hydrogen-Bonded [7]Helicenes*, Org. Lett. 2, 3169–3172 (**2000).**

[43] M. T. Reetz, E. W. Beuttenmuller, R. Goddard, *First enantioselective catalysis using a helical diphosphane*, Tetrahedron Letters 38**,** 3211-3214 **(1997).**

[44] S. D. Dreher, T. J. Katz, K.-C. Lam, A. L. Rheingold, *Application of the Russig-Laatsch Reaction to Synthesize a Bis[5]helicene Chiral Pocket for Asymmetric Catalysis,* J. Org. Chem. 65, 815–822 (**2000).**

[45] Y. Xu, Y. X. Zhang, H. Sugiyama, T. Umano, H. Osuga, K. Tanaka, *(P)-Helicene Displays Chiral Selection in Binding to Z-DNA*, J. Am. Chem. Soc. 126, 6566–6567 (**2004).**

[46] T. Nakamura, H. Kondoh, M. Matsumoto, *Scanning tunneling microscopy observations of [7]thiahelicene adsorbed on Au(111),* Molecular Crystals and Liquid Crystals Science and Technology Section A-Molecular Crystals and Liquid Crystals 337, 273 – 276 (**1999).**

[47] M. Taniguchi, H. Nakagawa, A. Yamagishi, K. Yamada, *Molecular chirality on a solid surface: thiaheterohelicene monolayer on gold imaged by STM*, Surf. Sci. 454, 1005-1009 (**2000).**

[48] K.-H. Ernst, Y. Kuster, R. Fasel, M. Müller, U. Ellerbeck, *Two-Dimensional Separation of [7]Helicene Enantiomers on Cu(111),* Chirality 13, 675- 678 (**2001).**

[49] M. Taniguchi, H. Nakagawa, A. Yamagishi et al., *STM observation of thia[11]heterohelicene on gold(111) and gold(110) surface,* Surf. Sci. 507**,** 458-462 **(2002).**

[50] M. Taniguchi, H. Nakagawa, A. Yamagishi et al., *STM observation of molecular chirality and alignment on solid surface*, J. Mol. Cat. A - Chemical 199**,** 65-71 **(2003).**

[51] R. Fasel, M. Parschau, K.-H. Ernst, *Chirality Transfer from Single Molecules into Self-Assembled Monolayers,* Angew. Chem. Int. Ed. 42, 5178–5181 (**2003**).

[52] R. Fasel, M. Parschau, K.-H. Ernst, *Amplification of chirality in two-dimensional enantiomorphous lattice,* Nature 439, 449–452 (**2006)**.

[53] G. R. Desiraju, S*upramolecular synthons in crystal engineering - a new organic-synthesis*, Angew. Chem. Int. Ed. 34**,** 2311-2327 **(1995).**

[54] T. Yokoyama, S. Yokohama, T. Kamikado et al. *Selective assembly on a surface of supramolecular aggregates with controlled shape and size.* Nature 413**,** 619-621 **(2001).**

[55] D. Bonifazi, H. Spillmann, A. Kiebele et al. *Supramolecular patterned surfaces driven by cooperative assembly of C-60 and porphyrins on metal substrates,* Angew. Chem. Int. Ed. 43**,** 4759-4763 (**2004).**

[56] H. Spillmann, A. Kiebele, M. Stöhr et al. *A two-dimensional porphyrin-based porous network featuring communicating cavities for the templated complexation of fullerenes,* Ad. Mat. 18**,** 275 **(2006).**

[57] A. Kiebele, D. Bonifazi, F. Y. Cheng et al., *Adsorption and dynamics of long-range interacting fullerenes in a flexible, two-dimensional, nanoporous porphyrin network,* ChemPhysChem 7**,** 1462-1470 **(2006).**

[58] N. Wintjes**,** D. Bonifazi, F. Y. Cheng, *A supramolecular multiposition rotary device*, Angew. Chem. Int. Ed. 46**,** 4089-4092 (**2007).**

3 Controlling the organization and heat induced coupling of biphenyl derivatives on metal surfaces through protecting group chemistry

In this section, the experimental results for the adsorption of the biphenyl derivatives **1**, **2** and **3** on Ag(111) and Cu(111) are presented and discussed.

The first subsection is a copy of the article published in the journal *Angewandte Chemie International Edition*. Herein, first, the formation of supramolecular arrangements of the biphenyl derivative **1** (figure 2.9) on Cu(111) and Ag(111) surfaces and second, the subsequent interlinking of the individual monomers by thermally releasing the protecting groups is presented. The molecules form two well-ordered structures that can coexist at room temperature on both surfaces. As a result of annealing these structures, covalently bound structures are formed. The molecule-substrate, the molecule-molecule interactions and the influence of the temperature on the self-assembled structures are studied.

The possibility to vary both the molecular core and the reactivity of the protecting group which will enable the creation of 2D polymers with well-defined functional properties will be discussed in the following subsections:

The reactivity of one of the protecting groups of molecule **1** is changed by replacing three hydrogen atoms by three fluorine atoms (biphenyl **2,** figure 2.9). Similar to the first study, the self-assembly behavior of the molecule and the influence of the temperature on Cu(111) and Ag(111)surfaces were studied and the results are presented in the second subsection. The molecules form similar structures at room temperature whereas the structures obtained after annealing differ compared to the previous case. Splitting of the fluorinated part of the molecule earlier than the non-fluorinated part after annealing the sample allow better ordering of the resulting interlinked structures.

In the third subsection the effect of placing one protecting group in meta instead of para position to the biphenyl core is examined (biphenyl **3**, figure 2.9). As in the previous cases the molecules exhibit well-ordered structures while similar to the second case, they form ordered interlinked structures after annealing the samples.

3.1 Heat induced coupling of a biphenyl derivative on metal surfaces

Publication A: Protecting-Group-Controlled Surface Chemistry-Organization and Heat-Induced Coupling of 4,4'-Di(tert-butoxycarbonylamino)biphenyl on Metal Surfaces

Serpil Boz, Meike Stöhr,* Umut Soydaner[§], and Marcel Mayor[§°]*

[*] Department of Physics, University of Basel, Klingelbergstrasse 82, 4056 Basel (Switzerland)
[§] Department of Chemistry, University of Basel, St. Johanns-Ring 19, 4056 Basel (Switzerland)
[°]Forschungszentrum Karlsruhe GmbH, Institute for Nanotechnology, P.O. Box 3640, 76021 Karlsruhe (Germany)

The combination of their almost infinite structural diversity and unique self-assembly properties makes molecules ideal building blocks for tailor-made materials. By utilizing the concepts of supramolecular chemistry[1] impressive results have been achieved for molecular self-assembly on surfaces.[2,3] Noncovalent interactions such as metal coordination,[4, 5] hydrogen bonding,[6] and dipolar coupling[7] are usually exploited to create extended supramolecular patterns in various dimensions. However, the formation of such thermodynamically controlled structures is reversible in most cases and the interaction between the molecular components is usually rather weak. A very appealing concept to obtain structures with higher stability (and in the ideal case, improved conductive properties) is to profit from the order of preorganized structures and to interlink the individual molecular building blocks to generate macromolecules. So far, there are only a very limited number of reports on the subsequent linking of (preorganized) molecules adsorbed on surfaces to provide new functional structures or materials.[8–17]

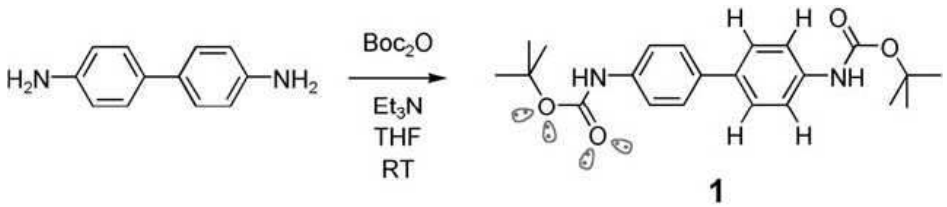

Scheme 1. One-step synthesis of the Boc-protected 4,4'-diaminobiphenyl 1. In the right half of molecule **1** the hydrogen atoms acting as potential hydrogen-bond donors are shown while in the left half the lone pairs of electrons of the oxygen atoms that act as potential hydrogen-bond acceptors are labeled in gray.

Herein we present a new concept to control both the two dimensional molecular self-assembly and the subsequent intermolecular coupling through the use of protecting groups. This concept may pave the way towards two-dimensional functional structures

which at present are only attainable on a larger scale by lithographic methods. Protecting groups are widely used to distinguish the reactivity of functional groups in synthetic chemistry.[18, 19] However, their potential as intermolecular "organizers" for the formation of well-ordered molecular patterns has not yet been explored to the best of our knowledge. Our investigations focus on tertbutoxycarbonyl (Boc) protected 4,4'-diaminobiphenyl (1) groups (Scheme 1). The use of a Boc-protected aryl amine was particularly appealing for numerous reasons: 1) deprotection generates intermediates that can undergo numerous reactions, 2) the Boc-protected amine should be able to act as both a hydrogen-bond donor and acceptor, and its self-assembly is expected to lead to the formation of intermolecular hydrogen bonds, and 3) Boc-protected amines can potentially be cleaved by a large range of stimuli, such as heat or pressure, which is particular appealing for our studies. The extent to which these solution-based properties can be expanded to immobilized molecules in an ultrahigh vacuum (UHV) experiment is one of the focuses of this study.

The deposition of Boc-protected diamine **1** at a coverage of less than a monolayer onto a Cu(111) surface resulted in its self-assembly into two different, but similarly ordered, structures. This was revealed by room-temperature as well as low-temperature scanning tunneling microscopy (STM) studies. The bright lobes in the STM images can be assigned to the tert-butyl groups of **1**.[20, 21] The molecular backbone can be distinguished in high-resolution STM images, thus enabling the identification of the arrangement of individual molecules within the network. Furthermore, atomically resolved STM images (Figure SI7 in the Supporting Information) allowed the orientation of the molecules with respect to the principal directions of the underlying Cu(111) substrate to be determined. It was found that the aromatic backbone is oriented along the $[11\bar{2}]$ direction. STM images of samples with a very low coverage of **1** led to the deduction that evolution of the assembly starts in both cases with the formation of individual molecular rows which are aligned along the $[01\bar{1}]$ direction (highlighted in yellow in Figure 1c, see also Figures SI3–SI5 in the Supporting Information). This arrangement allows the molecules to always be located in the same position with respect to the underlying Cu substrate. The molecules within these rows interact with each other through hydrogen bonds between the carbonyl oxygen atom of one molecule and a phenyl hydrogen atom of another molecule (O···H distance ca. 2.3 Å).

The two different densely packed surface patterns are formed at higher molecular coverage by either keeping the same orientation of the one-dimensional molecular rows during their assembly or by mirroring every second row in the $[01\bar{1}]$ direction of the Cu substrate. In the first arrangement (Figure 1a,c), which we call the parallel arrangement, the molecules are arranged with an oblique symmetry described by a rhomboid with sides of length (12.75±0.4) Å and (9.8±0.3) Å, and an angle of (75.5±1)°. In the second arrangement (Figure 1b, d), which we call the herringbone arrangement, the rhombic unit cell has sides of length (12.75±0.4) Å and (17.85±0.5) Å, and an internal angle of (82.5±1)°. The parallel arrangement has a slightly lower surface density (0.83 moleculesnm^{-2}) than the herringbone arrangement (0.89 moleculesnm^{-2}).

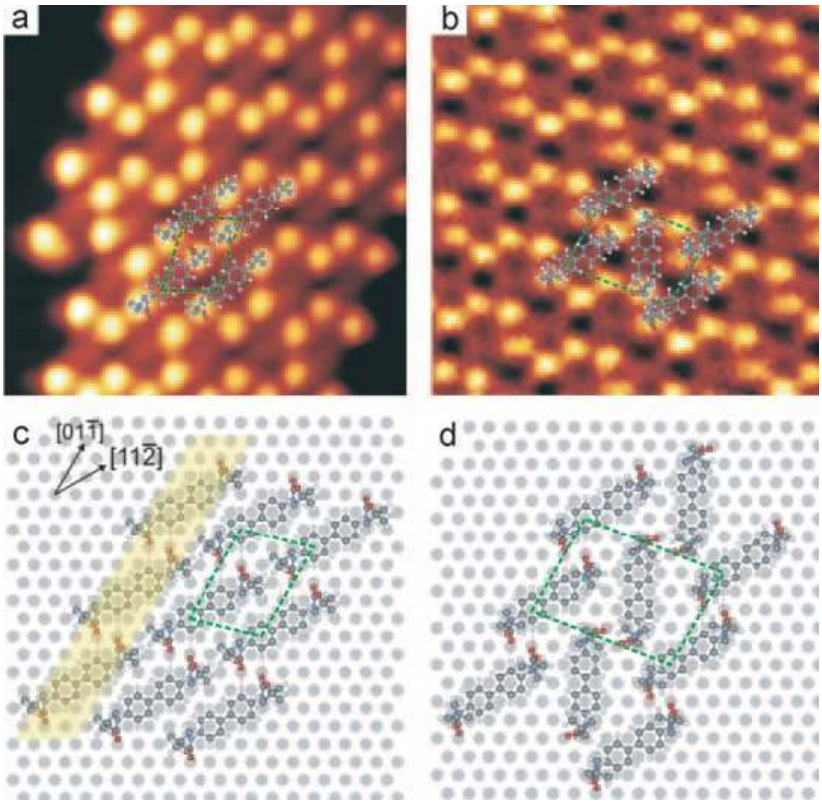

Figure 1. The STM images of **1** on Cu(111): a) the parallel arrangement (7x7 nm^2, 10 pA, 1.6 V, 77 K) and b) the herringbone arrangement (7x7 nm^2, 20 pA, 1.6 V, RT). A few molecules and the unit cell have been drawn in each STM image to illustrate their arrangement. c,d) Schematic representation of the two arrangements. The molecular row highlighted in yellow is the parent stripe motif which is stabilized by hydrogen bonding (red lines) and which leads to both observed arrangements.

Our first attempts to induce intermolecular reactions within the self-assembled monolayers of **1** utilized temperature as a trigger for deprotection. We hoped to be able to profit from the rich chemistry of potential reactive intermediates forming during the cleavage of the Boc group to interlink the preorganized molecular building blocks.

For this purpose, the samples were heated and subsequently investigated after recooling to room temperature. A considerably different and periodic molecular pattern emerged after heating the sample to 196°C. This new pattern (which we call a double-row arrangement) can be seen in the upper part of Figure 2a; the lower part shows the herringbone pattern. The unit cell for the double-row pattern is rhombic with sides of length (25.6±0.2) Å and (18.3±0.2) Å, and an internal angle of (73±1)°. Obviously, the number of bright spots arising from the bulky tert-butyl groups of the Boc protecting groups is reduced considerably. The pattern seems to consist mainly of molecular rods that still feature terminal Boc groups but which are about twice the length of the initial biphenyl rod **1**. Apparently, each monomer **1** loses one Boc group upon annealing, and two of these modified biphenyl units become interlinked to form a dimer (Figure SI6 in

the Supporting Information). Since desorption-reaction-readsorption mechanisms are very unlikely, or even impossible, under UHV conditions, this dimerization reaction must have taken place when the molecules were immobilized on the surface. This hypothesis is further supported by the fact that the number of biphenyl units per surface area remains the same in both surface patterns.

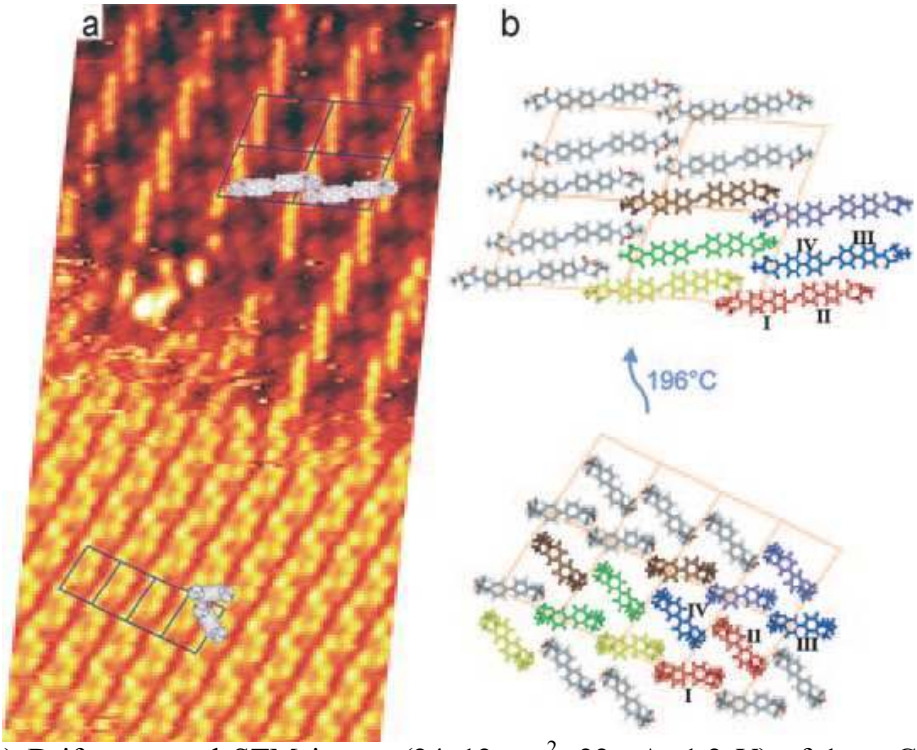

Figure 2. a) Drift-corrected STM image (24x12 nm^2, 22 pA, 1.2 V) of **1** on Cu(111) annealed at 196°C. The upper half shows the double-row pattern, which is only observed after the annealing procedure. The lower half shows the herringbone surface packing of the doubly Boc protected biphenyl **1**. The drawn molecules illustrate their arrangement in each of the two patterns. b) Schematic representation of the transition from the herringbone arrangement of **1** to the double-row arrangement of **2**.

The linking group between the two biphenyl subunits seems to be quite rigid and aligns both biphenyl units parallel to each other and also parallel to the $[11\bar{2}]$ direction, as already observed for both monomer phases. The interaction with the underlying Cu substrate appears to play an important role in the arrangement of both the dimers and the monomers. However, the most interesting feature is the selective cleavage of only one of the two Boc groups of **1** to form perfectly organized rows of dimers. While electronic effects may be responsible for the cleavage of a single protecting group, a selection rule that is communicated between individual molecules is required to enable the surprising perfect transformation from the ordered monomer pattern to the double-row pattern of the dimers. A potential mechanism could be a cleavage of individual Boc groups induced by the spatial rearrangement of the neighboring molecules upon formation of the dimer. Both the azo structure R-N=N-R and the hydrazine structure R-NH=NH-R are considered as possible linking structures that would allow the two biphenyl subunits to be aligned at

a distance of about 2.5 Å. However, we favor the azo structure R-N=N-R as the linker because of the stiff parallel arrangement of both biphenyl subunits in the dimers. Furthermore, the weak signal in the STM images for the linking unit is in line with previous reports on molecules with azo linkers.[22, 23] Assuming that a covalent coupling reaction between pairs of neighboring molecules is the origin of the dimers, the rearrangement sequence shown in Figure 2b may explain qualitatively both the formation of the dimers and their assembly in to the double-row pattern. While the position of one of the two molecules remains almost unchanged (molecules **I** and **III** in the lower part of Figure 2 b), the second rotates by about 60° and moves slightly on the surface to react with the first one (molecules **II** and **IV**), thereby forming the pairs of dimers. Assuming a conformational rearrangement of individual dimers comparable to the one reported by Besenbacher and co workers,[24] these pairs of dimers may even be stabilized by two hydrogen bonds between the carbonyl oxygen and hydrogen atoms of the biphenyl core of neighboring dimer molecules. The resulting pairs of dimers are separated from each other by terminal tert-butyl groups.

A potential reaction mechanism that not only explains the products formed but also the observed monodeprotection of the parent building block **1** is shown in Scheme 2. Upon heating, **1** is expected to lose an isopropene moiety to give the hydroxycarbamate **3**, which decomposes either by decarboxylation to the amine **4** or by condensation to the isocyanate **5**. The isocyanate **5** may even be formed directly through coordination of the lone pair of electrons on the nitrogen atom of **1** to the metal surface and elimination of tert-butanol. Subsequent reaction of the free amine **4** with the isocyanate **5** provides the urea derivative **6**. Either formaldehyde or carbon monoxide and hydrogen have to be expelled to obtain the azo derivative **2** from urea derivative **6**. Although urea derivatives are rather stable in solution and comparable reactions have not yet been reported, the coordination of CO to the metal surface might assist this reaction step. Strong indications supporting the proposed reaction step have been obtained by simulating the reaction with suitable model compounds. Furthermore, the decreasing electron-withdrawing character of the terminal substituents of **1**, **3**, **4**, and **5** and also reduced electron-withdrawing ability of the central linker of **2** and **6** compared with **1** increase the stability of the second Boc protecting group, thus providing a chemical argument for the observed monodeprotection during the transformation from **1** to **2**.

In analogy to **1**, the obtained dimer **2** also has two terminal Boc groups which are in proximity in the double-row arrangement, and thus might react further to give even longer structures upon annealing at higher temperatures. In fact, as displayed in Figure 3, the formation of more complex linked structures surrounded by a mobile phase[25] is observed after annealing the sample at ≥198°C. Mainly longer chains and cross-type structures—both consisting of the same prolate building blocks—are observed. We assign these prolate building blocks to the biphenyl subunits, which are interlinked to form these larger structures.[26]

Of particular interest is the structure of the dimer **2** and the structure of the resulting covalently linked molecules after heating at ≥198°C under UHV conditions. However, the very low yield and the polymeric nature of the reaction products did not allow their

analysis by traditional surface-science techniques. In spite of the successful synthesis of **2**, its sublimation under UHV failed because of its rather low decomposition temperature.

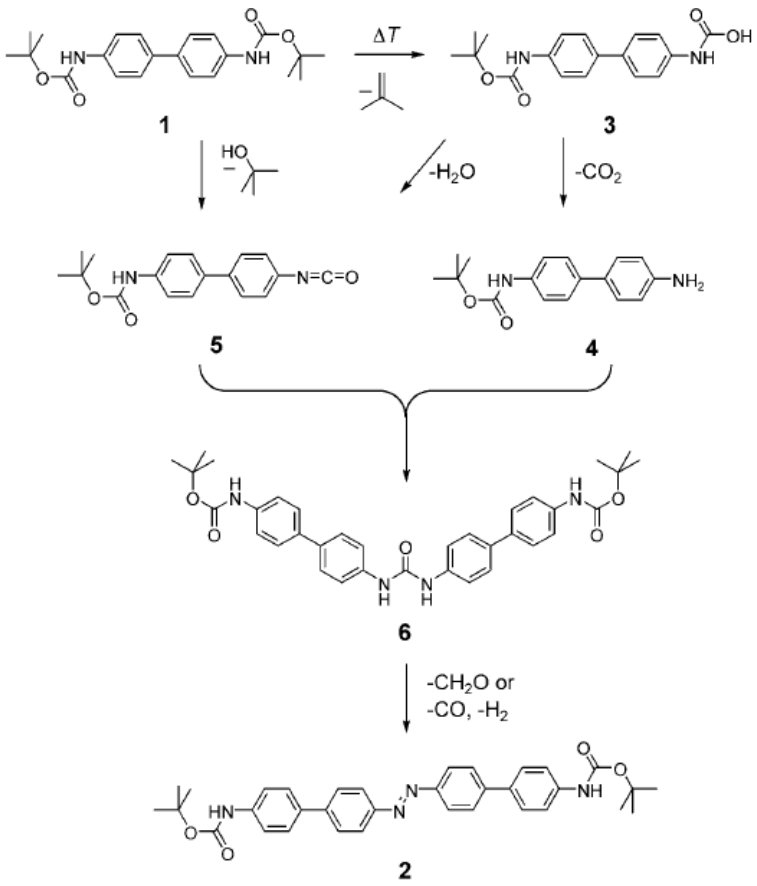

Scheme 2. Possible reaction sequence for the thermal transformation of monomer **1** to dimer **2** on the metal surface.

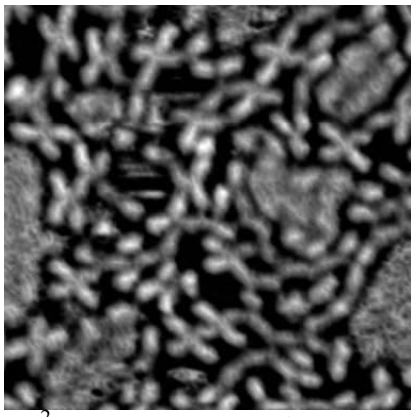

Figure 3. STM image (15x15 nm^2, 1.2 V, 20 pA) of **1** on Cu(111) annealed at >198°C. Chains and cross-type structures consisting of interlinked biphenyl subunits were formed.

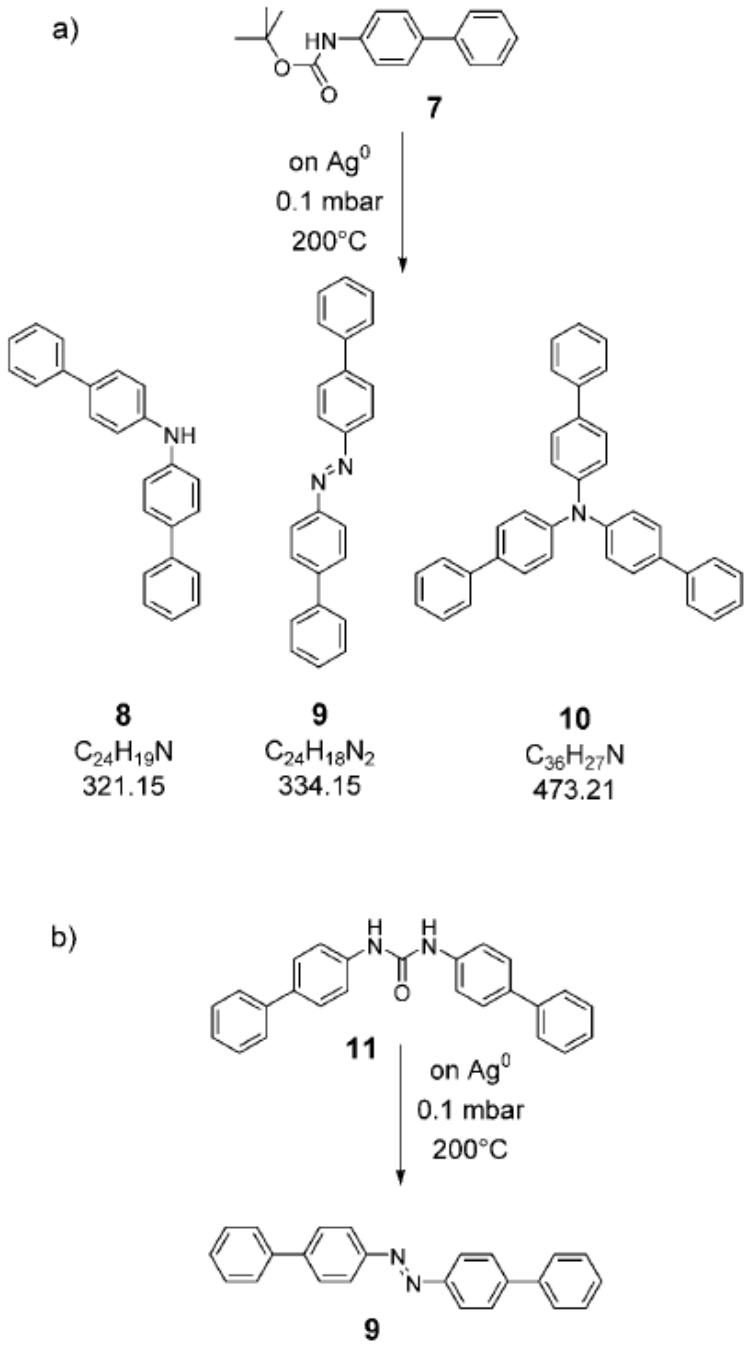

Scheme 3. Simulation of surface reactions: a) Reaction products **8**–**10** obtained by thermal decomposition of **7** on silver nanoparticles at reduced pressure. b) Thermal degradation of the urea derivative **11** to the azo derivative **9** on silver nanoparticles at reduced pressure.

To investigate the chemical processes leading to coupling, model compounds **6** and **7** adsorbed on silver nanoparticles were heated under reduced pressure (0.1 mbar) at 200°C for 6 h. Silver nanoparticles were used instead of copper nanoparticles as the surface purity of the latter was complicated by oxidation processes.[27] To decrease both

the number of potential reaction products and their molecular weights the bifunctional biphenyl **1** was replaced by its monofunctionalized derivative **7** (Scheme 3). Three main reaction products were isolated by preparative thin-layer chromatography (TLC) of the CH_2Cl_2 extract of the nanoparticles. The MALDI-TOF mass spectra of the products showed signals corresponding to structures **8**–**10**, thus supporting the formation of new N-N and N-C bonds under the reaction conditions. In particular, the isolation of the azobiphenyl **9** corroborates the hypothesized formation of an azo compound on the metal surface. In the proposed reaction sequence shown in Scheme 2, the so far unprecedented step from urea derivative **6** to azo derivative **2** was of particular interest.

Indeed, a model reaction of urea **11** on silver nanoparticles under the reaction conditions described above led to the azo derivative **9** being identified by reversed-phase HPLC as a reaction product in the DMF extract.

In conclusion, a new strategy for the creation of surface confined polymeric structures starting from preorganized monomers has been presented which profits from concepts from supramolecular and protecting-group chemistry. The validity of the strategy has been demonstrated with the doubly Boc-protected diaminobiphenyl **1**, which was found to self-assemble in two different arrangements on a Cu(111) surface. Annealing these arrangements at 196°C provided a well-ordered pattern consisting of dimers, also with terminal Boc groups. Further annealing of the samples at ≥198°C led to the formation of cross-type and chainlike structures surrounded by a mobile phase. Experiments were carried out with silver nanoparticles to elucidate the underlying reaction steps and the reaction products. The formation of new N-N and N-C bonds was identified. This observation in turn supports the proposed covalent interlinking of the monomers upon annealing under UHV conditions, a process that is facilitated by the release of the protecting groups. The results demonstrate the potential of using suitably designed protecting groups to arrange monomers on surfaces as well as their cleavage by an external trigger to allow the interlinking of the preorganized monomers. This concept offers various perspectives for the future formation of polymeric structures, since both the molecular core and the protecting group can be modified easily to tune the properties of the obtained surface immobilized polymers.

Supporting information for publication A

1. Synthesis and characterization of model compounds and their precursors

General: All chemicals were directly used for the synthesis without purification if nothing else is remarked. The solvents for chromatography and extractions were distilled once before use. Dry THF was distilled over sodium and potassium. Reaction vessels were flame dried and kept under a protection gas atmosphere. The following instruments have been used: ^{1}H-Nuclear Magnetic Resonance (^{1}H-NMR): Bruker DPX-NMR (400 MHz), Bruker BZH-NMR (250 MHz) instruments were used to record the spectra. Chemical shifts (δ) are reported in ppm relative to residual solvent peaks, and coupling

constants, *J* are in Hertz (Hz). NMR solvents were obtained from Cambridge Isotope Laboratories, Inc. (Andover, MA, USA). The measurements were done at room temperature unless temperatures are given. The multiplicity's are written as: *s* = singlet, *d* = doublet, *t* = triplet, *q* = quartet, *quin* = quintet, *m* = multiplet and *b* = broad. ^{13}C–Nuclear Magnetic Resonance (^{13}C-NMR): Bruker DPX-NMR (400 MHz was used to record the spectra. Chemical shifts (δ) are reported in ppm relative to residual solvent peaks. The measurements were done at room temperature. Electron impact massspectrometry (EI-MS) was performed with a Finnigan MAT 95Q massspectrometer. Elementary analysis (EA): The elementary analysis was measured on a Analysator 240 from Perkin-Elmer. Melting points (MP) have been measured with a Stuart SMP3 melting point apparatus and are uncorrected. Column chromatography (CC): For column chromatography silica gel 60 (40-63 µm) from Merck was used. Thin layer chromatography (TLC): Silica gel 60 F254 glass plates with a thickness of 0.25 mm from Merck were used. The detection was observed with a UV-lamp at 254 nm. Analytical reversed phase HPLC (RP-HPLC) was performed on Lichorspher® 100 RP-18 silica gel from Merck (5µm particle size, 4x250 mm column) with HPLC-grade MeCN.

Synthesis: The model compounds **1**, **2**, **7**, **9** and **11** are labeled according to the manuscript text and their synthesis is displayed in scheme 1.

***tert*.Butyl biphenyl-4,4'-diyldicarbamate (1):**

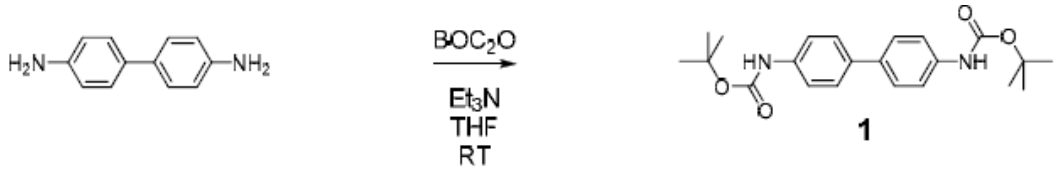

tert.Butyl biphenyl-4,4'-diyldicarbamate (**1**) was synthesized according to a reported procedure. [SI-1] In a 250 ml tree neck flask benzidine (0.41 g, 2.2 mmol, 1eq) was dissolved in THF (100 ml) and triethylamine (0.9 ml, 6.5 mmol, 3 eq.). A solution of di-*tert*.-butyl dicarbonate (1.37 g, 6.3 mmol, 2.9 eq.) in THF (75 ml) was added slowly to the reaction mixture. After stirring for 16 h at RT, the solvents were removed under reduced pressure. Purification by CC (Hexane/EtOAc:1/1) provided **1** as white solid (0.5 g, 1.3 mmol, 59%). MP: decomposition; ^{1}H-NMR (400 MHz, d6-DMSO): δ = 9.38 (*s*, 2H, -NH), 7.49 (*s*, 8H, phenyl), 1.46 (*s*, 18H, -CH_3); ^{13}C-NMR (100 MHz, d6-DMSO) δ = 153.61 (NH-CO_2), 139.35, 134.31, 127.12, 119.26 (phenyl); 79.90 (C(Me_3)), 28.99 (CH_3); EI-MS: 384.1 [M^+]; E.A. calcd. for $C_{22}H_{28}N_2O_4$ (384.47 g/mol): C 68.73, H 7.34, N 7.29, found: C 68.48, H 7.19, N 7.22.

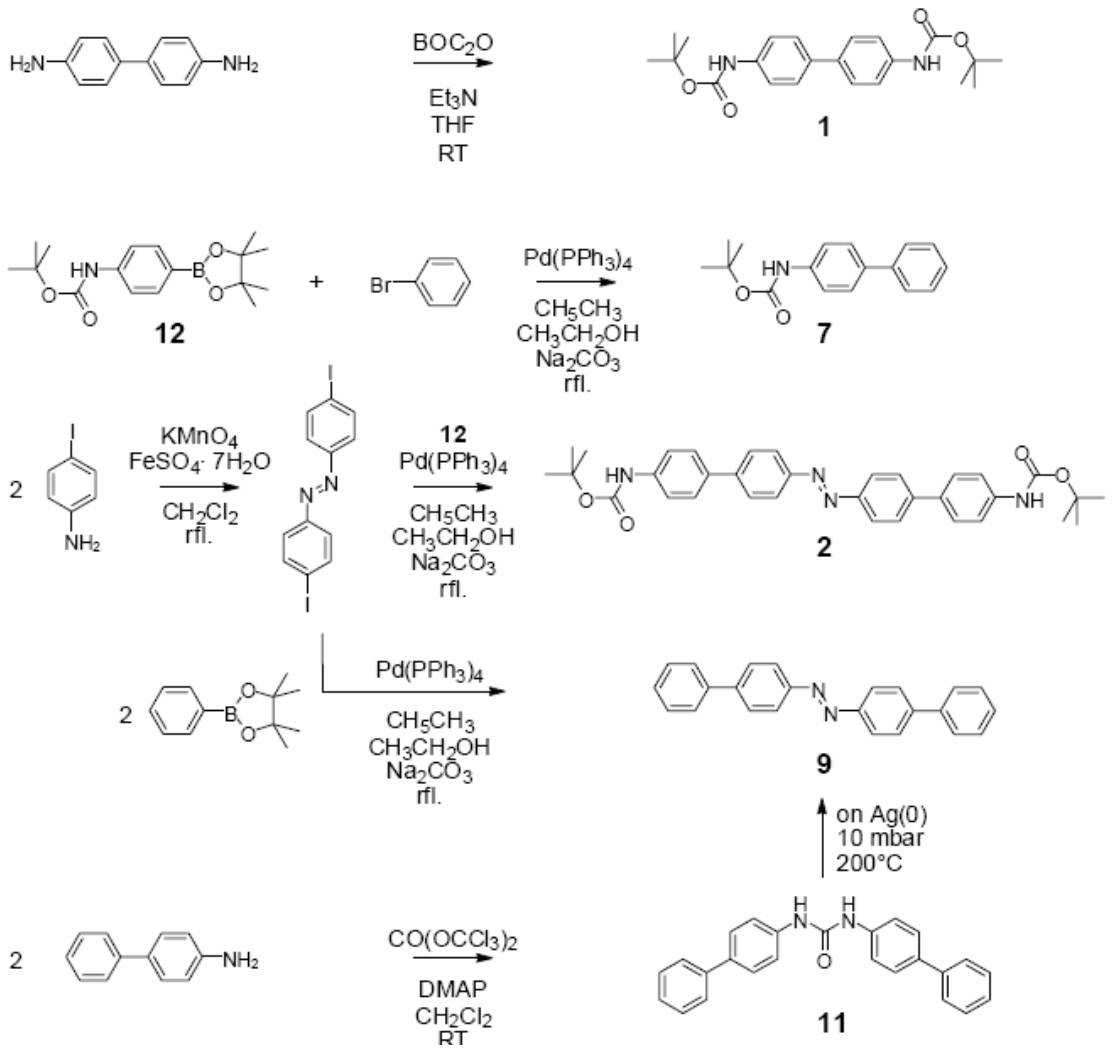

Scheme SI 1. Synthesis of the monomer **1**, the dimer **2** and the model compounds **7**, **9** and **11**.

1,2-bis(4-iodophenyl)diazene was synthesized following a reported procedure: [SI-3]

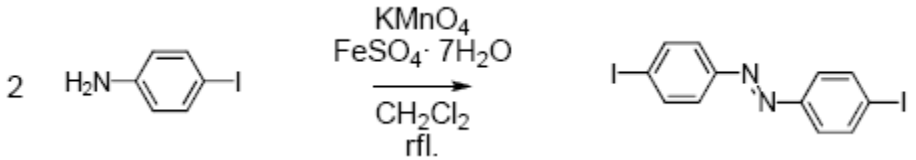

4-Iodo-aniline (1.1 g, 5 mmol, 1eq.) was dissolved in CH_2Cl_2 (50 ml). Equal amounts of oxidants $KMnO_4$ (2.5 g, 15.8 mmol) and $FeSO_4 \cdot 7H_2O$ (2.5 g, 9 mmol) were prepared by grinding in a mortar and added to the solution. The mixture was refluxed for 6 h and subsequnetly filtered through cellite. After washing with water and brine, the organic layer was dried over Na_2SO_4. After evaporation of the solvent CC (Hexane/CH_2Cl_2: 3/1) provided 1,2-bis(4-iodophenyl)diazene as orange solid (0.39 g, 0.9

mmol, 18%). MP: 242-244°C; ^{1}H-NMR (400 MHz, $CDCl_3$): δ = 7.87 (*d*, 2H, phenyl, *J* = 8.6 Hz); 7.64 (*d*, 2H, phenyl, *J* = 8.6 Hz); ^{13}C-NMR (100 MHz, $CDCl_3$): δ = 152.13 (I-C_{phenyl}); 138.84 (C_{phenyl}); 124.94 (C_{phenyl}); 98.55 (N-C_{phenyl}); EI-MS: 433.8 [M^+].

***tert*.Butyl 4',4''-(diazene-1,2-diyl)bis(biphenyl-4',4-diyl)dicarbamate (2):**

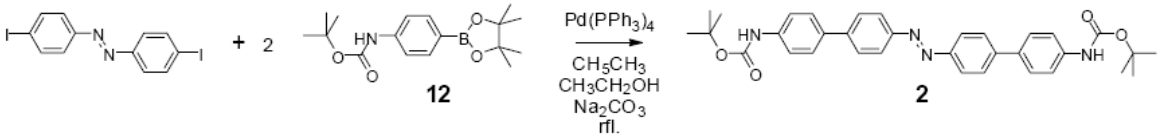

A 25 ml flask was charged with a toluene/ethanol: 6/1 mixture (14 ml) and a 2M aqueous Na_2CO_3 solution (1 ml). The solution was degassed by bubbling with argon while 1,2- bis(4-iodophenyl)diazene (86.95 mg, 0.2 mmol, 1 eq), 4-(Boc-amino)benzeneboronic acid pinacol ester **12** (143.8 mg, 0.44 mmol, 2.2 eq) and tetrakis(triphenylphosphine)- palladium (26 mg, 0.02 mmol, 10 mol%) were added. The reaction mixture was refluxed for 16 h. After cooling down to RT the solvents were removed and the crude dissolved in CH_2Cl_2, washed with water and brine and dried over Na_2SO_4. After evaporation of the solvent CC (CH_2Cl_2) provided the azo derivative **2** as orange solid (75.7 mg, 0.13 mmol, 67%). MP: decomposition; ^{1}H-NMR (400 MHz, d6-DMSO): δ = 9.54 (*s*, 2H, NH-CO_2R), 7.98 (*d*, *J* = 8.4 Hz, 4H, phenyl), 7.88 (*d*, *J* = 8.4 Hz, 4H, phenyl), 7.72 (*d*, *J* = 8.4 Hz, 4H, phenyl), 7.60 (*d*, *J* = 8.4 Hz, 4H, phenyl), 1.50 (*s*, 18H, -CH_3); The limitted solubility of **2** did not allow to record a ^{13}C-NMR spectrum; EI-MS: 564.3 [M^+], 464.2 [M^+-BOC], 364.1 [M^+-2BOC]; EA calcd. for $C_{34}H_{36}N_4O_4$ (564.67 g/mol): C 72.32, H 6.43, N 9.92, found: C 71.67, H 6.43, N 9.53.

1,3-Bis(4-iodophenyl)urea (6) was synthesized according to a reported procedure: [SI-4]

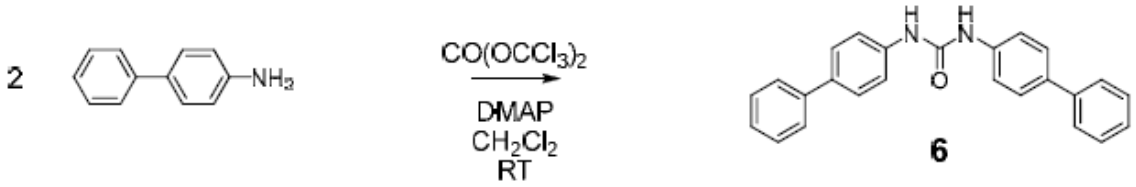

4-Biphenylamine (113.3 mg, 0.67 mmol, 6 eq.) and 4-(Dimethylamino)-pyridin (109.13 mg, 0.89 mmol, 8 eq.) in CH_2Cl_2 (2 ml) were kept under argon in a 25 ml flask. Triphosgene (32.64 mg, 0.11 mmol, 1 eq.) dissolved in CH_2Cl_2 (2 ml) was added dropwise at RT and the reaction mixture was stirred for additional 15 min. while the precipitation of a white solid was observed. The solid was collected by filtration, washed extensively with CH_2Cl_2 and dried at reduced presure to provide **6** as white solid (103.07 mg, 0.28 mmol, 85 %). MP: decomposition; ^{1}H-NMR (400 MHz, d6-DMSO): δ = 8.85 (*s*, 2H, -NH), 7.67-7.58 (*m*, 12H), 7.45 (*bt*, 4 H, *J* = 8 Hz); 7.32 (*bt*, 2 H, *J* = 7.6 Hz); The limitted solubility of **6** did not allow to record a ^{13}C-NMR spectrum; MALDI-ToF-MS: 364.82 [M^+]; RP-HPLC (MeCN) Rt = 7.6 min, purity 99%.

***tert*.Butyl biphenyl-4-ylcarbamate (7)**

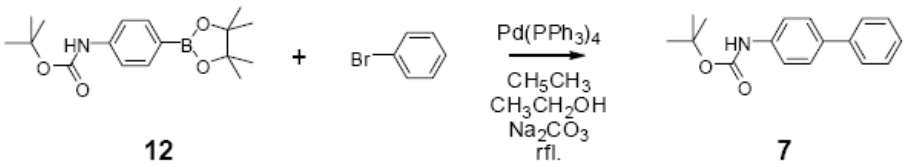

12 **7**

tert.Butyl biphenyl-4-ylcarbamate (**7**) was synthesized according to a reported procedure.[SI-2] In a 100 ml flask a mixture of toluene/ethanol: 6/1 (35 ml) and an aqueous Na_2CO_3 solution (2 M, 1 ml) were bubbled with argon while bromobenzene (0.11 ml, 1 mmol, 1 eq.), 4-(Boc-amino)benzeneboronic acid pinacol ester (0.32 g, 1 mmol, 1 eq.) and tetrakis(triphenylphosphine)palladium (0.06 g, 0.05 mmol, 5 mol%) were added. The reaction mixture was refluxed for 16 h. The solvents were removed under reduced pressure and the crude dissolved in CH_2Cl_2 and washed with water and brine and dried over Na_2SO_4. After evaporation of the solvent, purification by CC (hexane/EtOAc: 6/1) provided **7** as white solid (0.23 g, 0.85 mmol, 85%). MP: 148-150°C; ^{1}H-NMR (400 MHz, $CDCl_3$): δ = 7.57-7.52 (*m*, 4H, phenyl), 7.44-7.40 (*m*, 4H, phenyl), 7.31 (*tt*, 1 H, J_1 = 7.6 Hz, J_2 = 1.2 Hz, phenyl), 6.52 (*s*, 1H, -NH), 1.52 (*s*, 9H, -CH3); ^{13}C-NMR (100 MHz, $CDCl_3$) δ = 153.13, 141.04, 138.06, 136.35, 129,14, 128.03, 127.33, 127.18, 119.21, 81.05, 28.76; EI-MS: 269.2 [M^+]; EA calcd. for $C_{17}H_{19}NO_2$ (269.34 g/mol): C 75.81, H 7.11, N 5.20, found: C 75.56, H 7.17, N 5.14.

1,2-di(biphenyl-4-yl)diazene (9)

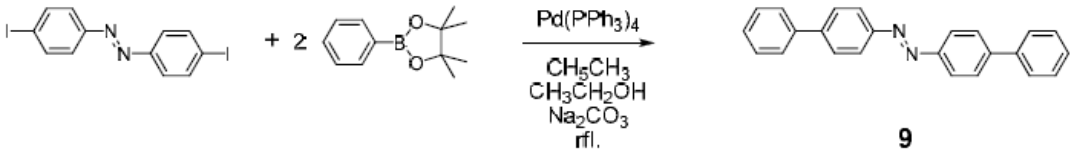

9

In a 25 ml flask a mixture of toluene/ethanol: 6/1 (14 ml) and an aqueous Na_2CO_3 solution (2 M, 1 ml) were bubbled with argon while 1,2-bis(4-iodophenyl)diazene (108.5 mg, 0.25 mmol, 1 eq.), phenylboronic acid pinacol ester (112.2 mg, 0.55 mmol, 2.2 eq) and tetrakis(triphenylphosphine)palladium (28.9 mg, 0.025 mmol, 10 mol%) were added. The reaction mixture was refluxed for 16 h. The solvents were removed under reduced pressure and the crude dissolved in CH_2Cl_2 (50 ml) and washed with water and brine and dried over Na_2SO_4. After evaporation of the solvent, purification by CC (CH_2Cl_2) provided **9** as orange solid (40.5 mg, 0.12 mmol, 48%). MP: 253-255°C; ^{1}H-NMR (250 MHz, d4-THF): δ = 8.03 (*d*, *J* = 8.5 Hz, 4 H), 7.84 (*d*, *J* = 8.5 Hz, 4 H), 7.74 (*d*, *J* = 7 Hz, 4 H), 7.46 (*t*, *J* = 7 Hz, 4 H), 7.38 (*t*, *J* = 7 Hz, 2 H); The limitted solubility of **9** did not allow to record a ^{13}C-NMR spectrum; EI-MS: 334.2 [M^+]; EA calcd. for $C_{24}H_{18}N_2$ (334.41 g/mol): C 86.20, H 5.43, N 8.38, found: C 85.79, H 5.66, N 8.25. RP-HPLC (MeCN) Rt = 18.7 min, purity 99%.

2. Experimental

Surface deposition: The experiments were carried out in an UHV system consisting of several chambers for sample preparation and characterization (base pressure of 1×10^{-10}

mbar). STM (scanning tunneling microscopy) measurements were carried out both at room temperature with a home-built microscope and at 77 K with a commercially available microscope (Omicron NanoTechnology GmbH). As substrate for the molecular films both a (111)-oriented Cu single-crystal and a (111)-oriented Ag single-crystal were used which were cleaned by cycles of sputtering with Ar^+ ions and subsequent annealing. The molecular compounds were deposited by thermal evaporation onto the substrate which was held at room temperature. The deposition rate was controlled by a quartz crystal microbalance.

Simulation of the surface reaction: The reaction conditions were mimicked by adsorbing **7** (5 mg, 0.0186 mMol) dissolved in dichloromethane on Ag nanoparticles with a diameter of about (2±1) µm (1.01g) by evaporation of the solvent at the rotavap. Subsequently, the surface functionalized particles were treated at 200°C and 0.1 mbar for 6h in a glass reaction vessel. To analyze the emerging organic compounds, the particles were extracted extensively with CH_2Cl_2. After concentration of the eluent and preparative TLC three new compounds have been isolated together with considerable amounts of unreacted starting material **7**. Analysis by MALDI-ToF displayed their molecular weights of 321.12, 334.11 and 471.22 suggesting the structures **8** - **10** displayed in Scheme 2 as reaction products.

In a similar procedure the urea derivative **11** (5 mg, 0.0137 mMol) was dissolved in DMF and immobilized on Ag nanoparticles with a diameter of about (2±1) µm (1.01g) by evaporation of the solvent at reduced pressure. After similar treatment of the particles as described above, the cooled down particles were extracted with DMF. The solvent of the extract was removed under reduced pressure and the remaining material was redissolved in acetonitrile for subsequent analysis by reversed phase HPLC. The analysis of the extract displayed three main compounds: unreacted starting material **11**, an unknown reaction product and the expected azo derivative **9** (see figure SI 1).

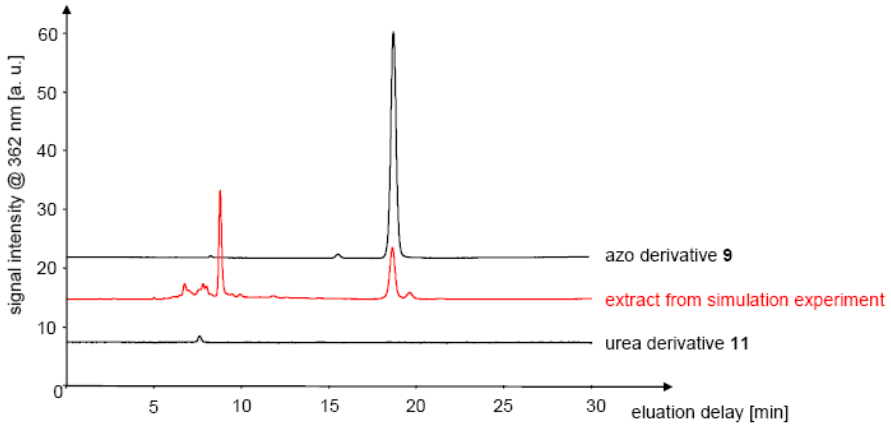

Figure SI 1. Reversed phase HPLC (CH_3CN, flow 0.4ml/min, λ_{det} = 362 nm, t = 25°C) of the azo derivative **9** (top), the DMF extract of the Ag nanoparticles (middle in red) and of the urea derivative **11** (bottom). Due to the poor adsorption at λ_{det} = 362 nm the signal of the urea derivative **11** after 7.6 min. is weak. However, a strong signal can be recorded at λ_{det} = 284 nm.

3. STM-Measurements for 1 adsorbed on Ag(111) / Cu(111)

1 adsorbed on Ag(111)

For **1** adsorbed on Ag(111) a molecular arrangement similar to the one of **1** adsorbed on Cu(111) was observed. Additionally, after annealing the samples at temperatures around 200°C, chainlike structures were found which indicates that a chemical reaction occurred: the BOC groups are released and such, the remaining biphenyl units can interlink.

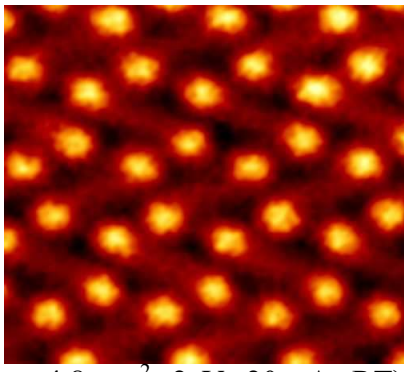

Figure SI 2. STM image (5.2 x 4.8 nm^2, 2 V, 20 pA, RT) of **1** on Ag(111). As for Cu(111) as substrate, again the molecules assemble in a herringbone arrangement.

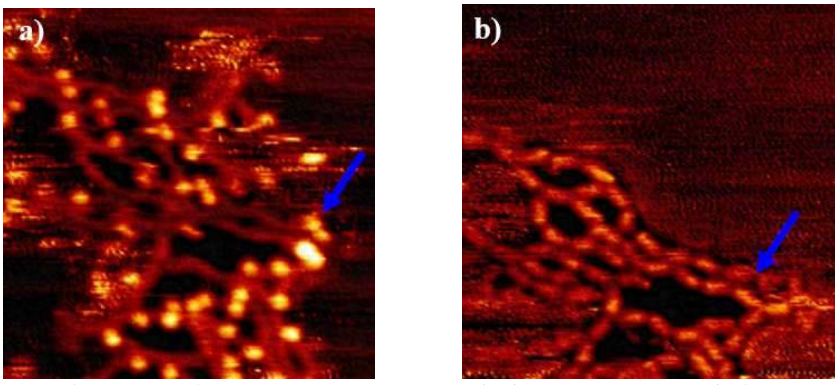

Figure SI 3. STM images of **1** on Ag(111) annealed at 200°C. Both images show the same area on the surface. Since the tip conditions were different during acquiring the images, in a) the tert-butyl groups are mainly imaged (15 × 15 nm^2, -2.18 V, 6 pA, RT) while in b) primarily the π-system is observed (15 × 15 nm^2, -1.18 V, 6 pA, RT). Because of thermal and piezoelectric drift the imaged sample area shifted toward the bottom. The same position on the sample is marked by a blue arrow.

1 adsorbed on Cu(111)

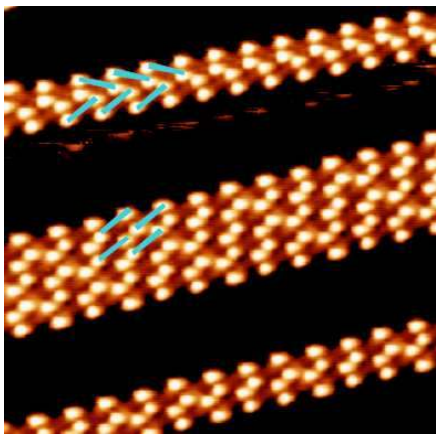

Figure SI 4. For submonolayer coverage of **1** on Cu(111) both the parallel and the herringbone arrangements can be seen (16 × 16 nm^2, 1.6 V, 10 pA, 77 K). The position of the individual molecules is indicated by the blue lines.

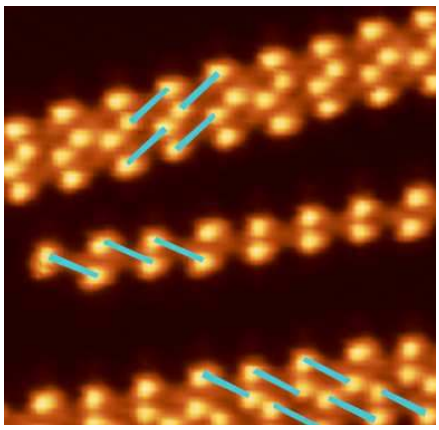

Figure SI 5. STM image for submonolayer coverage of **1** on Cu(111) (10.8 × 10.5 nm^2,1.21 V, 10 pA, 77K). In the middle part of the image, a single row of **1** can be seen (the orientation of the individual molecules is indicated by a blue line). Such a molecular row can be considered as the building block for both the parallel and the herringbone arrangements. In the upper and the lower part of the image the molecules are arranged in double rows in the parallel pattern.

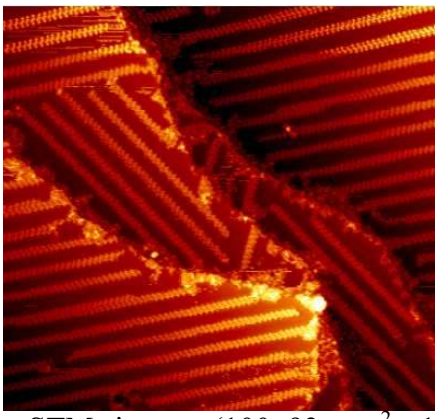

Figure SI 6. Large scale STM image (100x93 nm^2, 1.6 V, 10 pA, 77 K) for submonolayer coverage of **1** on Cu(111). Molecular double and triple rows are visible which are aligned along the three principle directions of the underlying Cu substrate.

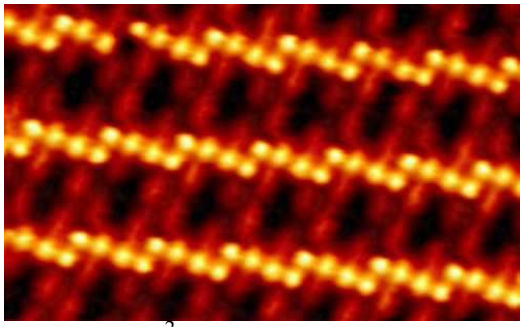

Figure SI 7. STM image (12x7.5 nm^2, 1.4 V, 16 pA, room temperature) of **1** adsorbed on Cu(111) after annealing at 196°C.

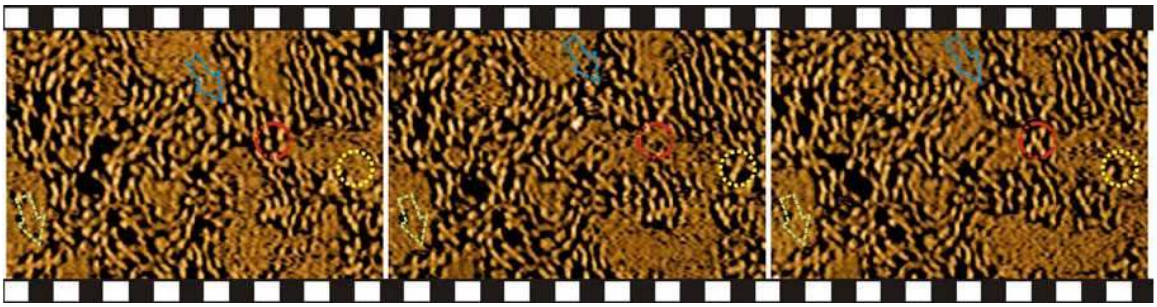

Figure SI 8. Time lapse series of STM images (34x17 nm^2, 1.5 V, 20 pA) of **1** on Cu(111) annealed at 198°C. The green arrow points to representative cross shaped structures, which did not move during the acquisition of the series of STM images, while the blue arrow denotes a moving cross-type structure. In contrast, the encircled structures show two representative areas in which emerging and vanishing aggregated structures can be observed. We thus conclude that the cross-type structures are covalently interlinked biphenyl building blocks forming large macromolecules while the aggregated structures consist of modified monomers or dimers which have lost either one or both Boc protection groups.

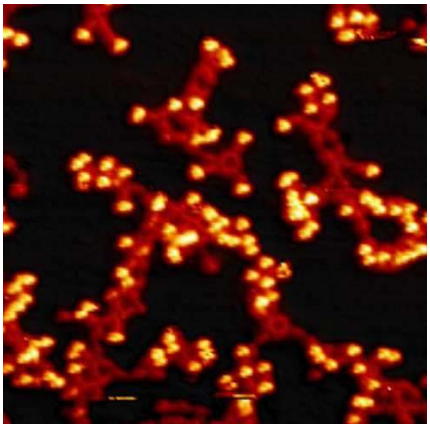

Figure SI 9. STM image (28x28nm^2, 20 pA, 2 V, 77 K) of **1** on Cu(111) annealed at 200°C.

Atomic resolution on Cu(111)

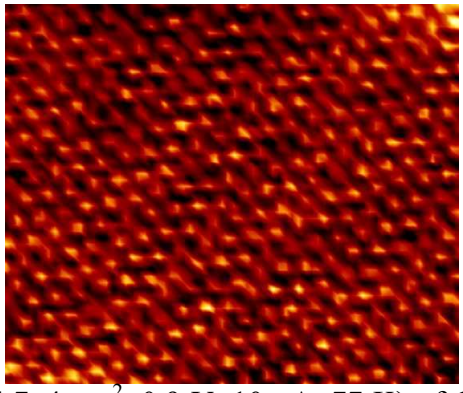

Figure SI 10. STM image (4.7x4 nm^2, 0.9 V, 10 pA, 77 K) of Cu(111) showing atomic resolution which was possible at the given tunnelling parameters because a molecule was picked up with the STM tip. Since the orientation of the substrate was maintained during all experiments done at the LT STM the orientation of the molecules with regard to the principle directions of the Cu substrate can be determined.

3.2 Heat induced coupling of a fluorinated biphenyl derivative on metal surfaces

In the previous work, we presented a new strategy for thermally induced formation of polymeric nanostructures from pre-organized molecular building blocks using protecting group chemistry under UHV conditions. Interlinking of individual monomers was obtained by thermally releasing the protecting groups. This concept offers the possibility to vary both, the molecular core and the reactivity of the protecting group which shall enable the creation of 2D polymers with well-defined functional properties.

Here, we show how the modification of one of the two protecting groups of the reactants effects the self-assembly and the resulting polymerized structures. The investigated compound (see biphenyl **2** in figure 2.9) contains a biphenyl core at each side of which a Boc protecting group is attached. As a difference to our previous work, we replaced three hydrogen atoms with three fluorine atoms at one of the side groups. We expected that an enhanced reactivity of this side group could in turn enhance the control of the formation of polymerized structures. In fact, STM images reveal a more pronounced ordering of the structures formed after annealing over larger islands. On both substrates, Ag(111) and Cu(111), the pre-organized structures evolve into well-ordered islands formed by dimeric, trimeric or even longer interlinked structures depending on the annealing temperature.

3.2.1 Ag(111)

Upon adsorption of biphenyl **2** onto Ag(111), a densely packed surface pattern is formed for a coverage close to a monolayer. An STM image of this arrangement is shown in figure 3.1a. As it can be seen in this high resolution STM image, intramolecular features are resolved. Thus, each molecule is identified as a linear backbone to which two bright lobes corresponding to the Boc protecting groups are attached. The surface structure is identified as a herringbone arrangement in which the molecules are stabilized by hydrogen bonding interactions between the carbonyl oxygen atom of one molecule and a phenyl hydrogen atom of the neighboring molecule. The O…H distance of neighboring molecules is measured to be ~2.7 Å. The nearly rectangular unit cell (a=18 ± 0.7Å, b=13.2 ± 0.7Å, Θ=88° ± 1°) and a few molecules are inserted to illustrate the molecular arrangement. Figure 3.1b shows the corresponding molecular model of the observed herringbone pattern. The structure possesses a molecular density of 0.84 molecules/nm^2.

The evolution of the pattern starts with the formation of molecular rows (building blocks) shown by green arrows in the molecular model. We note here that probably the fluorine atoms are arranged in such a way that the neighboring building blocks interact with each other via halogen bonds. Either the fluorine atoms bind to the carbonyl oxygen atoms of the neighboring molecules[28] or C-F…H-C bonds are formed between the fluorinated groups and the phenyl hydrogen atoms of neighboring molecules. The latter interaction is observed in many crystal structures [29-30] as well as in STM studies. [31-32]

Thus, in the molecular model in figure 3.1b, the C-F…H-C bonds are marked while the alternative model is not shown.

In addition to the herringbone arrangement, we observe also formation of parallel arrangements in either double (green circle) or triple rows (blue circles). The STM image in figure 3.2 shows the alternating rows of the parallel and the herringbone structures.

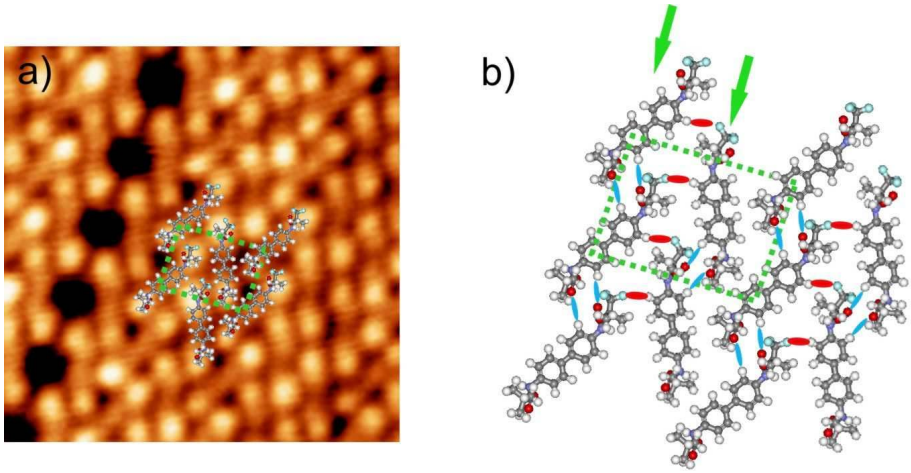

Figure 3.1. a) STM image (8x8 nm^2, 1.7 V, 20 pA, RT) of biphenyl **2** adsorbed on Ag (111). The bonding pattern reveals a herringbone arrangement as can clearly be identified from the high resolution STM image. b) The tentative molecular model in which the two building blocks of the herringbone pattern are indicated by green arrows. O…H bonds are shown with blue ellipses whereas red ellipses indicate the F…H bonds.

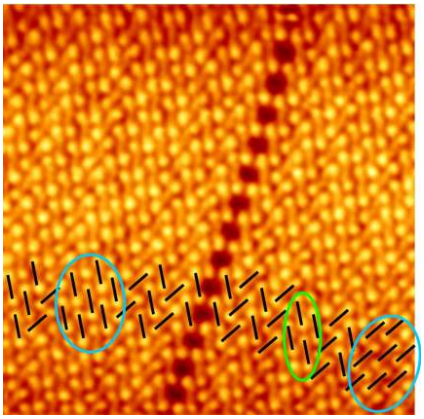

Figure 3.2. STM image of biphenyl **2** on Ag(111) showing the alternating parallel and herringbone arrangements (20x20 nm^2, 1.7 V, 20 pA, RT). The parallel rows can be formed by either double (green circle) or triple rows (blue circles). Some molecules are marked by black lines for better illustration of the arrangements.

To perform on-2D surface reactions, the samples were annealed at elevated temperatures and then imaged by STM after re-cooling to room temperature. The temperature is increased step-by-step on the same sample. Heating cycles at the elevated temperature were of 2-3 minutes each time. It should be noted here that separated experiments when heating the sample directly at the elevated temperature for 2-3 minutes led to comparable results.

As revealed from the STM measurements, the herringbone pattern formed at room temperature evolves into a completely new arrangement after annealing. The annealing process activates the monomers and by thermally releasing the Boc groups converts them into rod-like features whose lengths depend on the annealing temperature. The discrimination of the fluorinated Boc group from the non-fluorinated Boc group is not possible from the STM signature. However, due to the enhanced reactivity of the fluorinated side, we propose as a model that the molecules initially loose the fluorinated side group which leads to the formation of dimeric structures at temperatures between ~150-165°C.

In figure 3.3a, an STM image of a dimeric arrangement formed after annealing the sample at 160°C is shown. Each monomer looses its fluorinated Boc group and two of these unbound ends pair head-to-head to form a dimer. Each is measured in the STM images to be ~2.1 nm in length which is in good agreement with twice the length of a biphenyl unit. In figure 3.3b, the proposed molecular model is presented. The unit cell, as obtained from the analysis of several STM images, has sides of lengths of (24.6 ± 0.6 Å) and (16 ± 0.5 Å) with an angle of (75° ± 1°). H-bonding interactions between the carbonyl oxygen and the phenyl hydrogen atoms in addition to H-bonding interactions between the carboxyl oxygen and the H-N groups of the neighbouring dimers govern the formation of the pattern.

While dimeric structures are observed in majority, some biphenyl units are observed to be linked up into even longer structures (between ~160-170°C) assembling in small islands. The trimeric arrangement in the STM image in figure 3.3c is obtained after annealing the sample at 168°C. These trimers are arranged in a parallel pattern as proposed in the tentative molecular model in figure 3.3d. As found from the analysis of STM images, the unit cell parameters of the pattern are (22.9±0.3) Å and (17.5 ± 0.7) Å with an angle of (44°±1°). H-bonding interactions similar to the dimeric arrangement govern the formation of the trimeric arrangement. These dimers and trimers are found to be formed simultaneously on the surface. STM image in figure 3.4a reveals two such structures, in which a disordered phase and even longer structures are observed between the two phases.

For temperatures larger than ~165°C we observe a considerable large area containing only a mobile phase on the surface and some small islands consisting of only trimeric structures. In addition, the remaining components which loose both Boc groups evolve into even longer structures (figure 3.4b). The correlation between the formation of different structures and the temperature is summarized in a scheme in figure 3.5.

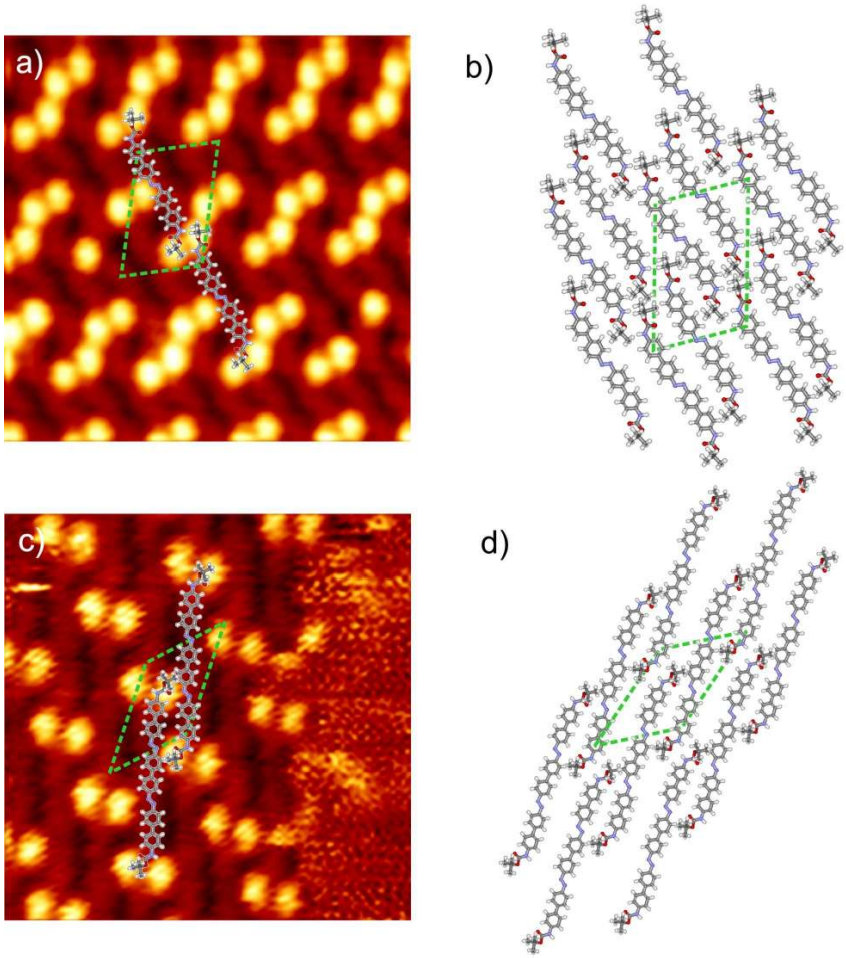

Figure 3.3. a) STM image of the dimeric arrangement of biphenyl **2** on Ag(111) after annealing the sample at 160°C (8x8 nm^2, -1.8 V, 20 pA, RT), and b) corresponding molecular model. c) STM image of the trimeric structures formed after annealing the sample at 168°C (8x8 nm^2, -1.9 V, 20 pA, RT), and d) schematic representation of the arrangement.

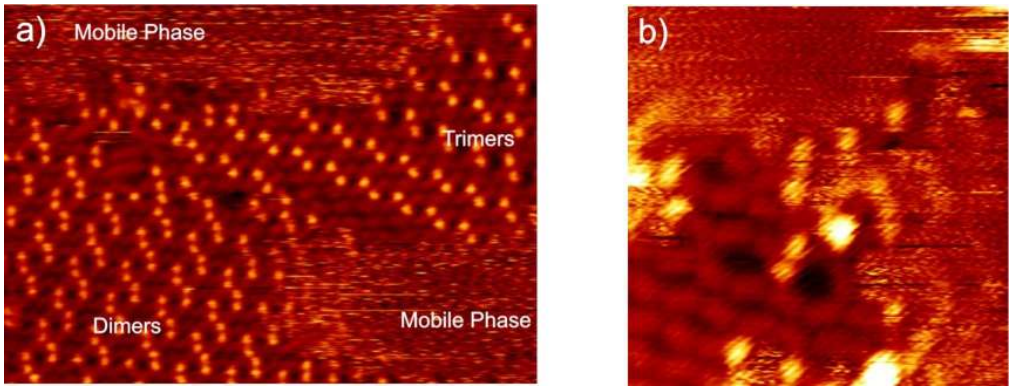

Figure 3.4. a) STM image of dimeric and trimeric structures on Ag(111) after annealing the sample at 160°C (24.9x17.8 nm^2, -1.9V, 20 pA, RT). b) Long chains obtained after annealing the sample at 168°C (10x10 nm^2, -1.9 V, 20 pA, RT).

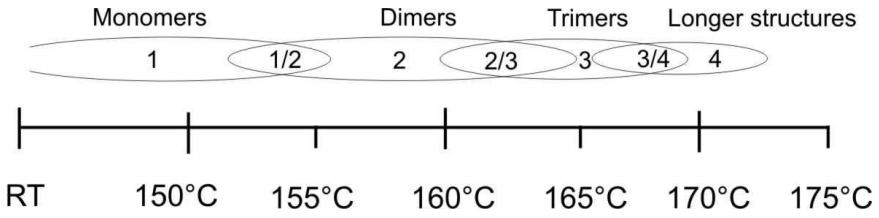

Figure 3.5. A scheme summarizing the relationship between the temperature and the formation of different structures on Ag(111). In the overlap points of the ellipses, coexistence of the different structures is observed on the surface.

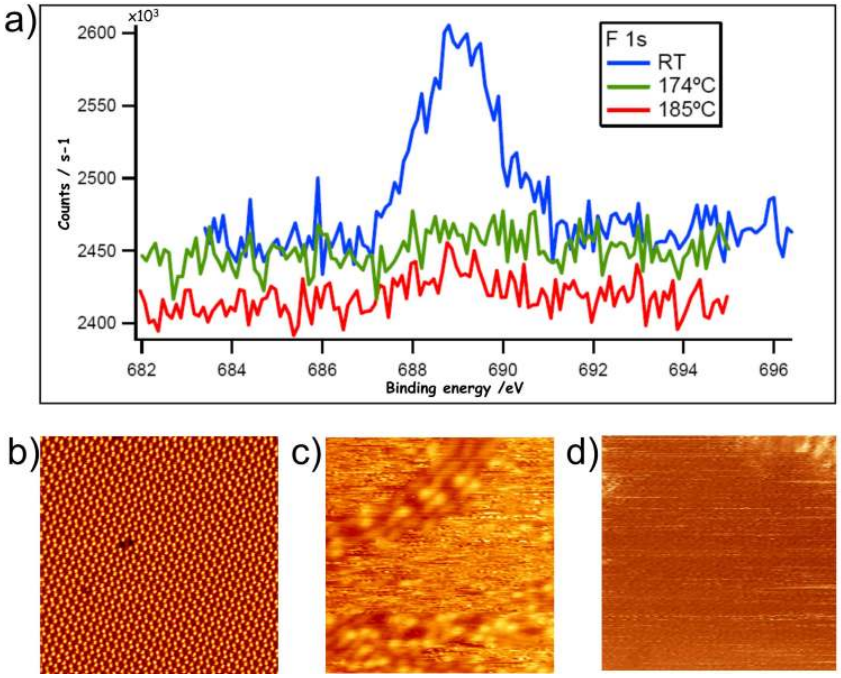

Figure 3.6. a) F1s XPS spectra of biphenyl **2** on Ag(111) obtained at the ordered phase (RT, blue curve) at the intermediate phase (174°C, green curve) and at the mobile phase (185°C, red curve). STM images of the b) ordered phase (30x30 nm^2, 1.78 V, 20 pA, RT), c) intermediate phase (10x10 nm^2, 1.78 V, 20 pA, RT) and d) the mobile phase (20x20 nm^2, 2 V, 20 pA, RT).

Comparing the STM signature of the resulting product to the structures found previously for a similar compound (biphenyl **1)** under similar conditions (section 3.1**)**, we attribute all interlinks to covalent bonds and the linking units to azo linkers.[22-23]

To obtain spectroscopic confirmation that the surface reaction occurred and the fluorinated Boc groups desorbed from the surface, we performed XPS studies on Ag(111) before and after annealing the sample at different temperatures (figure 3.6). The F1s peak observed at room temperature arising from the fluorine atoms at E= 689.4 eV is not observed after annealing the sample at higher temperatures. As a result, we conclude from our XPS experiments that desorption of the fluorinated Boc groups takes place in the temperature range in which coupling occurs.

3.2.2 Cu (111):

Deposition of biphenyl **2** on Cu(111) leads to the assembly of molecules in a parallel arrangement (figure 3.7a) as the structure obtained from biphenyl **1** presented in section 3.1. The unit cell exhibits the same parameters (12.75 Å x 9.8 Å; Θ=75.5°). However, biphenyl **2** molecules interact with each other via halogen bonds in addition to the C-H…O bonds as proposed on the Ag(111) surface. The proposed molecular model is illustrated in figure 3.7b.

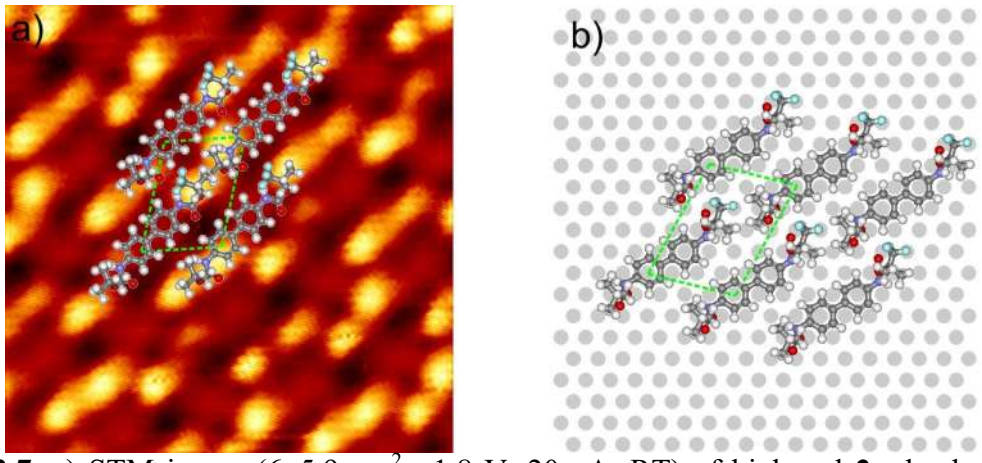

Figure 3.7. a) STM image (6x5.9 nm^2, -1.8 V, 20 pA, RT) of biphenyl **2** adsorbed on Cu(111) and b) the tentative molecular model.

The arrangement is stable up to ~145°C. Above this temperature, a new periodic pattern emerges. This pattern consists of molecular rods which are about twice the length of the initial biphenyl **2** rod: Namely, dimeric structures are formed through ligation of the N functions of the molecules to the N functions of the neighbouring molecules after releasing the fluorinated Boc groups. The STM image of the dimeric structure is shown in figure 3.8a in which the unit cell and two molecules revealing their arrangements are inserted. Similar to the parallel arrangement obtained before annealing, these perfectly organized rows of dimers are consistent with our previous findings, as well. The dimeric arrangement is the same as the one obtained from biphenyl **1** after annealing at elevated temperatures. Increasing the annealing temperature of the same sample in steps reveals that the dimeric pattern is stable in a temperature range of ~150-180°C. The unit cell size is (25.6x18.3) $Å^2$ with an angle of 73°. Each pair of dimers is held together by two hydrogen bonds between the carbonyl oxygen and the hydrogen atoms of the biphenyl

core of neighbouring molecules.

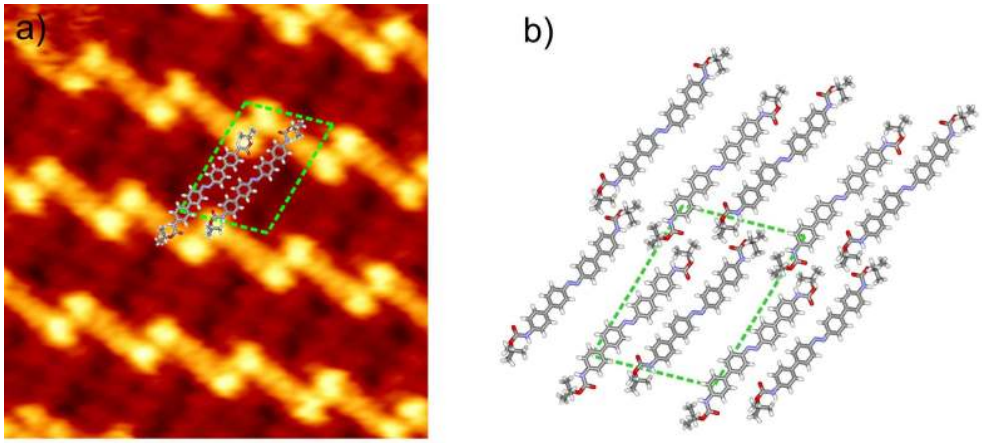

Figure 3.8. a) STM image (8x8 nm^2; -1.95 V, 19 pA, RT) of the dimeric structures consisting of interlinked biphenyl units formed after the sample was annealed at 150 °C and b) the tentative model which represents the arrangement of the molecules.

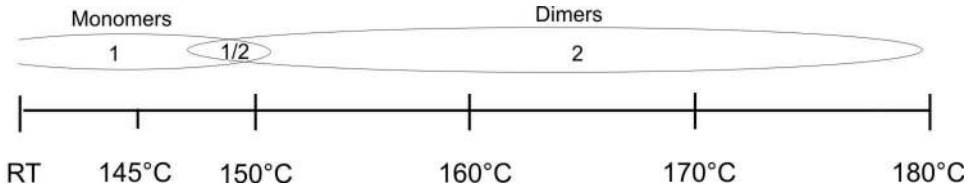

Figure 3.9. A scheme summarizing the relationship between the temperature and the formation of different structures on Cu(111).

On Cu(111), longer than dimeric structures are not observed. In a scheme in figure 3.9, the correlation between the formation of different structures and the temperature is summarized.

In summary, we have shown that a selective cleavage of Boc protecting groups can be achieved by their modification. By an appropriate choice of the annealing temperature, the length of the interconnected structures can be tuned. However, the molecule-substrate interactions have to be taken into account since the length of the polymeric structures differs depending on the substrate. The reason could be either the different catalytical behavior of the Ag and the Cu substrates or different diffusion rates of the molecules on these substrates.

3.3 Heat induced coupling of an asymmetric biphenyl derivative on metal surfaces

The concept of heat induced interlinking of functional units from pre-organized molecular building blocks studied in section 3.1 and 3.2 is applied here to an asymmetric molecule, biphenyl **3** (see figure 2.9), to get a complete understanding about the self-assembly and the interlinking mechanism of different biphenyl units on Ag(111) and Cu(111).

3.3.1 Ag(111)

The deposition of ~0.15 ML of biphenyl **3** on Ag(111) results in the formation of predominantly chain like structures which coexist with flower like structures. The STM image displayed in figure 3.10 shows an overview of the structures which are uniformly distributed over the surface.

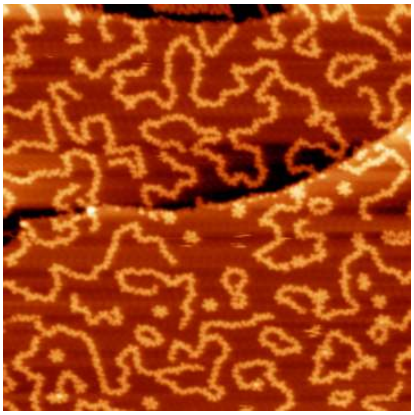

Figure 3.10. Overview STM image of the molecular chains and flowers of biphenyl **3** on Ag(111) formed at low coverage. The structures are uniformly distributed over the Ag(111) terraces (100x100 nm^2, 1.8 V, 20 pA, 77 K).

In high resolution STM images submolecular features can be resolved. Assigning the bright lobes to the tert-butyl groups and the less bright feature between two lobes to the molecular backbone of biphenyl **3**, it can clearly be identified that each flower-like structure consists of 6 molecules revealing a six-fold symmetry: a hexamer. This structure has a side of length a= (10.1±0.5) Å. An STM image of an individual hexamer and the tentative molecular model are shown in figure 3.11a and 3.11b, respectively. To enable intermolecular interactions in a circular arrangement to form such a hexamer, the two carbonyl oxygen atoms of each monomer point to the opposite directions of its molecular backbone. Consequently, the structure is stabilized by 12 H-bonds which arise between carbonyl oxygen and phenyl hydrogen atoms of neighboring molecules. The lengths of the H-bonds arising in the inner and the outer parts of the structure are measured to be ~2.3 Å and ~2.6 Å, respectively.

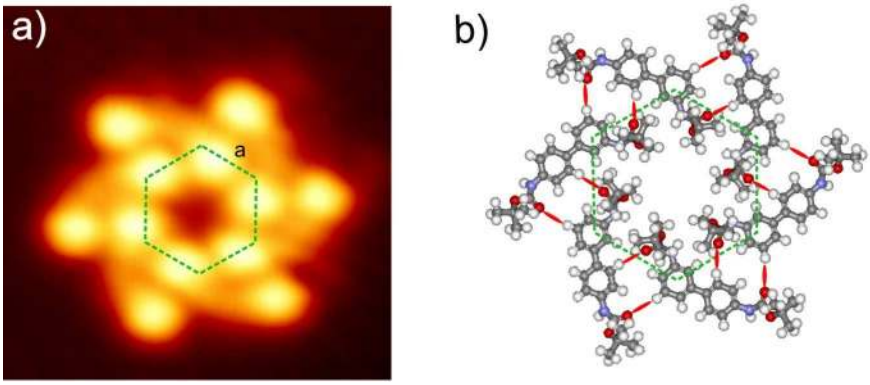

Figure 3.11. a) Closeup view of a hexamer of biphenyl **3** on Ag(111) (4.7x4.7 nm^2, -1.57 V, 20 pA, 77 K) showing submolecular features. It consists of 6 molecules. b) The tentative molecular model. H-bonds are shown with red lines.

The molecular chains at this low coverage (0.15 ML) are distributed randomly on the surface and exhibit no influence of the underlying silver substrate onto their arrangement. They are mainly formed by rows of molecules in which single molecules have different appearances due to the different rotational directions of the Boc groups, i.e., Boc groups are sometimes on the same side or at different sides of the molecular backbone of the single molecules. The zoomed image of such supramolecular chains displayed in figure 3.12 resolves the individual molecules, in which different appearances of the molecules in a molecular row are marked as a guide to the eye.

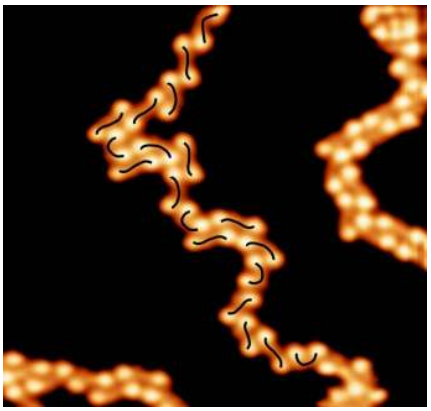

Figure 3.12. STM image showing **s**ingle molecular rows of biphenyl **3** on Ag(111). The molecules are randomly oriented with different molecular conformations (15x14 nm^2, -1.57 V, 20 pA, 77 K).

Upon increasing the coverage of biphenyl **3** to 0.5 ML, we observe chains formed by double rows (two single molecular rows lying parallel to each other). In contrast to the random arrangement and different appearances of the molecules within single rows at lower coverage, the molecules are well-arranged and have the same appearance inside double rows. The carbonyl oxygen atoms of each molecule point to the same direction with respect to their molecular backbone and within the double row arrangement neighboring molecules are rotated by 180° with respect to each other in order to enable the molecules to face each other with their functional groups. Consequently, H-bonding

interactions between carbonyl oxygen atoms of one molecule in the first row and the phenyl hydrogen atoms of the molecule in the neighboring row form the observed molecular double row. In the STM image in figure 3.13a, a few molecules are superimposed in a double row (indicated with a yellow arrow) to illustrate their arrangement. In figure 3.13b, the tentative model of the double row is shown.

Such a double row can be considered as the building block for the formation of the densely-packed arrangement at coverages above 0.5 ML. Namely, double rows pack in a parallel fashion at increasing coverage to evolve into the densely-packed arrangement. This result can clearly be deduced by a detailed analysis of the STM images. For example, the arrangement pointed out with the blue arrow in figure 3.13a is formed by two parallel double rows indicating that larger islands originate from the double rows.

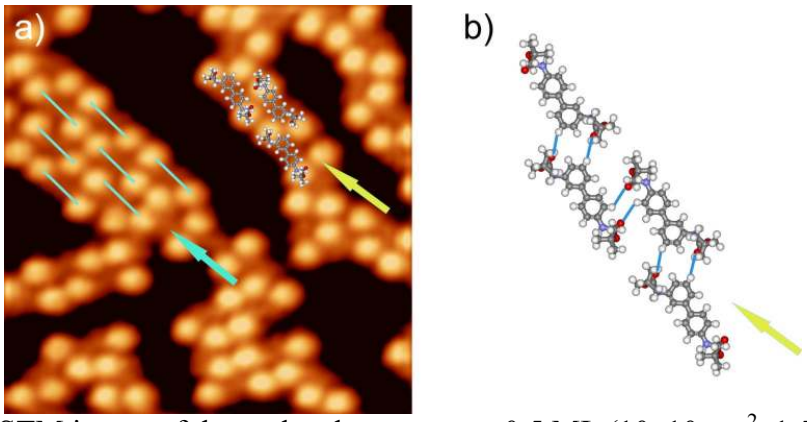

Figure 3.13. a) STM image of the molecular pattern at 0.5 ML (10x10 nm^2, 1.57 V, 20 pA, 77 K). Evolution of the densely packed arrangement starts with the formation of double rows (building block). A few molecules are inserted in the double row shown with a yellow arrow. The arrangement shown with a blue arrow is formed by the packing of two double rows and is a close-packed parallel arrangement which evolves into bigger domains at higher coverage. b) Tentative molecular model of the double row. The H-bonds are marked by blue lines.

When the coverage is increased to 0.85 ML, most of the areas covered by biphenyl **3** consist of double row arrangement, as can be seen in the STM image in figure 3.14a. The unit cell size is obtained by the analysis of several STM images and has sides of lengths (15.2±0.5) Å and (20.2±0.6) Å, and an internal angle of (70±1)°. Figure 3.14b shows a closeup view of the arrangement together with the unit cell. In the schematic representation of the parallel arrangement (figure 3.14c), the double row highlighted in red represents a building block. It is stabilized by hydrogen bonds and repetition of the double rows leads to the observed arrangement. The arrangement exhibits a surface density of 0.65 molecules/nm^2.

At room temperature, the chains and the hexamers are not stable and only a mobile phase is observed at low coverage. This indicates weak intermolecular interactions. Only close to the saturation coverage, the parallel close-packed arrangement is observed.

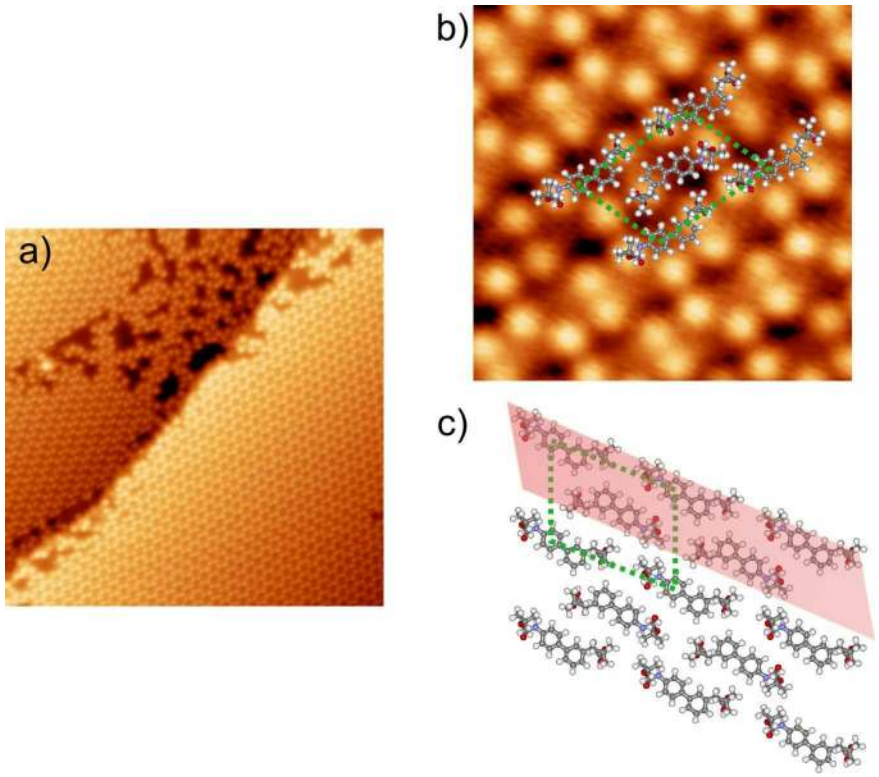

Figure 3.14. a) Overview of the close-packed parallel arrangement of biphenyl **3** on the Ag(111) surface (40x40 nm^2, 1.2 V, 20 pA, 77 K). b) Zoomed view of the arrangement (5.7x5.7 nm^2, 1.3V, 20 pA, 77 K). The molecules in the unit cell are superimposed in the STM image to illustrate their arrangement. c) Schematic representation of the arrangement in which the double molecular row is highlighted in a red stripe.

To induce intermolecular reactions within the self-assembled monolayers of biphenyl **3**, temperature is exploited as a trigger for deprotection, as in the previous cases (biphenyl **1** and **2**). The temperature is increased step-by-step on the same sample. Heating cycles at the elevated temperature are of 2-3 minutes each time. Annealing the samples enables the cleavage of the Boc groups which results in interlinking of pre-organized molecular building blocks into longer structures.

Upon annealing the sample at 155°C, new structures are observed which appear as dark and long single rows within the close-packed arrangement as well as at the border of the arrangement with the mobile phase (figure 3.15a). Having a close look (figure 3.15b), it is clearly seen that the number of bright dots which correspond to the Boc groups is reduced along these rows indicating an interlinking of monomers into longer structures. Along the row at the border (indicated by a blue arrow), a monomer lies next to a longer structure which has twice the length of a monomer, and thus corresponds to a dimer. However, the row inside the network is formed exclusively from the dimers that are rotated by 180° with respect to the neighboring one. A few monomers and dimers are marked along the rows at the border and inside the network in figure 3.15b in order to illustrate their arrangement. These observations can be explained as follows.

The annealing process activates the monomers and due to the release of the Boc groups in para positions, a dimer can be formed. The Boc groups in para position are splitt off easier than the ones in meta position which is due to the electron distribution within the molecule. When two of these activated monomers meet, they interlink through an azo linker into a dimer which has two terminal Boc groups in meta position.

From the STM image in figure 3.15a, it can be seen that the molecular arrangement is influenced by the Ag substrate. The angle between the domains amounts to 120° which coincides with the angle measured between the principal directions of the Ag(111) substrate.

Upon slightly increasing the annealing temperature (161°C), more monomers loose their Boc groups in para positions and the interlinked dimers form extended islands (figure 3.16a). A closeup view of the self-assembled dimer arrangement is shown in figure 3.16b. The Boc groups and the molecular cores can clearly be resolved. The unit cell and the arrangement of the dimers are illustrated in the molecular model in figure 3.16c. The unit cell has vector sizes of (12.7±0.6) Å and (31.7±0.5) Å with an angle of 84° in between. Each dimer interact with a neighboring one via H-bonding interactions between the carbonyl oxygen and the H-N groups at one side and an H-bonding interaction between the carbonyl oxygen and a phenyl hydrogen atom on the other side.

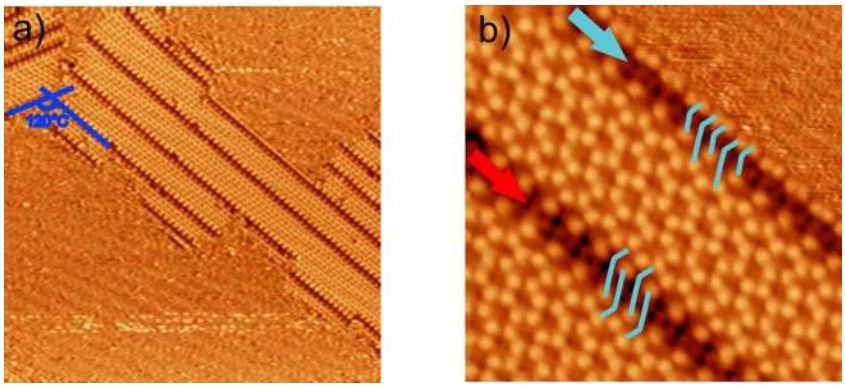

Figure 3.15. a) STM image of biphenyl **3** on Ag(111) annealed at 155°C (80x80 nm^2, -1.94 V, 20 pA, RT). The structures follow the principle directions of the underlying Ag(111) substrate. b) Zoomed view in which some monomers and dimers at the borders (red arrow) and some dimers inside the network (blue arrow) are marked with blue lines (15x15 nm^2, -1.94 V, 20 pA, RT).

Upon annealing at higher temperatures (168°C), the dimers react further and evolve into longer structures. A dimer looses one of its Boc groups in meta position and interlinking to another monomer which looses a Boc group in para position happens. This interlinking results in a longer structure: a trimer. In figure 3.17a and b, an STM image of the trimeric arrangement and its tentative molecular model are shown, respectively. As obtained from the analysis of several STM images, the unit cell parameters were determined to (13.2±0.6) Å and (39.7±0.7) Å with an angle of (83±1.5)°.

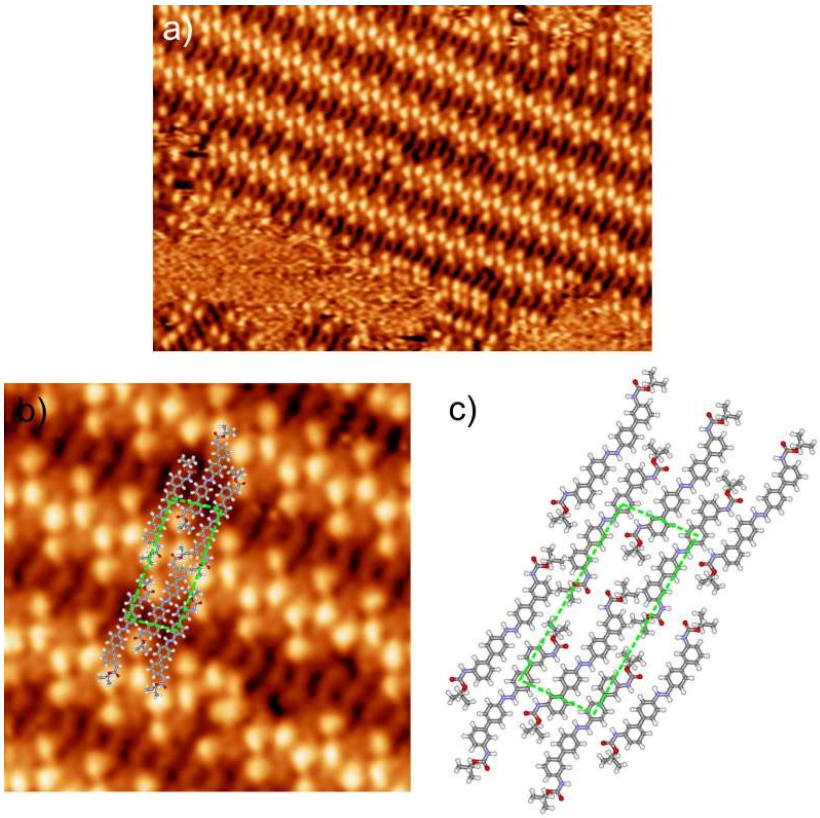

Figure 3.16. a) STM image of biphenyl **3** on Ag(111) annealed at 161°C revealing extended densely packed dimeric islands (29.8x20.8 nm^2, -1.9 V, 20 pA, RT). b) Closeup view of the structure showing the dimers with submolecular resolution. The molecules within the unit cell are superimposed in the STM image to show their arrangements (10x10nm^2, -1.9V, 20pA, RT). c) The tentative molecular model.

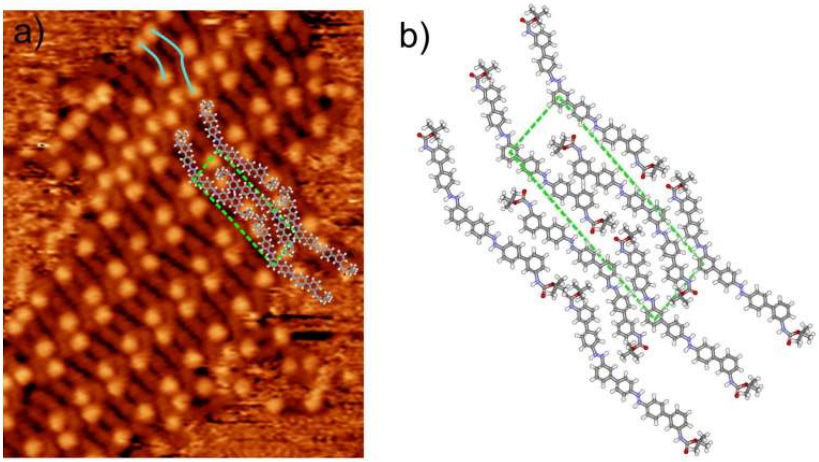

Figure 3.17. a) STM image of the trimeric structure (13.6x16.8 nm^2, -1.9 V, 20 pA, RT) formed after annealing the sample at 168°C. Close to the borders monomers and dimers can be observed simultaneously (marked in blue). b) Tentative molecular model of the trimeric arrangement.

Another appealing feature is the finding of monomers, dimers and trimers simultaneously on a well-ordered island. In figure 3.17a, a monomer and a dimer which coexist at the border of an island of trimeric structures are marked in blue. Similar dimeric and trimeric structures were previously obtained after annealing the self-assembled monolayers of biphenyl **1** (section 3.1) and **2** (section 3.2). However, the dimeric pattern obtained after deprotection of biphenyl **3** exhibits a different appearance in the STM images due to the asymmetric shape of the molecule.

3.3.2 Cu(111):

Compared to the curled and disordered chains in which the molecules exhibit different molecular appearances (Boc groups rotate freely around the molecular backbone) at low coverage on Ag(111), the molecules on Cu(111) organize mainly into double rows (building block) in which they are arranged in a parallel fashion with the same appearance. In order to form such straight double rows Boc groups of the neighboring molecules face each other. However, at the kink points which change the direction of the chains, the position of the Boc groups with respect to the molecular backbone might be different compared to the position of the Boc groups forming the straight double rows. Apart from this observation, the hexamers are found to exist more frequently on the Cu(111) surface. The STM image in figure 3.18a shows both structures formed at a coverage of 0.35 ML of biphenyl **3**. The zoomed view of the area marked by the dashed frame in this image is shown in figure 3.18b. Individual molecules within a double row are marked to illustrate their arrangement.

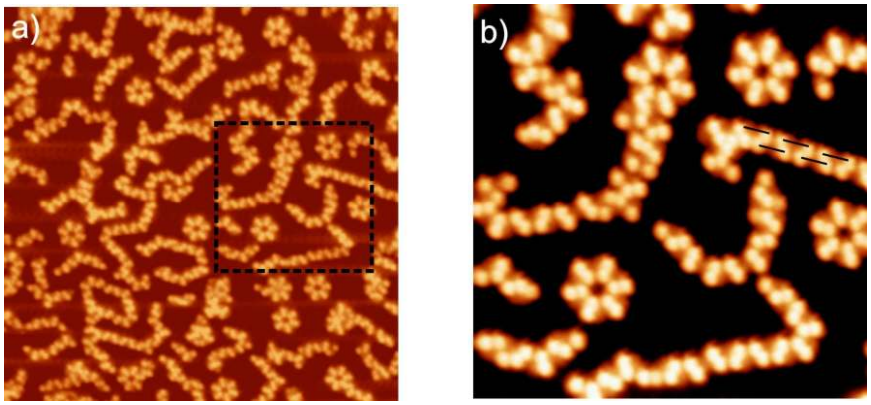

Figure 3.18. a) STM image of biphenyl **3** on Cu(111) at 0.35 ML. Chains and hexamers (50x50 nm^2, 1.1 V, 20 pA, 77 K). b) Zoomed view of the area indicated with a dashed frame in (a) (20x20 nm^2, 1.5 V, 20 pA, 77 K). A few molecules are marked by black lines to show their arrangement within the double row.

An interesting property of the self-assembly of biphenyl **3** into hexamers is found upon further evaluation. Even though the submolecular features cannot always be resolved in the STM images, by displaying the contours of the structures, more information can be gained. The STM image in figure 3.19a displays the contours of two hexamers which lie next to each other on the surface. The orientation of the outer lines of

the two structures reveals that the molecules in the left hexamer are rotated clockwise with respect to the molecules in the right hexamer which are rotated in the opposite direction. This clockwise and counterclockwise adsorption preference of the molecules introduces a chiral signature of the hexameric structures. For the right and left handed hexamers shown in the STM image in figure 3.19b (same image in figure 3.19a, but in a normal contrast), the rotational directions of the molecules are marked.

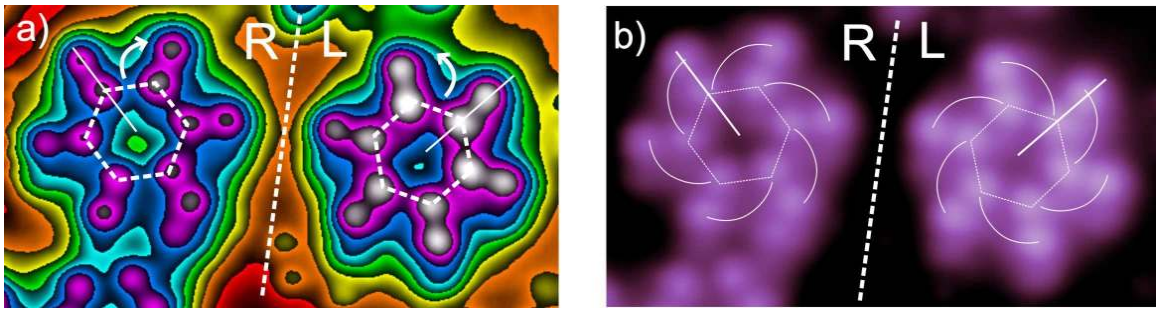

Figure 3.19. a) STM image of two mirror image hexamers displayed in all colors in order to enhance the submolecular contrast. b) The same STM image as in (a) but with "normal" contrast (8.5x4.7 nm^2, 1.58 V, 20 pA, 77 K).

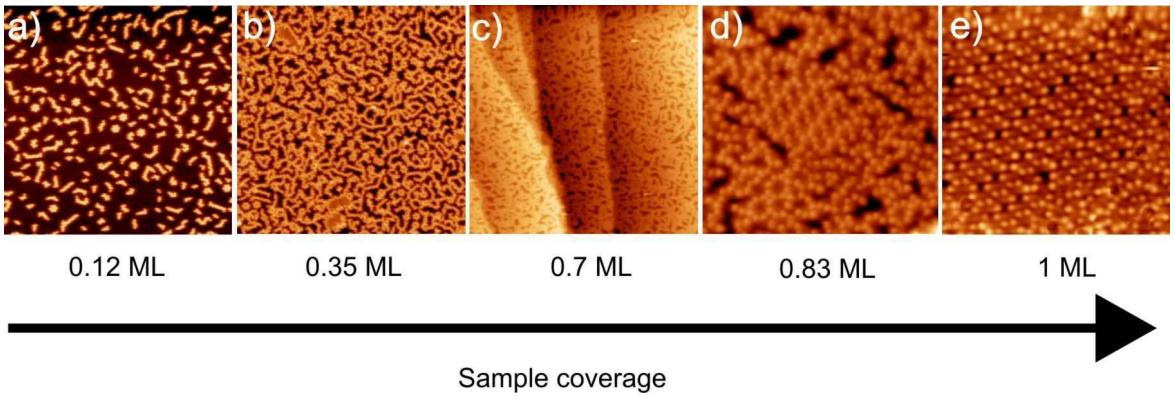

Figure 3.20. STM image showing the coverage dependent growth of self-assembled structures of biphenyl **3** on Cu(111) obtained by adding molecules in a consecutive manner. a) Randomly distributed short chains (mainly double rows) and hexamers (100x100 nm^2, 1.65 V, 20 pA, 77 K). b) and c) densely distributed supramolecular chains and hexamers at increased coverage (100x100 nm^2, 1.65 V, 20 pA, 77 K). The number and lengths of the chains as well as the number of hexamers increase. d) and e) Small self-assembled islands surrounded by a disordered phase for a coverage of ~0.8 ML and higher (19x18 nm^2, 1.6 V, 20 pA, 77 K (d); 15x15 nm^2, -1.26 V, 20 pA, 77 K (e)). Non-periodic structures are dominant at high coverages.

The growth mechanism of supramolecular structures formed from biphenyl **3** as a function of coverage on Cu(111) differs compared to the growth mechanism on Ag(111). At low coverage, as mentioned above, the chains exhibit a better ordering and the hexamers are formed more dominantly on Cu(111). On Ag(111), the molecules start to

form the parallel arrangement even at low molecular densities (~0.4 ML) and the domain size increases with increasing coverage until all terraces are completely filled. On the contrary, biphenyl **3** prefers to form only the chains mainly composed of double rows or the hexameric structures on Cu(111) until all the free area between these structures are filled. This results in a random distribution of the chains for coverages close to a ML. In figure 3.20, a series of STM images presenting the coverage dependent growth of biphenyl **3** on Cu(111) is shown. While only randomly distributed chains and hexamers exist on the surface for coverages below 0.8 ML, the surface structure is mainly a disordered close-packed phase above this molecular density. Only just above 0.8 ML, as seen in figure 3.20d and 3.20e, tiny patches of well-ordered islands between the disordered phases can be observed. This well-ordered structure is shown in a zoomed STM image in figure 3.21a. A close look reveals that the molecules interact with each other dominantly in a parallel manner by H-bonding interactions between carbonyl oxygen and phenyl hydrogen atoms of neighboring molecules whereas a herringbone arrangement can be observed at some regions. The tentative molecular model for the parallel arrangement illustrated in figure 3.21b is inserted in the STM image in figure 3.21a. The unit cell has sides of length (14.8 ±0.6) Å and (23.8±0.7) Å, and an internal angle of (68±2)°. In the upper part of the STM image the herringbone arrangement of the molecules is illustrated by black lines.

Similar to the previous cases, temperature is used to interlink the monomers into longer structures. Cleavage of Boc groups and coupling of the molecules are observed to occur but no ordered interlinked structures are found on Cu(111) with this asymmetric molecule. Figure 3.22 displays such structures formed after annealing the sample at 160°C.

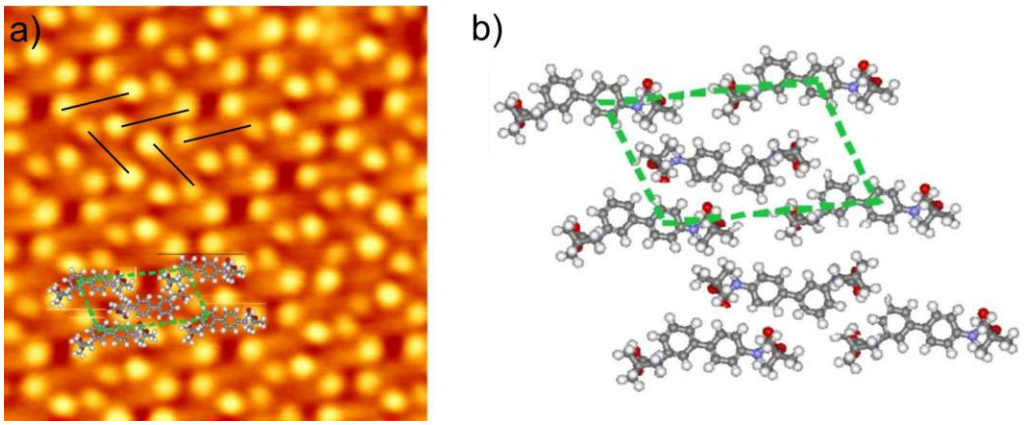

Figure 3.21. a) STM image of the parallel arrangement in which the unit cell and a few molecules are inserted to illustrate their arrangement (10x10 nm^2, -1.26 V, 20 pA, 77 K). Besides this structure, rarely a herringbone arrangement of the molecules can be observed, which is illustrated with black lines inside the network. b) Tentative molecular model of the close-packed parallel arragement.

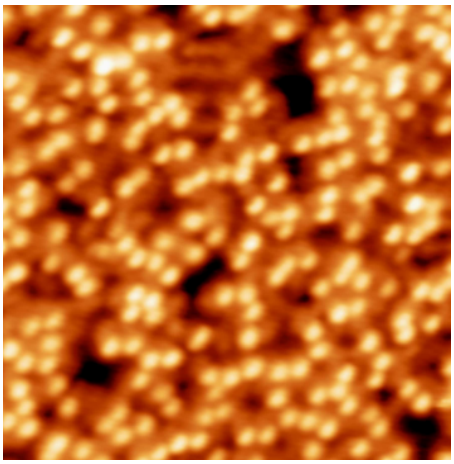

Figure 3.22. STM image of the sample after annealed at 160°C (12.7x12.8 nm^2, 1.5 V, 20 pA, 77 K). Some interlinking is observed but there is no ordering of the structures.

In summary, we have shown that a selective cleavage of Boc protecting groups can be achieved by playing with the position of the Boc group. However, the role of the substrate on the formation of the polymeric structures has to be taken into account since the experimental results performed under similar conditions for the same molecule differ depending on the substrate.

References 3

[1] J. M. Lehn, Supramolecular chemistry: concepts and perspectives, Wiley-VCH, Weinheim (**1995**).

[2] S. De Feyter, F. C. De Schryver, Chem. Soc. Rev. 32, 139 (**2003**).

[3] J. V. Barth, Annu. Rev. Phys. Chem. 58, 375 (**2007**).

[4] N. Lin, A. Dmitriev, J. Weckesser, J. V. Barth, K. Kern, Angew. Chem. 114, 4973 (2002); Angew. Chem. Int. Ed. 41, 4779 (**2002**).

[5] S. Stepanow, M. Lingenfelder, A. Dmitriev, H. Spillmann, E. Delvigne, N. Lin, X. Deng, C. Cai, J. V. Barth, K. Kern, Nat. Mater. 3, 229 (**2004**).

[6] J. A. Theobald, N. S. Oxtoby, M. A. Phillips, N. R. Champness, P. H. Beton, Nature 424, 1029 (2003).

[7] M. De Wild, S. Berner, H. Suzuki, H. Yanagi, D. Schlettwein, S. Ivan, A. Baratoff, H.J. Güntherodt, T. A. Jung, ChemPhysChem 3, 881 (**2002**).

[8] H. Ozaki, T. Funaki, Y. Mazaki, S. Masuda, Y. Harada, J. Am. Chem. Soc. 117, 5596 (**1995**).

[9] S. W. Hla, L. Bartels, G. Meyer, K. H. Rieder, Phys. Rev. Lett. 85, 2777 (**2000**).

[10] Y. Okawa, M. Aono, Nature 409, 683 (**2001**).

[11] A. Miura, S. De Feyter,M. M. S. Abdel-Mottaleb, A. Gesquiere, P. C. M. Grim, G. Moessner, M. Sieffert, M. Klapper, K. Mullen, F. C. De Schryver, Langmuir 19, 6474. (**2003**).

[12] J. Barner, F. Mallwitz, L. Shu, A. D. Schlüter, J. P. Rabe, Angew. Chem. 115, 1976 (**2003**); Angew. Chem. Int. Ed. 42, 1932 (**2003**).

[13] L. Grill, M. Dyer, L. Lafferentz, M. Persson, M. V. Peters, S. Hecht, Nat. Nanotechnol. 2, 687 (**2007**).

[14] a) S. Weigelt, C. Busse, C. Bombis, M. M. Knudsen, K. V. Gothelf, T. Strunskus, C. Wöll, M. Dahlbom, B. Hammer, E. Laegsgaard, F. Besenbacher, T. R. Linderoth, Angew. Chem. 119, 9387 (**2007**); Angew. Chem. Int. Ed. 46, 9227 (**2007**); b) S. Weigelt, C. Busse, C. Bombis, M. M. Knudsen, K. V. Gothelf, E. Laegsgaard, F. Besenbacher, T. R. Linderoth, Angew. Chem. 120, 4478 (**2008**); Angew. Chem. Int. Ed. 47, 4406 (**2008**).

[15] M. Matena, T. Riehm, M. Stöhr, T. A. Jung, L. H. Gade, Angew. Chem., 120, 2448 (**2008**); Angew. Chem. Int. Ed. 47, 2414 (**2008**).

[16] M. In`t Veld, P. Iavicoli, S. Haq, D. B. Amabilino, R. Raval, Chem. Commun. 1536 (**2008**).

[17] a) N. A. A. Zwaneveld, R. Pawlak, M. Abel, D. Catalin, D. Gigmes, D. Bertin, L. Porte, J. Am. Chem. Soc. 130, 6678 (2008); b) M. Treier, N. V. Richardson, R. Fasel, J. Am. Chem. Soc. 130, 14054 (**2008**).

[18] P. G. M. Wuts, T.W. Greene in Greene`s Protective Groups in Organic Synthesis, 4th ed., Wiley, Hoboken, NJ (**2007**).

[19] P. J. Kocienski in Protecting Groups, 3rd ed., Thieme, Stuttgart (**2005**).

[20] F. Moresco, G. Meyer, K.-H. Rieder, J. Ping, H. Tang, C. Joachim, Surf. Sci. 499, 94 (**2002**).

[21] T. A. Jung, R. R. Schlittler, G. K. Gimzewski, Nature 386, 696 (**1997**).

[22] J. Henzl, M. Mehlhorn, H. Gawronski, K. H. Rieder, K. Morgenstern, Angew. Chem. 2006, 118, 617; Angew. Chem. Int. Ed. 45, 603 (**2006**).

[23] M. J. Comstock, N. Levy, A. Kirakosian, J. Cho, F. Lauterwasser, J. H. Harvey, D. A. Strubbe, J. M. J. Frechet, D. Trauner, S. G. Louie, M. F. Crommie, Phys. Rev. Lett. 99 038301 (**2007**).

[24] S. Weigelt, C. Busse, L. Petersen, E. Rauls, B. Hammer, K. V. Gothelf, F. Besenbacher, T. R. Linderoth, Nat. Mater. 5, 112 (**2006**).

[25] S. Berner, M. Brunner, L. Ramoino, H. Suzuki, H.-J. Güntherodt, T. A. Jung, Chem. Phys. Lett. 348, 175 (**2001**).

[26] See the Supporting Information.

[27] 1 self-assembles in a herringbone structure on Ag(111) and the formation of polymers has been observed upon annealing at 2008C. These experiments are described in detail in the Supporting Information.

[28] K. E. Riley, K.M. Merz, J. Phy. Chem. A 111**,** 1688**-**1694 (**2007**).

[29] J.A.K. Howard, V.J. Hoy, D.O. Hagan et al., Tetrahedron 52**,** 12613-12622 (**1996**).

[30] L. Shimoni, J.P. Glusker, Struct. Chem. 5**,** 383-397 (**1994**).

[31] V. Oison, M. Koudia, M. Abel et al. Phy. Rev. B 75**,** Article Number: 035428 **(2007**).

[32] E. Salomon, Q. Zhang, S. Barlow et al., J. Phy. Chem C, 112**,** 9803-9807 (**2008**).

SI

[SI-1] Y. Basel, A. Hassner, J. Org. Chem**.** 65, 6368 (**2000**).

[SI-2] A. M. Brown, M. V. Ovchinnikov, C. L. Stern, C. A. Mirkin, J. Am. Chem. Soc. 126, 14316 (**2004**).

[SI-3] Barman D. C., Saikia P., Prajapati D., Sandhu J. S. Heterogeneous permanganate oxidations. A novel method for deamination reactions using solid supported iron-permanganate. Synth. Commun. 32: 3407-3412 (**2002**).

[SI-4] George S., Nangia A. N,N'-Bis(4-biphenyl)urea. Acta Cryst. E59: o901-o902 (2003).

4 Control of chirality in 2D structures by the chirality of their building blocks: Cyano helicene on Cu(111)

In this section the self-assembly of enantiopure (**P4**) as well as racemic 6,13-dicyano-[7]-helicene (figure 2.10) on Cu(111) is studied, predominantly by STM. Two different phenomena are observed: 1) the self organization and layering of cyano helicene, as it derives from the cyano functionalisation and the particular surface-molecular interaction, and 2) the phase behaviour of ad-surface molecular layers of cyano helicene at close to monolayer coverages.

In the first subsection, low temperature STM measurements obtained for different coverages are discussed. With increasing coverage, the enantiopure molecules form 1D molecular chains, tetrameric and well-ordered dimeric structures. Interestingly a unique "upright standing" configuration of molecular chains is observed in addition to the different network patterns. Moreover, a transfer of the chirality of the molecules to the self-assembled structures occurred at higher coverages.

Upon adsorption of the racemic mixture on Cu(111), with increasing coverage, chains, tetramers and dimers are observed as it is the case for enantiopure molecules. However, these structures co-exist in mirror domains on the surface in the racemic case.

In the second subsection, an interesting phase behaviour for **P4** observed at room temperature on the Cu(111) substrate are presented. At low coverages, the molecules exhibit a mobile phase whereas upon increasing the coverage (0.7 ML), a metastable nanoporous network is observed in coexistence with the mobile phase, thereby suggesting a thermodynamic equilibrium. Re-investigation of the sample after 12 hours showed that a slow transition of this surface phase occurred: The terraces on the Cu sample were either covered by the dimeric phase or by a mobile phase. Possible reasons for the observation of co-existing phases and the observed transitions are presented.

In the following, we briefly discuss the choice of cyano helicene which resulted from the groups experience with cyano functionalisation of porphyrins impacting their self-assembly and the prominent earlier literature on helicene derivatives: Nakamura et al. studied for the first time the self-assembly behavior of [7]thiahelicene molecules on surfaces by STM under HV conditions.[1] Subsequently, Taniguchi et al. studied thia [11]heterohelicenes on Au(111) under UHV conditions.[2] More recently, Ernst and

coworkers were the first to introduce a pure [7]-helicene system on surfaces[3] and to study it by STM.[4,5] Building upon this molecular backbone we have attached two opposed cyano side groups to the [7]-helicene core in position 6 and 13 (figure 2.10).

4.1 Low temperature measurements

4.1.1 Enantiopure cyano helicene

Upon deposition of **P4** on a Cu(111) surface, for coverages below 0.4 ML, domains of parallel 1D chains are formed, which exhibit an angle of ~20° with the principle directions of the underlying copper substrate as depicted in figure 4.1a. Each molecule is identified by one lobe in the STM data. Even in high resolution STM images the intramolecular structure cannot be resolved. This makes it impossible to determine the helicity of the individual molecules in this phase. Based on geometric considerations, helicenes as three-dimensional objects may take two different configurations upon their adsorption on surfaces: an “upright standing” and a “flat-lying (parallel to the substrate with their π-system)” configuration. The latter configuration which allows the identification of chirality for individual helicenes is expected to be predominant due to the considerable interaction expected between the delocalised π-system of the molecules and the metallic substrate surface. This expectation is consistent with the earlier reports of helicenes which were predominantly found to adsorb in the co-planar configuration on metal surfaces.[2,4-6] In only one publication a tilted local adsorption geometry by (43 ± 5°) from the surface for a P-[7]H on Ni(100) is described for a saturated monolayer. The reported angle has been derived from NEXAFS measurements.[7]

The fact that the intramolecular structure and thus the enantiomeric discrimination of the individually adsorbed molecules can not be identified even in high resolution STM images of our data suggests a non-planar adsorption geometry. This assignment is further supported by the STM cross-section analysis of the molecular chains in comparison to the literature.[4-6] On the basis of this assessment, a tentative first model for the chain structure in "standing” configuration of the helicenes is proposed in the inset of figure 4.1a (side view). The wealth of experience with cyano substituent driven self-assemblies of porphyrins[8-11] suggests that the cyano groups are involved in the binding and are therefore oriented parallel to the chain direction. The observed preferred orientation of the chains implies that the substrate molecular interaction is also influencing the formation of the chains. Interestingly, the chains are not aligned with the symmetry axes of the substrate as they are indicated in figure 4.1a. In the contrary, the chains are oriented at an estimated angle of -20 degrees. Note that the contrary orientation +20 degrees is not observed. This implies that upon deposition of the other helicity compound the alternate alignment shall be found and that the binding site of the chains to the substrate is chirally selective. Chains formed from the racemate could be expected to align with both directions after partial segregation of the two helicities.

By superimposing the model demonstrated in figure 4.1a (inset) on the STM image in figure 4.1b, we can further develop the assumed model situation for two binding motifs observed: The linear chain link (blue circle), and the symmetric node connecting three

chain arms (red circle). The linear chain link would be consistent with an antiparallel arrangement of cyano dipole-cyano dipole interactions assisted by C-H…N hydrogen bonds (blue circle). In this arrangement the dipoles are clearly antiparallel and the C-H...N hydrogen bonds are linear which makes this bonding motif most stable. Such interactions were previously observed in the self-assembly of benzonitriles,[12] of CNN derivatives,[13] of TCBDs in organic crystals, [14] and recently of tetraarylporphyrins.[15] From the STM data the distance between two neighboring molecules in the linear chains is estimated to approximately 14 Å which would result in an estimated distance of the C-H…N bond of approximately 4 Å. This estimated bond distance from the data, however is significantly larger than the typical length of a H-bond of ~ 2.3 Å taken from the literature and from the above cited references. In this arrangement, the dipole forces between the cyano groups would not be expected to be energetically favourable, and it is difficult to imagine how the flexibility of the helicene could compensate for the difference of 1.7 Å thereby providing some counter-evidence for this first model.

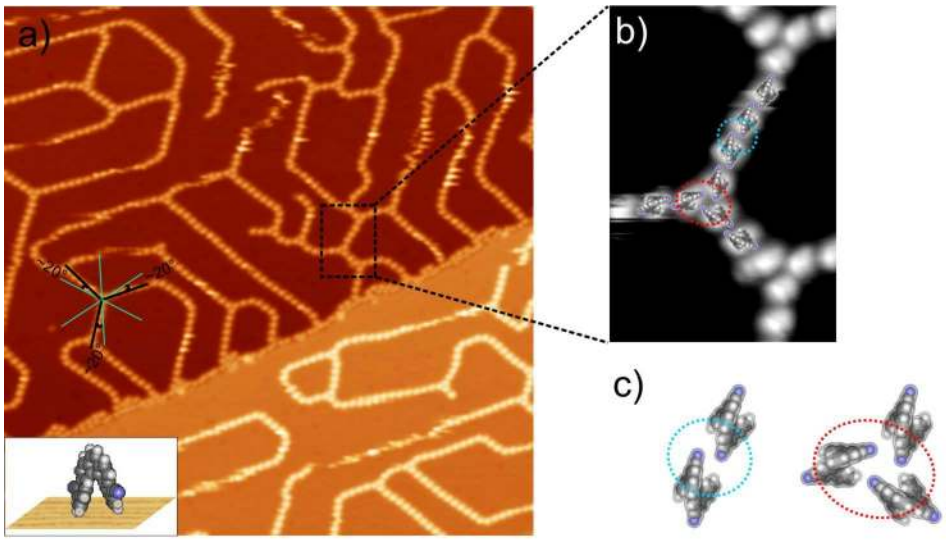

Figure 4.1. a) STM image which shows the straight chains of upright standing molecules observed at low coverages of **P4** on Cu(111). The side view of the adsorption geometry of the molecule is shown in the inset (170x170 nm^2, 1.3 V, 20 pA, 77 K). On the left-middle part of the image, the principal directions of the underlying copper substrate and the growth directions of the chains are marked in blue and black lines, respectively. Chains form an angle of ~ 20° with the principal direction. b) Detail of the area marked by a black dotted line in (a) in which a possible molecular model is sketched (7.7x17.7 nm^2, 1.3 V, 20 pA, 77 K). c) Tentative models to explain the formation of the chains and of branching points, respectively. Between two molecules along the chain both dipole-dipole interactions and H-bonding interactions may contribute to the stabilization of the chain and branching point.

In view of the further development of this model it seems a remarkable feature that the cyano helicenes in the chains are showing a lateral extension which is larger than expected for a single helicene aligned along with the chain direction. The second and alternative explanation of the observed linear structures could be the orientation of the helicenes by 90° in each lobe compared to the orientation depicted in figure 4.1b.

However, such an alignment is difficult to justify provided the long distance between the two neighbouring molecules within a chain which prevents both dipole-dipole and van der Waals interactions (figure 4.2; 2.option).

The third explanation (figure 4.2; 3.option) assumes a π-π stacking between helicenes in antiparallel orientation within one lobe, a motif that could in principle gain energy both from the condensation of the molecules and from the dipolar arrangement of the cyano residues. There is quite some evidence for π-π stacking in the observed crystal structures of helicenes, while, however, there are a few possibilities regarding the positions of the cyano groups and the stacking of the chains on the substrate which are currently under investigation using theoretical calculations performed at EMPA.

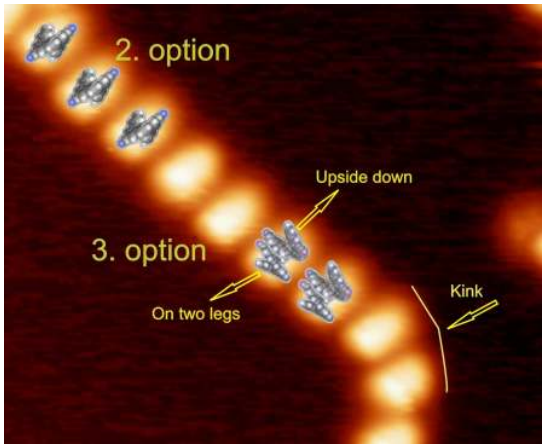

Figure 4.2. STM image which shows how the molecules might be positioned within a lobe of the chains. In the first option each molecule has an upright standing adsorption geometry perpendicular to the chain growth direction while in the 2. option each lobe hosts two molecules which are stacked by π-π interaction. The first option is rather unexpected in view of earlier publications, while the second option seems more attractive in view of the energetics. However, there are still open issues which need to be assessed by numerical simulations.

At the branching points of the molecular chains, there is the possibility that three cyano helicene molecules join in an angle of 60° forming a trimer, where the closest distance of a cyano group of one molecule to the H atom of the neighboring molecule is ~2.4 Å, which corresponds to the length of a usual H-bond. Such trimers of cyano-hydrogen bonding motifs have been identified previously in one or two dimensional assemblies with molecules possessing cyano functions.[11-13, 15-17] It is particular to this case, however, that the molecules are in a standing configuration, and the cyano interactions thus take place at a certain elevation above the surface.

Within the kinks, which changes the direction of a chain (see figure 4.2), the molecular association involves dipole-dipole and C-H...N interactions but since the dipoles are not perfectly antiparallel and the H-bonds are not fully directional (in the C-H…N interactions involving cyano groups, H-bonds can have variable angles[18]), the dipole-dipole interaction is weakened.

The deposition of a higher molecular coverage (~0.4 ML) of **P4** on Cu(111) leads to the formation of tetramers which nucleate from the chain intersections. Below this coverage, 1D molecular chains tend to repel each other, and thus do not get close or intersect in any other than the trimer motif discussed above. Below a certain threshold coverage tetramers are not formed. In the transition regime between a high density of chains and the nucleation of the tetramers as it is depicted in figure 4.3, the minimal separation of the chain motif is estimated to about 10 Å. This suggests that the coverage needs to be high enough to fill the gap between the chains which for a reason (registry, symmetry with the substrate or dipole charges) can not be filled by insertion of another chain. Therefore, only above a certain threshold coverage, the tetramers start to evolve at the chain intersections. With further increased coverage, the fraction of the surface which is covered by the tetramers increases steadily.

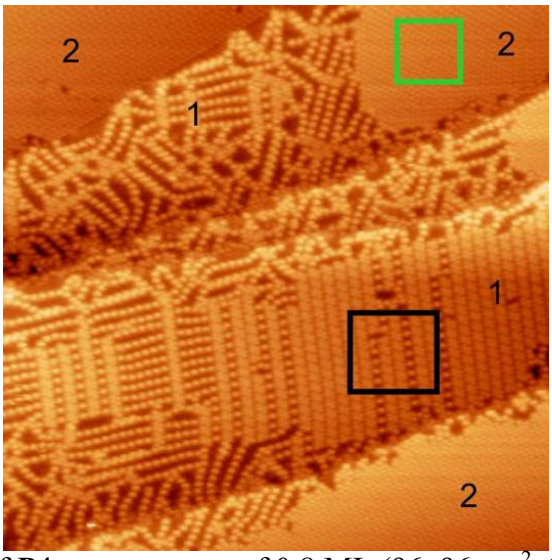

Figure 4.3. STM image of **P4** at a coverage of 0.8 ML (96x96 nm^2, 20 pA, 1.2 V, 77 K). Chains, tetramers and dimers are observed simultaneously. In the image the tetrameric structures are numbered as 1 while the dimeric structures are numbered with 2. The areas marked with green and black frames are shown in detail in figure 4.5 and 4.6, respectively.

At further increased coverage of **P4** (~0.6 ML) two superstructure arrangements are observed to coexist with the molecular chains (figure 4.3). The first pattern is formed by tetramers connected either by a row of molecules or only by a single molecule (indicated by number 1). The packing density of the close-packed tetrameric arrangement (with no single molecules or rows of molecules in between) is ~0.73 molecules/nm^2. The second pattern is more densely packed (~0.84 molecules/nm^2) and composed of dimers (figure 4.3, indicated by number 2). At intermediate coverages both patterns coexist and for coverages close to 1 ML the tetrameric structures evolve into a fully packed layer of the dimers.

The unit cell of the dimeric arrangement has been determined from LEED measurements performed at room temperature. The sample is slightly tilted with respect to normal incidence to allow for the observation of the first order diffraction spots which

would otherwise be hidden by the electron gun. LEED data has been taken for different energies of the incident electron beam. Diffraction patterns measured at 6eV, 16eV and 31eV beam energies are presented in figure 4.4a, b and c, respectively. Some of the diffraction spots are marked in green to emphasize the periodicity of the observed patterns. The software LEEDpat 2.1[19] has been used to simulate the experimentally obtained LEED pattern (figure 4.4d). From the analysis of the experimental data which is in agreement with the simulated measurements, a superstructure which is commensurate to the underlying Cu substrate is found. The following matrix describes the molecular ad-layer:

$$\begin{pmatrix} 9 & 6 \\ -1 & 4 \end{pmatrix}$$

The unit cell, as obtained from the LEED measurements, is of rectangular symmetry characterised by one lattice dimension of 20.29 Å and the other of 11.7 Å. The lattice vectors form an angle of 90° and the unit cell contains 2 molecules. The very small unit cell size suggests that the molecules pack very densely. This can only be achieved by an upright standing configuration of the molecules. A molecularly resolved STM image of the dimeric arrangement and the corresponding molecular model is presented in figure 4.5a and 4.5b, respectively. The adsorption sites of the molecules have been chosen arbitrarily on the copper substrate in the model. The structure consists of alternating rows A and B (marked in the model) which are parallel to the short axis of the unit cell. In row A, the π-system of the molecules is parallel to the row direction. Thereby, H-bonding interactions between the N atom of one cyano group and the H atom of a phenyl ring of the neighbouring molecule are enabled. Moreover, antiparallel dipolar coupling between the cyano groups of neighbouring molecules stabilize the structure more. In row B, the π-system of the molecules is orthogonal to the row direction and hence, the molecules of this row interact with the molecules of row A via CH···NC bonds. A dimer is then formed in combination of a monomer in row A and a neighbouring monomer in row B. This is highlighted by a coloured rectangle in the tentative model in figure 4.5b.

The STM image in figure 4.6a shows the tetrameric arrangement. The tentative model for the tetramers in figure 4.6b reveals that each tetramer is formed by two dimers as highlighted in the coloured rectangle. It should be noted that these dimers are not the same as the ones in the dimeric arrangement. The difference of the dimers observed in the tetramers originates from the slightly different angles of the molecules with respect to each other. In the dimeric arrangement, the two molecules in a dimer are nearly perpendicular to each other whereas the molecules in the dimer within the tetrameric arrangement lie more parallel to each other. Antiparallel dipolar coupling between the cyano groups of two parallel dimers (illustrated in a dashed black circle) leads to the formation of a tetramer. The single helicene molecule indicated by a green arrow in figure 4.6a,b interacts with molecules belonging to two neighboring tetramers by antiparallel arrangement of dipole-dipole interactions assisted by C-H…N hydrogen bondings as it is the case in row A in the dimeric pattern.

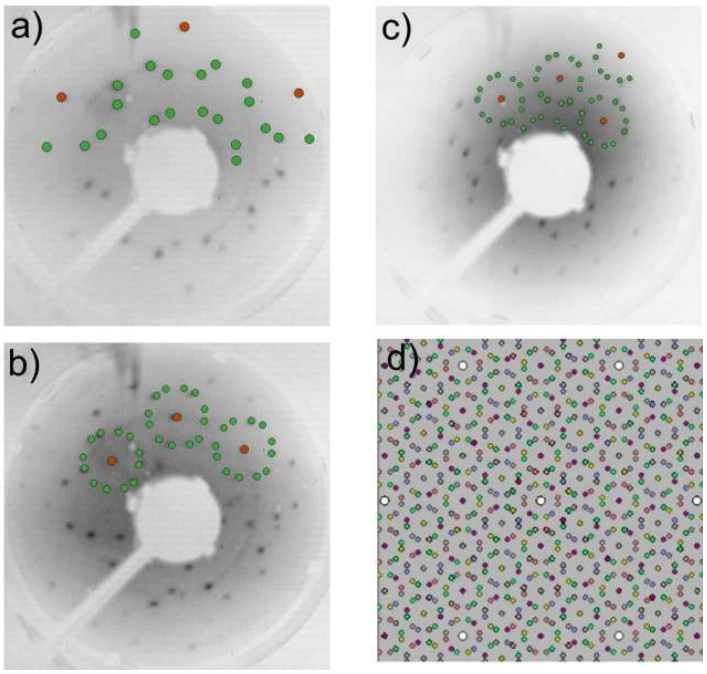

Figure 4.4. a) LEED pattern for the dimeric arrangement on Cu(111) obtained at electron energies of a) 6 eV b) 16 eV and c) 31 eV. The green dots act as a guide to the eye to be able to compare the LEED patterns obtained from our experiments with the simulated LEED pattern (d).

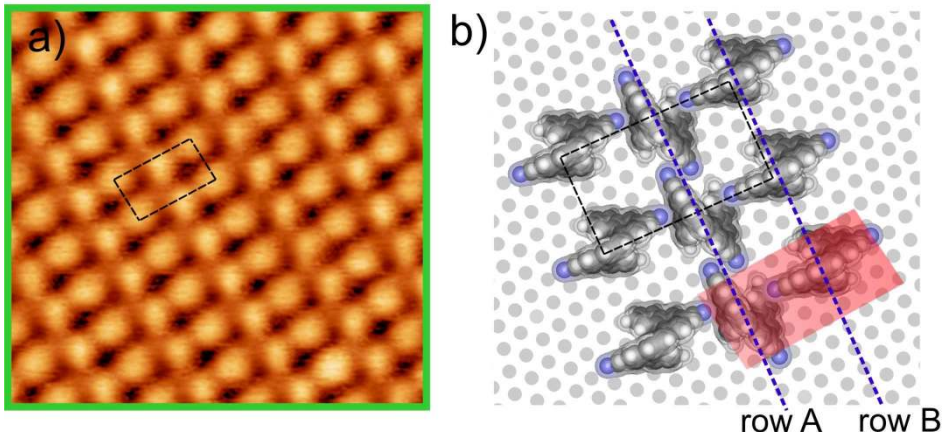

Figure 4.5. a) STM image of the dimeric structure (9.3x8.9 nm^2, 1.2 V, 20 pA, 77 K) formed by **P4**. b) Tentative molecular model for the dimeric arrangement. The red rectangle in the molecular model indicates a dimer.

Adsorption of the opposite enantiomer, **M4,** leads to structures which are mirror images of the ones observed for **P4**. In figure 4.7 mirror image tetrameric structures for **P4 (a)** and **M4 (b)** are shown. Similarly, dimeric arrangements of **P4** and **M4** reveal

mirror image structures when deposited separately onto the surface (figure 4.8 (a) and (b), respectively).

For one enantiomer, no mirror domains were observed. This is the first presented evidence in this thesis that the chirality of the enantiomer is programming the chirality of the assembly, as it was already observed in van der Waals aggregation of the unsubstituted helicenes.[4] Thereby this concludes that the chirality of a supramolecular assembly by cyano functionalisation – and most probably not restricted to these – can be programmed through the chirality of the building block. This was the aim of this project. In addition, for one enantiomer we found different rotational domains which differ by a 60° rotation with respect to each other. In the STM image in figure 4.9, two rotational domains of the dimeric structures formed upon adsorption of **M4** are seen.

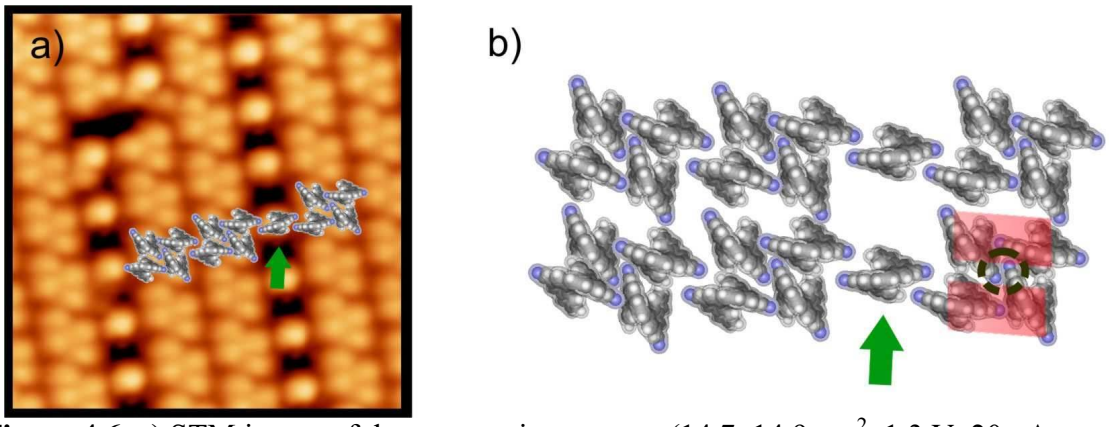

Figure 4.6. a) STM image of the tetrameric structure (14.7x14.9 nm^2, 1.3 V, 20 pA, 77 K) formed by **P4**. b) Tentative molecular model for the tetrameric arrangement. The red rectangles in the molecular model indicate two dimers which form a tetramer.

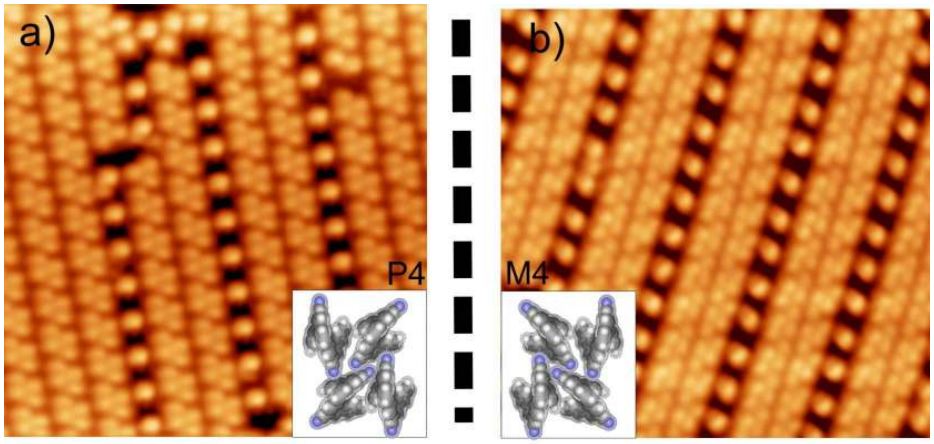

Figure 4.7. STM images of the tetrameric structures formed by a) **P4** (23x23 nm^2, 1.3 V, 20 pA, 77 K) and b) **M4** (26x26 nm^2, 1.2 V, 20 pA, 77 K) for coverages ~ 0.8ML on Cu(111). The tetrameric arrangement formed by **P4** is the mirror image to the arrangement formed by **M4**.

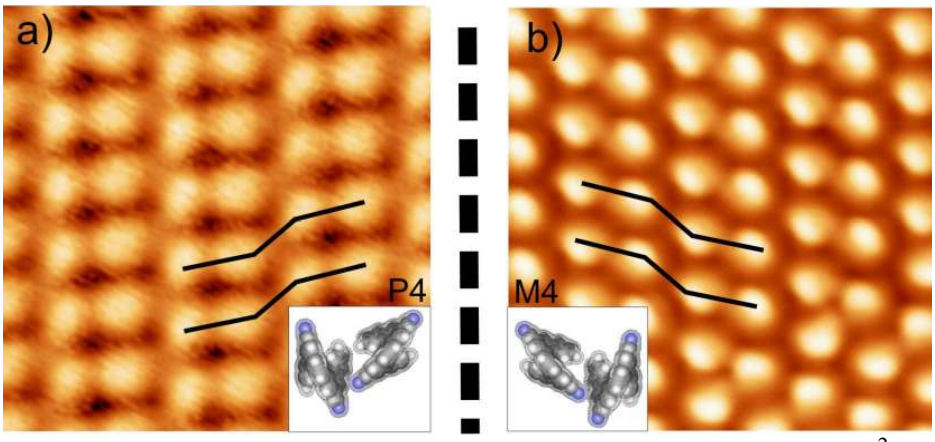

Figure 4.8. STM images of the dimeric structures formed by a) **P4** (8x8 nm^2, 20 pA, 1.2 V, 77 K) and b) **M4** (8.5x7.6 nm^2, 20 pA, 1.3 V, 77 K) for coverages above 0.8 ML on Cu(111). The dimeric arrangement formed by **P4** is the mirror image to the arrangement formed by **M4**.

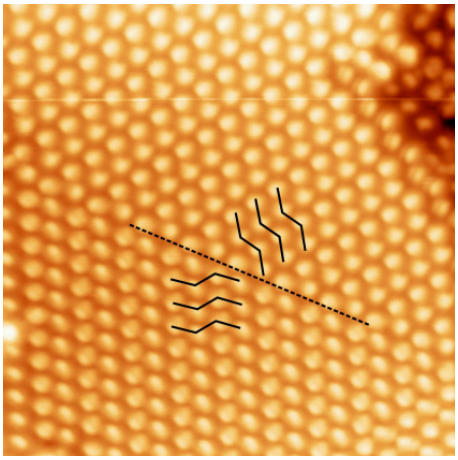

Figure 4.9. STM image of the rotational domains found upon adsorption of **M4** onto Cu(111) surface (20x20 nm^2, 1.3 V, 20 pA, 77 K). As expected due to the symmetry of the surface lattice, the domains are rotated by 60° with respect to each other.

4.1.2 Racemic cyano helicene

The finding that different enantiomers form similar but mirror image structures when deposited separately onto the surface gives rise to the question of how different enantiomers interact with each other when adsorbed simultaneously, leading either to homochiral (LL or RR) or heterochiral (LR or RL) supramolecular structures.

When mixtures of **P4** and **M4** are deposited onto the Cu(111) surface, similar structures are observed as they have been described above for the case of enantiopure helicenes. For coverages below 0.4 ML, straight chains which are distributed uniformly over the Cu(111) surface are seen (figure 4.10a). Since the enantiomeric discrimination is not possible due to the adsorption geometry of the molecule, it is not possible to identify if mirror image enantiomers are distributed randomly within the chains or if they are

separated. However, homochiral chains would possibly be more likely since electrostatic interaction might favour interactions between identical enantiomers as it has been discussed for other molecules previously.[20,21] Moreover, considering H-bond interactions between the molecules within the chains, it is known that strong H-bonds favour homochiral structures due to smaller distances between the interacting atoms.[22]

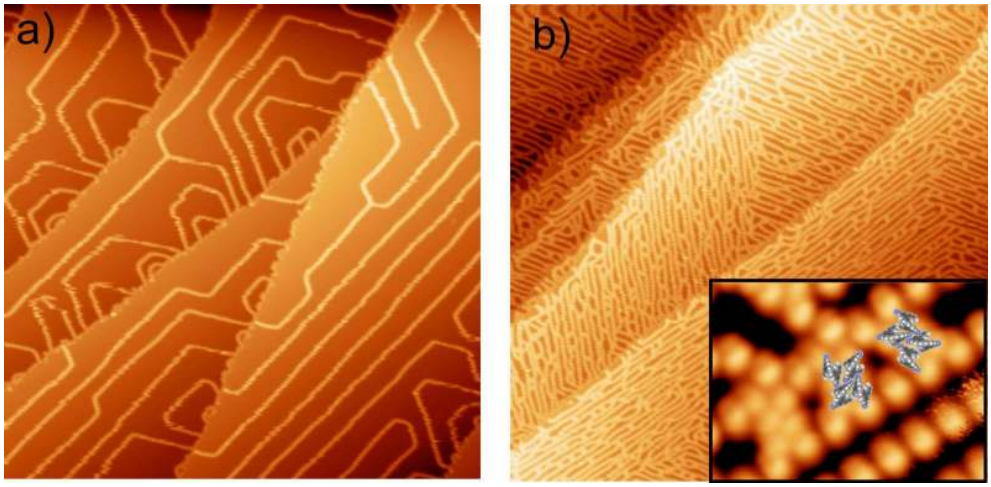

Figure 4.10. STM images of the racemic chains a) for a coverage of 0.08 ML (188 x 188 nm^2, 1.3 V, 20 pA, 77 K) and b) for a coverage of 0.4 ML (200x200 nm^2, 1 V, 20 pA, 77 K). In the inset two tetramers are shown which are mirror images of each other (11.8x8.6 nm^2, 1.3 V, 20 pA, 77 K).

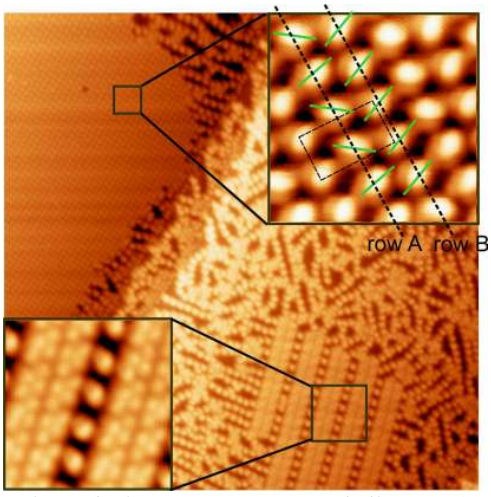

Figure 4.11. STM image showing chains, tetramers and dimers (96x96 nm^2, 1.2 V, 20 pA, 77 K) formed by the racemate. Closeup views of dimeric (5x5 nm^2, 1 V, 20 pA, 77 K) and tetrameric (10x10 nm^2, 1.3 V, 20 pA, 77 K) structures are shown in the insets in the upper and lower part of the STM image, respectively.

At intermediate coverages (~0.4 ML), tetramers at the chain intersections start to grow. Compared to the enantiopure case, tetramers self-assemble into mirror image aggregates in the racemate. In figure 4.10b, two mirror image tetramers (inset) are shown.

At higher coverages (above 0.6 ML), tetramers evolve into larger islands and dimers can be observed simultaneously (figure 4.11). In addition to the mirror image tetramers, we found mirror domains of dimers within the self-assembled layers of the racemate (figure 4.12). Since the adsorption of one enantiomer resulted in structures which are mirror images of those obtained after deposition of the opposite enantiomer, we conclude that the mirror domains are based on the separation of the enantiomers into enantiomorphous mirror domains in the racemate. This would mean that the self-assembly of cyano helicene molecules into homochiral tetramers and dimers of **M** or **P** type is due to a chiral recognition process and progressive segregation. We may therefore conclude that the bonding of different enantiomers is energetically disfavored compared to the homochiral combination.

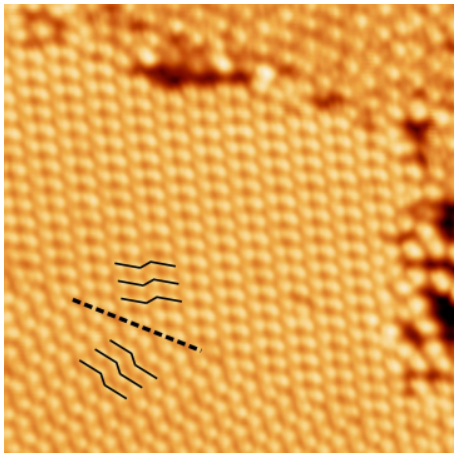

Figure 4.12. STM image of the racemic mixture adsorbed on Cu(111) which shows the mirror image domains of dimers (28x28 nm^2, 1. 2 V, 20 pA, 77 K).

As a result, the same molecular models for tetramers and dimers in the enantiopure case can be applied to the structures in the racemic case, as well. However, detailed examination of the dimeric structures in the racemic case shows that the interaction of the molecules in row B (figure 4.11) (compare with the model in figure 4.5b) reveals a better stability than the interaction of the molecules in row A in which the molecules are observed to exhibit different molecular orientations. (It should be noted that the dimeric pattern in figure 4.11 is formed by **M4** and thus row A and B are exchanged with row B and A in the dimeric pattern (formed by **P4**) in figure 4.5b, respectively). This result may be attributed to two reasons: 1) antiparallel dipolar coupling and directional H-bonding interactions result in a strong stabilization of neighbouring molecules along row B whilst C-H…NC bonds between two dimers have variable angles which results in relatively weak interactions[18] and thus different orientations of the molecules along row A; 2) in the racemic case the insertion of an enantiomer into a homochiral dimeric pattern formed with enantiomers with an opposite chirality may cause such defects leading to different orientations of the molecules.

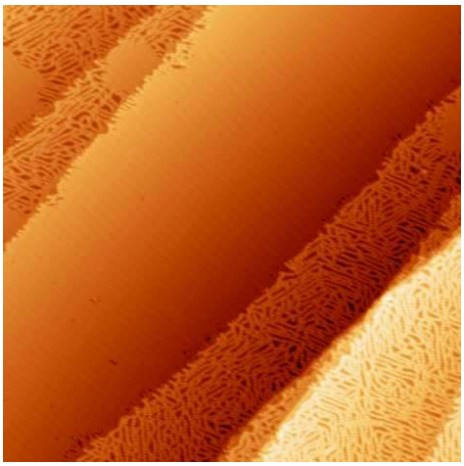

Figure 4.13. A large scale STM image which shows the very peculiar behaviour of the racemate that the molecules prefer to cover one terrace fully with the densest packing possible (dimeric pattern), then the dimers are started to be built in another terrace (200x200 nm^2, 1.4 V, 20 pA, 77 K).

To conclude, there is a chiral recognition between cyano-substituted helicene molecules. Enantiomers separate within the self-assembled monolayers and form homochiral tetrameric and dimeric close-packed structures at high coverages. Dimeric arrangement is thermodynamically the most favored phase. This result is also confirmed by annealing dependence measurements. The dimeric structures are stable up to 250°C and the tetramers evolve into the dimers upon annealing the samples. Moreover, the strong interaction between molecules to form the dimers can obviously be seen in the STM image presented in figure 4.13. The molecules prefer to fully cover a terrace with the most favorable arrangement. Subsequently, the growth of dimeric pattern starts again on another terrace and goes on extending until it is almost covered.

4.2 Room temperature measurements: Time-induced phase transition of a helicene porous network into a dimeric pattern

Nanoporous supramolecular networks raised increasing attention in recent years[23] owing to the fact that such networks expose specific surface sites with specific size, depth and shape in the nanometer regime and therefore are suitable to accommodate guest molecules within the cavities. Thereby host-guest binding and dynamic behaviours like (1) lateral or rotational mobility inside the pore or (2) hopping processes of guest molecules from one pore to another[24,9,10] have been studied, or guest molecules are manipulated by the STM tip.[11,25] Furthermore, such networks might essay chiral pores enabling enantioselective recognition of chiral guest molecules inside the pores, a phenomenon that was not observed before.

Such porous networks are often stabilized by rather weak and reversible interactions, such that the system is under thermodynamic control and displays a high degree of self-repair which leads to defect-free assemblies. Predominantly, nanoporous

structures are stabilized by hydrogen bonding interactions.[26] More robust porous network structures can be obtained by connecting building blocks through multiple hydrogen bonds[27] or by using even stronger metal-ligand interactions which also lead to well-ordered stable networks.[28]

The building blocks which form the porous structures can be designed to fit a specific guest molecule. The size and the symmetry of the building block or the functional groups to be attached, for example, can be chosen carefully. However, it is still not possible to predict the outcome of the self-assembly process since the outcome not only depends on the intermolecular interactions but is also driven by the interactions of the molecules with the substrate. Moreover, the surface coverage also plays an important role in the formation of the structures. Cyano helicene is a very good example for the latter case. Room temperature measurements of **P4** on Cu(111) give one of the most appealing findings on the self-assembly of helicenes for coverages ~0.65ML**,** which is a nanoporous network and critically depends on the surface coverage.

Upon adsorption of **P4** on Cu(111), only a mobile phase is observed at very low coverages. Upon increasing the coverage, a well-ordered nanoporous network evolves which is surrounded by a mobile phase (figure 4.14). Due to the effects of a thermodynamic equilibrium of rapid dissociation (from the 2D 'solid' network into the fluid) and re-condensation (from the 2D 'fluid' into the 2D 'solid') processes with respect of the characteristic time scale of the STM experiment (~msec), the fluid looks corrugated in the neigbouring area of the network, in similarity to the behavior of sub-phthalocyanine molecules on Ag(111) studied by S. Berner et al.[29] At the border between the mobile phase and the assembly, it can clearly be seen that the molecules combine into tetramers: a structure which has also been observed at low temperature measurements of the enantiopure helicenes, as described further above. The tetramers at the borders of the assembly are randomly placed while those which are closer to the inner part of a superstructure island form well-ordered hexagonal pores, where every pore consists of six tetramers. Each tetramer is formed by two dimers (figure 4.14b) each of which is stabilized by hydrogen bonding interactions between the nitrogen atom of one molecule and the hydrogen atom of the neighboring molecule. Two dimers then combine into a tetramer with a dipole-dipole coupling in between (green circle in the inset). A detailed description of the formation of the tetramers is presented in section 4.1.1. Each molecule in a tetramer interacts with another molecule in the neighbouring tetramer by antiparallel arrangement of dipole-dipole interactions assisted by C-H…N hydrogen bonds giving rise to the observed network in which the pores clearly reveal a six-fold symmetry and have a side of length a= 19.8±0.6Å. These characteristic distances for the lattice are provided in figure 4.14b together with the characteristic angles of a hexagon (α= 60°; β= 120°). The unit cell contains 1 pore and 12 molecules.

Parallel to the formation of the network, some molecules are seen to be trapped inside the pores (indicated with green arrows). However, the size of these guest molecules appears to be quite large compared to the molecules in the network. This indicates that either each pore hosts more than one molecule, owing to the relatively large

pore size (~ 19Å) or that the molecule rotates inside the pore at room temperature indicating a larger dimension.

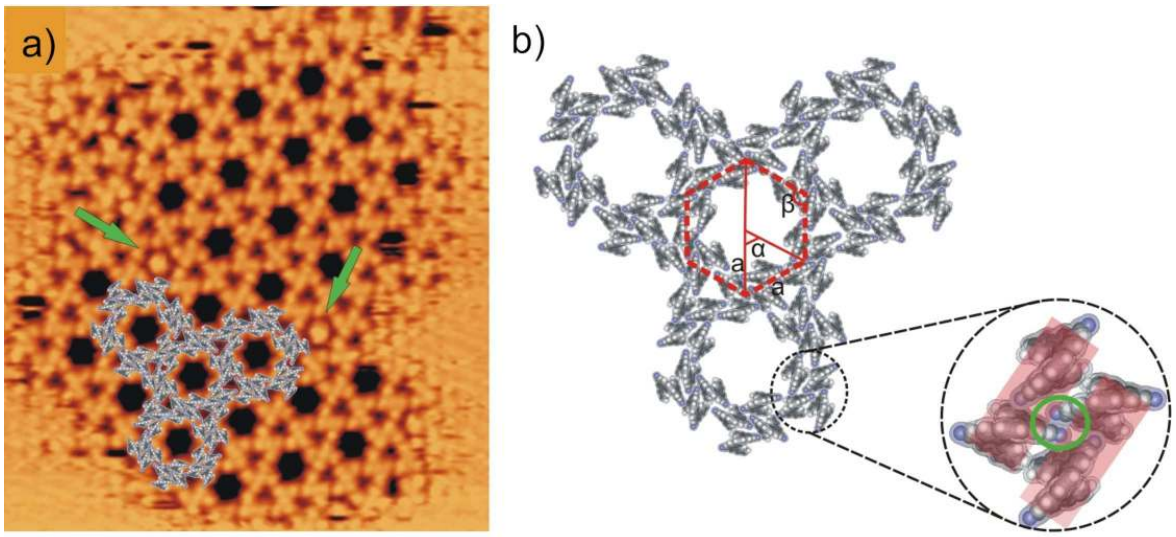

Figure 4.14. a) STM image of the porous network formed by **P4** (30x32 nm^2, 2.77 V, 7 pA, RT)**.** b) The tentative molecular model. A tetramer is encircled and zoomed out in which two dimers are highlighted in red.

The subsequent STM images of the same area in figure 4.15 demonstrate the behavior of the network over time. Apart from the fact that the network is observed to move on the surface, it also changes its shape and size which indicates the metastability of the network within the thermodynamic equilibrium of the 2D 'fluid' and 2D condensed phase.

Tetramers at the borders are randomly placed and not adapted to the underlying substrate to form the pores. The molecules here exhibit a significant volatility. It can be interpreted from this observation that initially the mobile molecules close to the border of the assembly form tetramers which by interaction with the mobile phase or by their 'incomplete' interaction at the 'surface' of the 2D environment are observed in a different arrangement. Only if the tetramers reside within the inner part of the supramolecular island, the porous network is formed. Apart from the influence of the substrate, the molecular coverage also plays a role in the formation of the network. At low coverage, only a mobile phase is observed whereas at higher coverages a close-packed assembly (dimeric pattern) evolves. However, coverage and the molecule-substrate interactions are not the only driving forces for the formation of the structure because at low temperatures, where the mobility of the molecules is reduced, straight chains and tetrameric structures were observed for the same coverage. This indicates that the mobility plays a key role for the formation of the porous network.

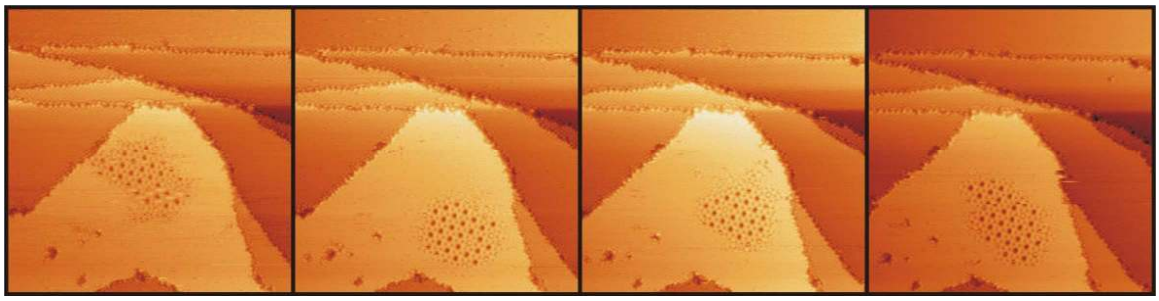

Figure 4.15. Subsequent STM images showing the metastability of the porous network (100x100 nm^2, 2.77 V, 7 pA, RT). The structure moves on the surface and it is surrounded by a mobile phase.

Surprisingly, leaving the sample for around 12 hours in the UHV chamber leads to a retarded transition of the mobile phase into the same dimeric arrangement, as it has already been described above (figure 4.16). Additionally, the metastable porous network is observed at a lower relative surface coverage or completely disappears and converts into the stable dimeric structures. Previously, coexistence of different phases formed by self-assembly of one type of molecule have been observed on surfaces for the same coverage[30,31] or depending on the surface coverage different phases have been obtained.[32-36] Recently, a network which undergoes a phase transition through thermally-induced change of the molecular conformation has been reported by Matena et al.[37]

In previous room temperature measurements the dimeric phase is observed only near the saturation coverage indicating that the molecules must be closely packed to be able to form the dimeric arrangement at room temperature. In the current case, however, observation of dimers below saturation coverage (in time) can be explained as follows. When the sample is measured after depositing the molecules directly, all terraces on the surface exhibit only a mobile phase and the network phase is observed in coexistence, but only if the molecular coverage is above the given threshold. After 12 hours some of the terraces are occupied with the densely packed dimeric arrangement leaving some of the terraces unfilled. This difference can clearly be seen in figure 4.17 in which only the terrace in the lower part contains the molecules forming dimers. This suggests a) that the system is kinetically retarded at room temperature to reach its thermodynamically most stable phase and b) that molecules diffuse from neigbouring terraces in order to form the most favored phase: dimeric arrangement. To cross a step-edge from one terrace to another, an atom or a molecule must overcome an additional potential barrier which is known as the Ehrlich-Schwoebel (ES) barrier.[38] In a further study, theoretical calculations of the diffusion and step-edge barrier for the helicene molecule are necessary in order to make more conclusive statements.

The STM image in figure 4.16 shows the dimeric arrangement that emerged in time. The unit cell of the dimeric packing, as determined from the LEED measurements (reported in section 4.1.1) has sides of lengths of 20.29 Å and 11.7 Å with an internal angle of 90° and contains 2 molecules. A tentative model for the close-packed dimeric

structure is presented in figure 4.16 in which a dimer is highlighted in a coloured rectangle. The detailed explanation of this arrangement has been given in section 4.1.1.

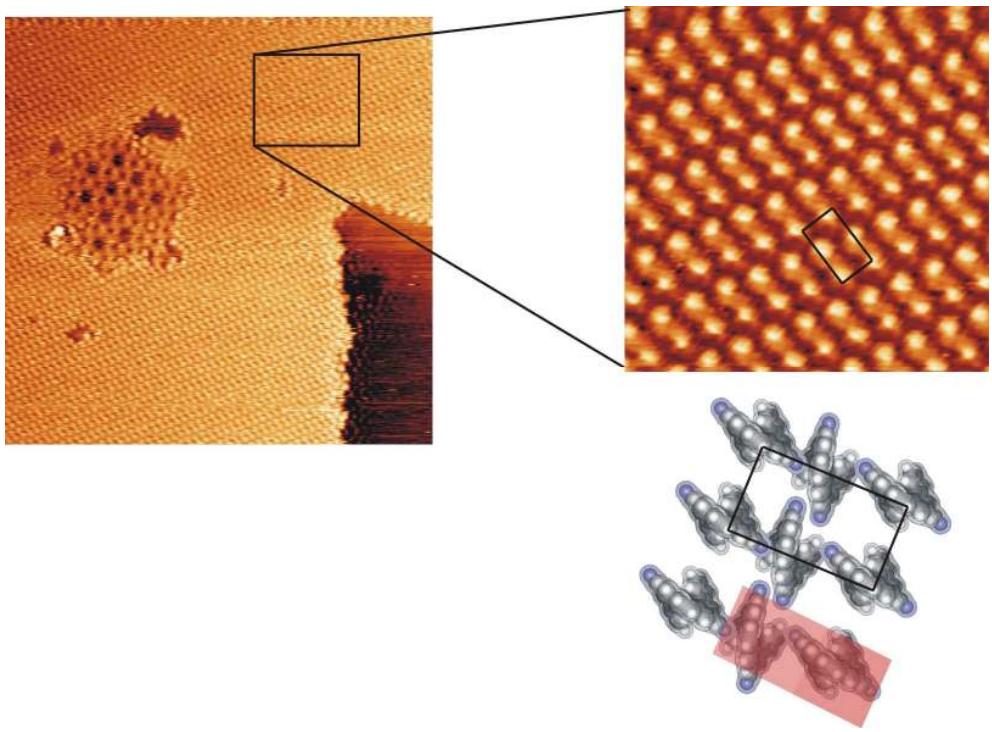

Figure 4.16. STM image of the porous network surrounded by the dimeric arrangement. (63x63 nm^2, 2.16 V, 20 pA, RT). A closeup view of the dimeric arrangement and the corresponding tentative molecular model is shown on the right (12x12 nm^2, 1.28 V, 20 pA, RT).

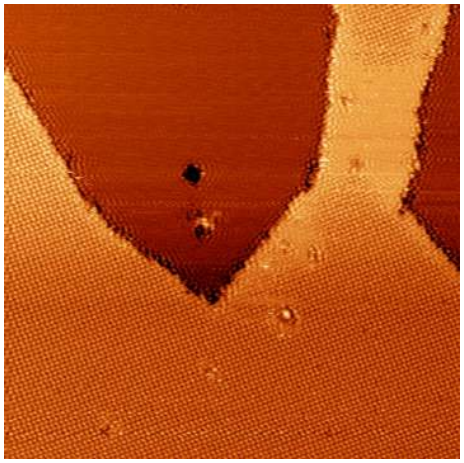

Figure 4.17. A large scale STM image of the surface after the phase transition. The molecules prefer to aggregate on the same terrace (lower terrace) while leaving some terraces unoccupied (upper terrace) (100x100 nm^2, 1.9 V, 14 pA, RT).

	Porous structure	Dimeric structure
(Dipole-dipole) /nm^2	0.324	0.42
(C-H...N) /nm^2	0.65	0.84
(N-pi bond) /nm^2	0.324	0.84
(N-N) /nm^2	0.162	0
molecules/nm^2	0.65	0.84

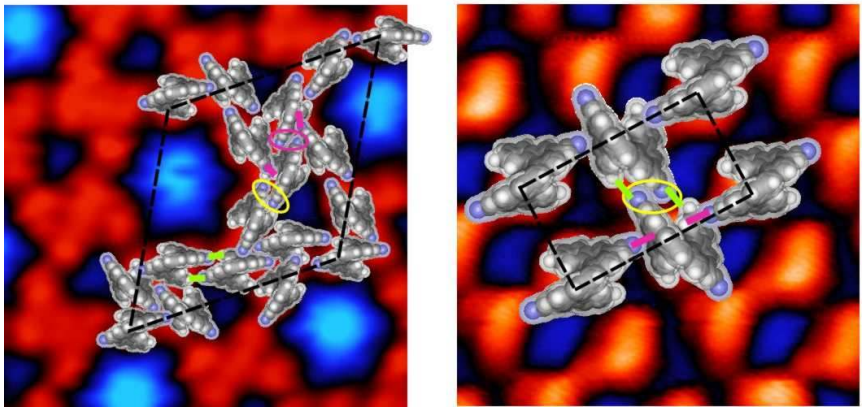

Figure 4.18. A scheme which shows the number of each interaction which takes place per nm^2 for the porous and the dimeric structures. The STM images for the porous (7.8x7.8 nm^2, 2.7 V, 7 pA) and the dimeric (4.2x4.2 nm^2, 1.3 V, 20 pA; 77 K) arrangements are shown below in which the molecules within the unit cells are superimposed. Dipole-dipole interactions (assisted by H-bonds) are shown in yellow circles whereas green lines indicate H-bonds and pink lines indicate N-pi bonds in both structures. The pink circle in the porous structure shows an N-N interaction which is not supported by H-bonds and does not exist in the dimeric arrangement.

Conversion of the porous network into the dimeric pattern in time without any external trigger approves that there is at least a small energy difference between these two phases. Another view on this energy difference can be gained by comparing the molecular interactions per nm^2 for each phase. In figure 4.18 the number of all these interactions per nm^2 for both phases is shown together with the STM images of two phases in which only the molecules within the unit cells are superimposed. The porous network contains four different interactions in the unit cell: (6) dipole-dipole assisted by H-bond interactions connecting each tetramer to a neighbouring one, (12) C-H…N (which assist the 6 dipole-dipole interactions in previous interaction), (6) N-π bond interaction and (3) N-N interaction that connects two dimers into a tetramer (figure 4.10b, green circle; we call this an N-N interaction instead of a dipole-dipole interaction to distinguish it from the initial interaction. The dipoles here are not participating in a H-bond interaction). The dimeric structure includes (1) dipole-dipole, (2) C-H…N, (2) N-π bonds and no N-N interaction in the unit cell. As the values confirm, the number of interactions per nm^2 is slightly higher for the dimeric pattern but still the difference is not too large and the N-N bond which connects two dimers into a tetramer in the porous

network does not exist in the dimeric structure which may more or less compensate for the energy difference between the two phases. A second important parameter is the average packing density which influences two terms: (1) the average separation between the molecules and as such the interaction via non-directional vdW interactions as well as the distances in directional interactions as those listed above and (2) the energy gained from the surface-molecular interaction per surface area which is generally considerable on metallic substrates. The packing densities of the porous and the dimeric structures are ~0.65 molecules/nm^2 and 0.84 molecules/nm^2, respectively.

References 4

[1] T. Nakamura, H. Kondoh, M. Matsumoto, *Scanning tunneling microscopy observations of [7]thiahelicene adsorbed on Au(111),* Mol. Crys. Liq. Cry. Sci. Tech. Sec. A-Mol. Crys. Liq. Crys. 337, 273 – 276 (**1999).**

[2] a) M. Taniguchi, H. Nakagawa, A. Yamagishi, K. Yamada, *Molecular chirality on a solid surface: thiaheterohelicene monolayer on gold imaged by STM*, Surf. Sci. 454, 1005-1009 (**2000)**; b) M. Taniguchi, H. Nakagawa, A. Yamagishi et al., *STM observation of thia[11]heterohelicene on gold(111) and gold(110) surface,* Surf. Sci. 507**,** 458-462 **(2002)**; c) M. Taniguchi, H. Nakagawa, A. Yamagishi et al., *STM observation of molecular chirality and alignment on solid surface*, J. Mol. Cat. A-Chemical 199**,** 65-71 **(2003).**

[3] K.-H. Ernst, Y. Kuster, R. Fasel, M. Müller, U. Ellerbeck, *Two-Dimensional Separation of [7]Helicene Enantiomers on Cu(111),* Chirality 13, 675- 678 (**2001).**

[4] R. Fasel, M. Parschau, K.-H. Ernst, *Chirality Transfer from Single Molecules into Self-Assembled Monolayers,* Angew. Chem. Int. Ed. 42, 5178–5181 (**2003**).

[5] R. Fasel, M. Parschau, K.-H. Ernst, *Amplification of chirality in two-dimensional enantiomorphous lattice,* Nature 439, 449–452 (**2006).**

[6] a) R. Fasel, A. Cossy, K.-H. Ernst, F. Baumberger, T. Greber, J. Osterwalder, *Orientation of chiral heptahelicene $C_{30}H_{18}$ on copper surfaces: An x-ray photoelectron diffraction study,* J. Chem. Phys. 115, 1020–1027 **(2001);** b) K.H. Ernst, Y. Kuster, R. Fasel et al. *Adsorption of helical aromatic molecules: heptahelicene on Ni(111),* Surface Science 530**,** 195-202 **(2003).**

[7] K. H. Ernst, M. Neuber, M. Grunze et al., *NEXAFS study on the orientation of chiral P-heptahelicene on Ni(100),* J. Am. Chem. Soc. 123, 493-495 (2001).

[8] D. Bonifazi, H. Spillmann, A. Kiebele et al. *Supramolecular patterned surfaces driven by cooperative assembly of C-60 and porphyrins on metal substrates,* Angew. Chem. Int. Ed. 43**,** 4759-4763 (**2004).**

[9] H. Spillmann, A. Kiebele, M. Stöhr et al. *A two-dimensional porphyrin-based porous network featuring communicating cavities for the templated complexation of fullerenes,* Ad. Mat. 18**,** 275 **(2006).**

[10] A. Kiebele, D. Bonifazi, F.Y. Cheng et al., *Adsorption and dynamics of long-range interacting fullerenes in a flexible, two-dimensional, nanoporous porphyrin network,* ChemPhysChem 7**,** 1462-1470 **(2006).**

[11] N. Wintjes**,** D. Bonifazi, F.Y. Cheng et al., *A supramolecular multiposition rotary device*, Angew. Chem. Int. Ed. 46**,** 4089-4092 (**2007).**

[12] Y. Okuno, T. Yokoyama, S. Yokoyama et al., *Theoretical study of benzonitrile clusters in the gas phase and their adsorption onto a Au (111) surface*, J. Am. Chem. Soc. 124, 7218-7225 **(2002).**

[13] M. Itoh, M. Takamatsu, N. Kizu et al., *Van der Waals cluster and excimer formations of 1-cyanonaphthalene and methyl-substituted 1-cyanonaphthalened in supersonic expansion*. J. Phy. Chem. 95**,** 9682-9687 **(1991).**

[14] T. Michinobu, C. Boudon, J.P. Gisselbrecht et al., *Donor-substituted 1,1,4,4-tetracyanobutadienes(TCBDs): New chromophores with efficient intramolecular charge-transfer interactions by atom-economic synthesis*, Chem. A European J. 12**,** 1889-1905 **(2006).**

[15] N. Wintjes, J. Hornung, J. L. Checa, et al., *Supramolecular synthons on surfaces: Controlling dimensionality and periodicity of tetraarylporphyrin assemblies by the interplay of cyano and alkoxy substituents,* Chem. A Eur. J. 14**,** 5794-5802 (**2008).**

[16] G.R. Desiraju, *Supramolecular synthons in crystal engineering - a new organic-synthesis*, Angew. Chem. Int. Ed. 34**,** 2311-2327 **(1995).**

[17] T. Yokoyama, S. Yokoyama, T. Kamikado et al., *Selective assembly on a surface of supramolecular aggregates with controlled shape and size,* Nature 413**,** 619-621 (**2001).**

[18] K.E. Maly, T. Maris, E. Gagnon et al. *Inclusion compounds of hexakis(4-cyanophenyl)benzene: Open networks maintained by C-H center dot center dot center dot N interactions*, Crystal Growth and Design 6**,** 461-466 **(2006).**

[19] K. Hermann, M.A. van Hove, *LEED pattern simulator LEEDpat Version 2.1* (**2006**).

[20] D. Andelman, *Chiral discrimination and phase-transitions in langmuir monolayers,* J. Am. Chem. Soc. 111**,** 6536-6544 (**1989**).

[21] M. Bohringer, W.D. Schneider, R. Berndt, *Real space observation of a chiral phase transition in a two dimensional organic layer*, Angew. Chem. Int. Ed**.** 39**,** 792 (**2000).**

[22] Q.Chen, C. W. Lee et al., *The formation of enantiospecific phases on a Cu{110} surface,* PhysChemComm, 9, 4 (**1999**).

[23] T. Kudernac, S.B. Lei et al. *Two-dimensional supramolecular self-assembly: nanoporous networks on surfaces,* Chem. Soc. Rev. 38**,** 3505-3505 (**2009).**

[24] a) G. Schull, L. Douillard, C. F. Debuisschert et al., *Single-molecule dynamics in a self-assembled 2D molecular sieve,* Nano Letters **6,** 1360-1363 (**2006)**; b) G. Schull, L.

Douillard, C. F. Debuisschert et al., *Selectivity of single-molecule dynamics in 2D molecular sieves,* Ad. Mat. 18, 2954**-+ (2006).**

[25] M. Stöhr, M. Wahl, H. Spillmann et al., *Lateral manipulation for the positioning of molecular guests within the confinements of a highly stable self-assembled organic surface network***,** Small 3, 1336-1340 **(2007).**

[26] a) S. Griessl, M. Lackinger, M. Edelwirth et al., *Self-assembled two-dimensional molecular host-guest architectures from trimesic acid*, Single Molecules **3**, **25-31** (**2002);** b) A. Dmitriev, N. Lin, J. Weckesser et al., *Supramolecular assemblies of trimesic acid on a Cu(100) surface***,** J. Phy. Chem. B 106**,** 6907-6912 **(2002);** c) Y.C. Ye, W. Sun, Y.F. Wang et al., *A unified model: Self-assembly of trimesic acid on gold***,** J. Phy. Chem. C 111, 10138-10141 **(2007).**

[27] J. A. Theobald, N. S. Oxtoby, M. A. Phillips et al., *Controlling molecular deposition and layer structure with supramolecular surface assemblies,* Nature 424**,** 1029-1031 **(2003).**

[28] a) A. Dmitriev, H. Spillmann, N. Lin et al., *Modular assembly of two-dimensional metal-organic coordination networks at a metal surface*, Angew. Chem. Int. Ed. 42**,** 2670-2673 (**2003);** b) S. Stepanow, M. Lingenfelder, A. Dmitriev et al., *Steering molecular organization and host-guest interactions using two-dimensional nanoporous coordination systems***,** Nature Materials 3, 229-233 **(2004).**

[29] S. Berner, M. Brunner, L. Ramoino et al., *Time evolution analysis of a 2D solid-gas equilibrium: a model system for molecular adsorption and diffusion,* Chem. Phys. Let. 348**,** 175**-181 (2001).**

[30] T. Samuely, S. X. Liu, N. Wintjes et al., *Two-dimensional multiphase behavior induced by sterically hindered conformational optimization of phenoxy-substituted phthalocyanines,* J. Phy. Chem. C 112**,** 6139-6144 **(2008).**

[31] K. Morgenstern, S. W. Hla, K. H. Rieder, *Coexisting superstructures of iodobenzene on Cu(111) near saturation coverage***,** Surface Science 523**,** 141-150 (**2003).**

[32] S. Berner, M. de Wild, L. Ramoino et al., *Adsorption and two-dimensional phases of a large polar molecule: Sub-phthalocyanine on Ag(111),* Phys. Rev. B 68**,** Article Number: 115410 **(2003).**

[33] M. Roos, H. E. Hoster, A. Breitruck et al., *Coverage dependent structures of oligopyridine adlayers on (111) oriented Ag films*, PhysChemChemPhys 9**,** 5672-5679 (**2007).**

[34] B. Xu, C.G. Tao, E.D. Williams et al., *Coverage dependent supramolecular structures: C-60 : ACA monolayers on Ag(111),* J. Am. Chem. Soc. **128, 8493-8499 (2006).**

[35] M. Stöhr, M. Wahl, C. H. Galka et al., *Controlling molecular assembly in two dimensions: The concentration dependence of thermally induced 2D aggregation of molecules on a metal surface*, Angew. Chem. Int. Ed. 44**,** 7394-7398 (**2005).**

[36] K. Muller, A. Kara, T.K. Kim et al., *Multimorphism in molecular monolayers: Pentacene on Cu(110),* Phys. Rev. B 79**,** Article Number: 245421 **(2009).**

[37] M. Matena, A. Llanes-Pallas, M. Enache et al. *Conformation-controlled networking of H-bonded assemblies on surfaces***,** Chem. Com. 24**,** 3525-3527 (**2009).**

[38] a) G. Ehrlich, F. G. Hudda, *Atomic view of surface self-diffusion - tungsten on tungsten,* J. Chem. Phys. 44, 1039-& (**1966);** b) R.L. Schwoebel, E.J. Shipsey, *Step motion on crystal surfaces,* J. App. Phys. 37**,** 3682-& (**1966).**

5 Conclusions and Outlook

In the work at hand, the focus was on two main subjects: formation of covalent bonds by making use of protecting group chemistry (chapter 3) and the control of chirality in an architecture by the chirality of its building blocks (chapter 4).

In the first part of chapter 3, we combined a biphenyl core with two Boc groups attached symmetrically at para positions of the core (biphenyl **1**). In view of the studies described therein, Boc protecting groups have proven to be potential candidates for surface self-assembly studies. They exhibit both hydrogen bond donor and acceptor functionalities which allow them to act as intermolecular organizers on surfaces. The experimental results definitely show that they provide lateral ordering for the compounds on both Ag(111) and Cu(111) surfaces. Biphenyl **1** formed two different self-assembled structures: A herringbone and a parallel arrangement regardless of the substrate. The main goal was to couple these pre-organized molecular building blocks benefiting from the rich chemistry of protecting groups. The chemical reaction was induced by the appropriate choice of the sample temperature. We have shown that, depending on the temperature, the molecules can form either interlinked dimers and interlinked cross-like structures on Cu(111) or interlinked compounds forming long chains on Ag(111).

In the second part of chapter 3, further deliberate controlling of the formation and the arrangement of the resulting interlinked structures was achieved by modification of one of the end groups of biphenyl **1**. In order to be able to induce a sequential splitting of the Boc groups of the molecule at elevated temperatures, we replaced three hydrogen atoms with three fluorine atoms at one of the end groups of the molecule (biphenyl **2**). Enhanced reactivity of this end group resulted in the formation of similar dimeric structures as obtained from biphenyl **1**, but more stable in a broader temperature range on both Cu(111) and Ag(111) surfaces. Moreover, interlinked trimers have also been found to form well-ordered arrangements stabilized by H-bonds.

In the third part of chapter 3, a similar study has been carried out. This time we played with the positions of the Boc protecting groups of biphenyl **1**: one of the Boc groups is placed at meta position instead of para position of the biphenyl core which resulted in an asymmetric molecule, biphenyl **3**. This molecule was able to form molecular chains, hexagonal flower-like structures and a densely-packed parallel arrangement depending on the coverage at low temperature. After annealing the sample, covalently bound dimeric and trimeric structures have been obtained similar to the previous case.

A similar study has been carried out with a similar but longer molecule (molecule **6**) which is described in appendix 2. The molecules self-assembled into four different phases at room temperature and gave rise to individual triangular shaped structures upon annealing the samples. However, we were unable to reproduce the structures obtained before annealing, due to sublimation problems (the molecules could not be deposited intact onto the surface by sublimation). Further evaluation is needed to understand the structures formed before and after annealing. Therefore, different deposition methods can be tried, e.g. electrospray deposition as described by James O'Shea.[1]

The next step would be the formation of a long-range-ordered and highly stable surface structure in two dimensions. A very promising approach towards such a goal seems to be the use of the protecting groups. However, in our work, we used compounds having only two functional groups which can, in principle, form 1D covalently bound structures. Using new compounds with multiple functional groups could lead to ordered 2D structures formed by covalent bonds, that can be studied in future experiments.

Additionally, cleavage of Boc groups using the STM tip may lead to covalently bound structures and can additionally be evaluated in the future.

In the fourth chapter of the thesis, a helicene derivative consisting of two cyano side groups have been introduced. The cyano groups have been found to have a high influence on the adsorption geometry of the molecules upon deposition on the surface as well as on the formation of the self-assembled structures. Since the helicene molecules are "3D objects" they can either have an "upright standing" or "flat lying" geometry. In our work, all self-assembled structures of cyano-helicenes revealed an upright standing adsorption geometry which is observed for the first time for helicenes.

Both racemic and enantiopure forms of the molecule have been found to exhibit 1D molecular chains, tetrameric structures and dimeric structures depending on the coverage. Mainly dipolar coupling and H-bonding interactions stabilize these structures.

Adsorption of different enantiomers gave mirror image structures of each other. Moreover, these mirror image structures have been observed simultaneously upon deposition of the racemic mixture, which shows a chiral seperation. As a result, the control of chirality in the self-assembled extended domains has been managed by the chirality of its building blocks.

Additionally, enantiopure form of the molecule has been deposited on Cu(111) and measured at room temperature. STM measurements revealed a metastable nanoporous network. This metastable phase transformed into energetically the most favoured phase in time: dimeric arrangement. Our proposal was that the molecules diffuse from an upper terrace to a lower one in order to form thermodynamically the most favored phase. For this step-crossing, molecules must overcome an additional potential barrier which is known as the Ehrlich-Schwoebel (ES)[2] barrier. As a further study, theoretical

calculations of the diffusion and step-edge barrier for the helicene molecules have to be performed in order to draw reliable conclusions.

As described already in appendix 3, hydrogen bonding amide-[7] helicene system has to be further examined, which will probably lead to stronger supramolecular interactions within the self-assembled structures of helicenes. Moreover, obtaining stable nanoporous networks would enable using these systems for host-guest studies. Furthermore, since helicenes are 3D objects, the pores are extended into 3D which allows further optimization of the host-guest chemistry and functionalization out of the plane of the monolayer. Moreover, obtaining chiral pores would enable enantioselective recognition of chiral guest molecules inside the pores.

Theoretical calculations of the investigated molecular systems, especially of the cyano helicenes presented in the second part of the experimental results, would be very helpful for the interpretation of the experimental data. Why molecules prefer to have an upright standing configuration and how they interact with each other within the 1D supramolecular chains are still open questions. In colloboration with M. T. Nguyen, C. Pignedoli and D. Passerone from EMPA Dübendorf, we expect to answer these questions.

References C&O

[1] J. C. Swarbrick, J.B. Taylor, J.N. O'Shea, *Electrospray deposition in vacuum*, Ap. Surf. Sc. 252**,** 5622-5626 **(2006).**

[2] G. Ehrlich, F. G. Hudda, *Atomic view of surface self-diffusion - tungsten on tungsten,* Journal of Chemical Physics 44, 1039-& (**1966);** b) R.L. Schwoebel, E.J. Shipsey, *Step motion on crystal surfaces,* J.Ap. Phy. 37**,** 3682-& (**1966).**

Appendix 1

This section presents the first experimental results of dicyano-[7]-helicene. The compound includes the pure helicenes (**P4** and **M4**; figure A1.1a) together with an impurity (**P5** and **M5**; figure A1.1b) which stems from the last step of synthesis that was inadvertently executed in an incomplete sense.

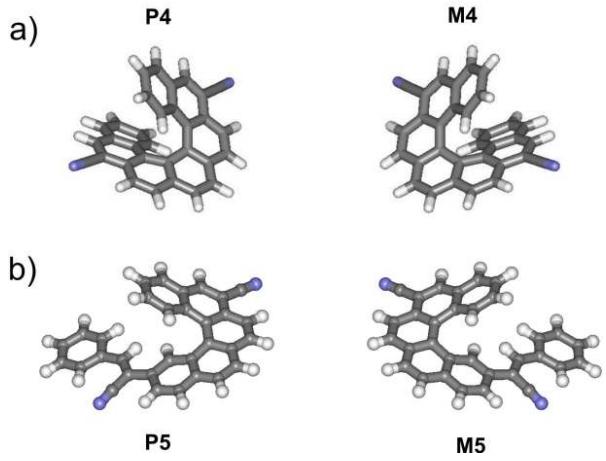

Figure A1.1. Two enantiomers of dicyano-[7]-helicene, a) **P4** and **M4,** and b) two enantiomers of the impurity compound, **P5** and **M5**.

Upon deposition of the mixture on Cu(111), for coverages below 0.8 ML, 1D molecular chains are formed which are randomly oriented with respect to the principal surface directions (figure A1.2a). Each molecule is identified as a lobe and shows different levels of brightness within the chains. The difference in brightness corresponds to a difference in height which can only be explained by different adsorption geometries. The very bright lobes are contributed to the upright standing molecules while the dim ones are the molecules lying parallel to the substrate with their π-system. Models based on "standing up" or "lying" geometries of the two compounds are illustrated in figure A1.2b (side view).

In high resolution STM images the intramolecular structure is resolved, thus enantiomeric discrimination can be possible by making use of the following model:

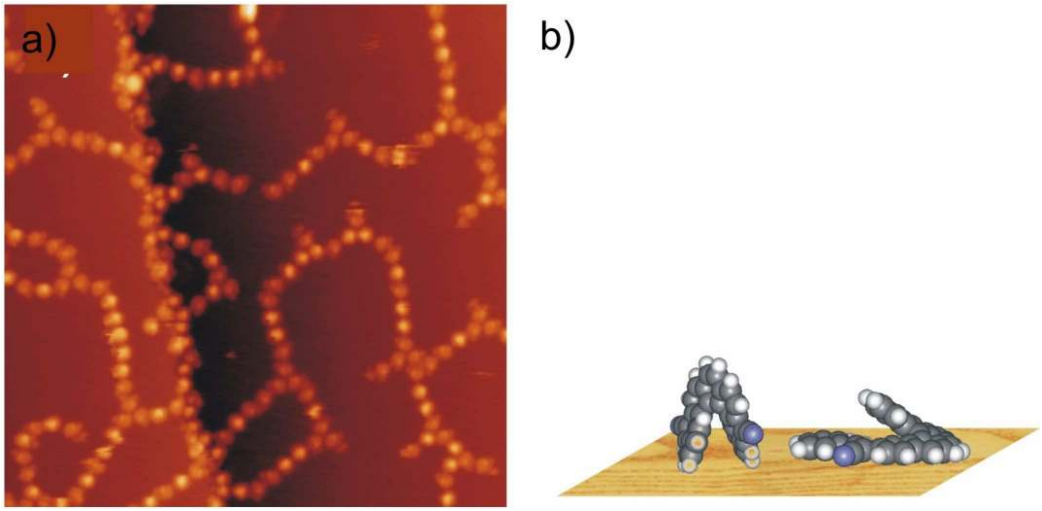

Figure A1.2. STM image of the molecular chains formed by the racemic mixture of **P4** also containing a fraction of some percent of **P5** after incomplete synthesis after sublimation onto Cu (111) (40x40 nm^2, 2 V, 20 pA, 77 K) (a). Adsorption geometries of both compounds in (b) reveal an upright standing geometry for the pure helicene while the impurity lies flat on the surface (side views).

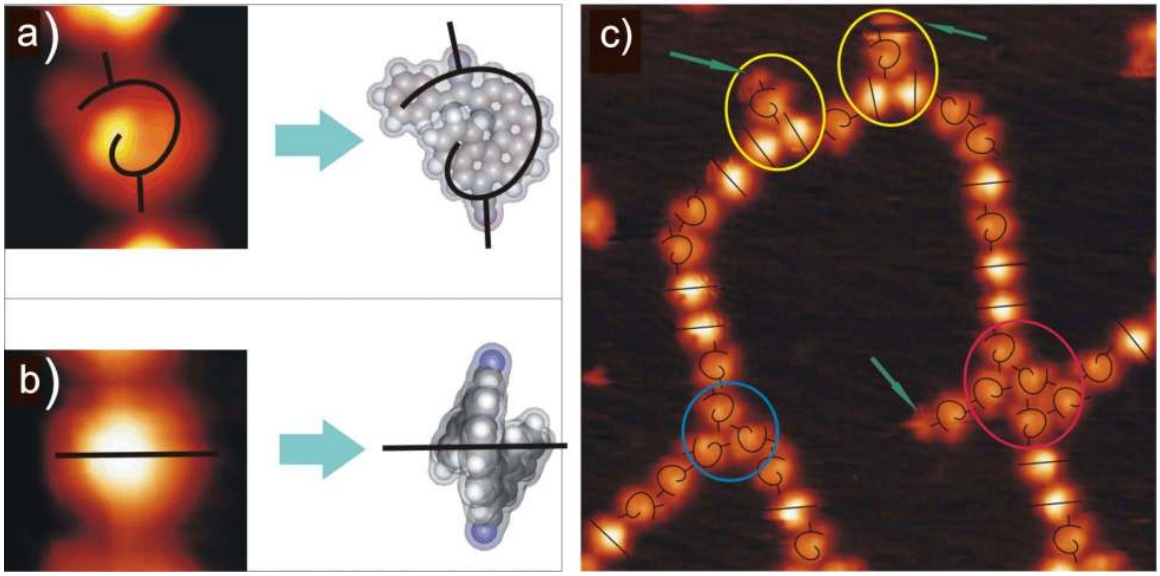

Figure A1.3. Models for flat lying (a) and upright standing (b) molecules used for interpretation of the STM images. By superimposing the models in (a) and (b) on the STM image (c), the molecular model of the chain can be estimated (d). (Parameters: 2 V, 20 pA, 77 K; a,b) 2.4x2.2 nm^2 c) 17x20 nm^2)

The brightness is not homogeneous for flat lying molecules in the STM images. Each lying molecule (figure A1.3a) looks like a spiral, the initial part of which is imaged brighter and correlated to the topmost part of the molecule. The end of the spiral corresponds to a dim appearance in the STM images which is the lowest part of the molecule and is in contact with the substrate. This dim protrusion corresponds to the single benzene ring of the impurity. Therefore, we can conclude that parallel lying molecules are the impurities (**P5** and **M5**) while standing molecules should correspond to the mixtures of **P4** and **M4**. In fact, upon deposition of the pure helicenes on the surface, only upright standing molecules have been observed (chapter 4). Since there is no significant difference in the appearance of different enantiomers for the upright standing molecules, they are shown as a line perpendicular to the chain growth direction (figure A1.3b). The cyano groups are also not resolved but lie parallel to the growth directions of the chains. By superimposing the two models demonstrated in figure A1.3a and A1.3b on the STM image in figure A1.3c, possible interactions between the molecules can be studied.

The random orientation of the chains implies that the substrate is not dominating the assembly and the intermolecular interactions are relevant for the chain formation. In particular, dipole-dipole and C-H…N interactions govern the arrangement of the chains. It may also be worth to note that the relative fraction of **P4** and **P5** is strongly shifted towards **P5** after the sublimation. This suggests that the impurity **P5**, some percent in the raw material used for these experiments is preferentially sublimed, an effect which is also confirmed by our observation that the observed fraction of **P5** was continuously reduced with progressive use of the same batch of molecules in the Knudsen cell and then diminished.

Two upright standing helicene units form a linear connection and basically lengthen the chains. Self-assembly of such two standing molecules is observed upon deposition of the pure helicene compound and the possible interactions are explained in section 4.1.1 (molecular structure of such two upright standing units is shown in figure A1.4a).

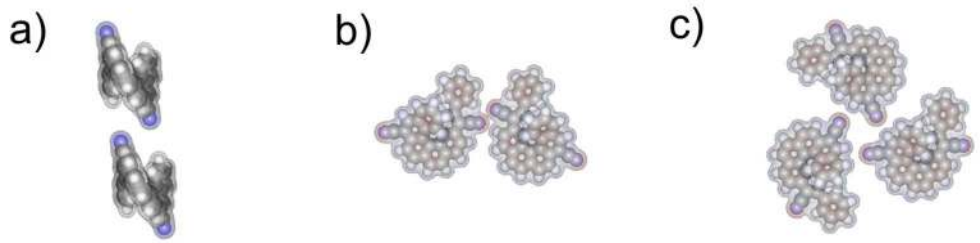

Figure A1.4. The molecular models for two upright standing molecules (pure helicene) (a), two flat lying molecules (impurity) (b) and a trimer (impurity) (c).

Kinks are mainly formed by two lying molecules (impurities) with opposite helicity and change the direction of the chains. The formation of kinks with the molecules having

opposite chiralities has been previously observed for porphyrin chains[1] and even though the interaction is different, Böhringer observed kinks in the chains of NN molecules on Au (111) surface when two molecules with opposite chiralities interact.[2] Within the kinks, the molecular association involves dipole-dipole and C-H...N interactions that takes place between lower cyano groups and H-atoms of the benzene ring of the neighboring molecules (figure A1.4b). However, the dipole-dipole interaction is weakened because the dipoles are not perfectly antiparallel.

At the branching points of the molecular chains, the impurities integrate to form trimeric structures in which a trimeric cyano interaction takes place. Such trimers were also observed at the branching points of pure helicene chains as described in detail in section 4.1.1. The closest distance of a cyano group of one molecule to the H atom of the neighboring molecule is 1.5 Å. As two type of cyano groups in different heights relative to the helix-axis exist, with the impurity in "lying down" geometry there should be one possible cyano interaction close to the surface and another located in a certain distance above the surface. The trimeric motif shown in blue circle in figure A1.3c includes both enantiomers and the interaction takes place above the surface. On the other hand, it is also possible to see the packing of two trimers at the branching points of the chains (red circle). In the case of enantiopure trimeric arrangement (figure A1.4c), three C-N…H interactions above the surface are possible in addition to the interaction between the lower cyano groups of the neighboring molecules.

Another trimeric structure observed in the chains consists of two upright standing and a flat-lying molecule (inside yellow circle in figure A1.3c). This structure was never observed within the branches but only observed as attached to a chain and generally leaves an open end. The molecules at the open ends of this type of trimers are always the flat lying ones (impurities). The protrusions at the open ends generally reveal a mobile appearance which might be due to the movement of the benzene ring of the impurity molecule (green arrows).

For coverages 0.8 ML to 1 ML, two different close-packed arrangements are observed which reveal different apparent heights (figure A1.5). The upright standing helicene units observed within the chains form a dimeric arrangement while the flat lying impurities form a trimeric arrangement at high coverage. A detailed description of the dimers was given in section 4.1.1. The trimeric closed-packed arrangement is formed by the integration of individual trimers (as observed at the branching points of the chains) when the coverage is increased. As obtained from the LEED measurements, the unit cell of the dimeric arrangement has vector sizes of 20.3 Å and 11.7 Å with an angle of 90° and exhibits 0.842 molecules/nm^2.

The unit cell size of the trimeric arrangement is obtained from the analysis of several STM images. The unit cell has 27.7 ± 0.4Å and 25.8 ±0.5 Å vector sizes with an angle of 62±1° in between and contains ~0.48 molecules/nm^2. The adsorption geometries, the STM images and the corresponding molecular models are shown in figure A1.6a and A1.6b for dimeric and trimeric arrangements, respectively.

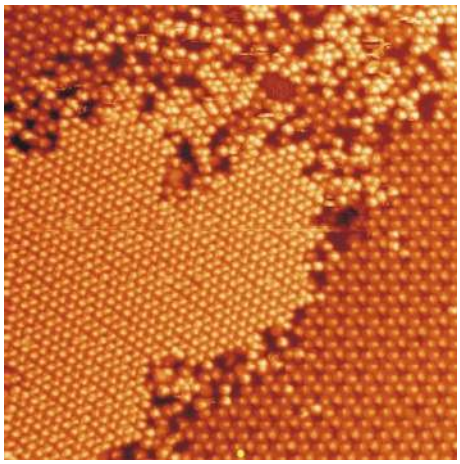

Figure A1.5. STM image of the two different closed-packed structures which exhibit different apparent heights (50x50 nm^2, 2 V, 20 pA, 77 K). Dimers are formed by mixtures of **P4** and **M4** whereas mixtures of **P5** and **M5** form the trimeric arrangement.

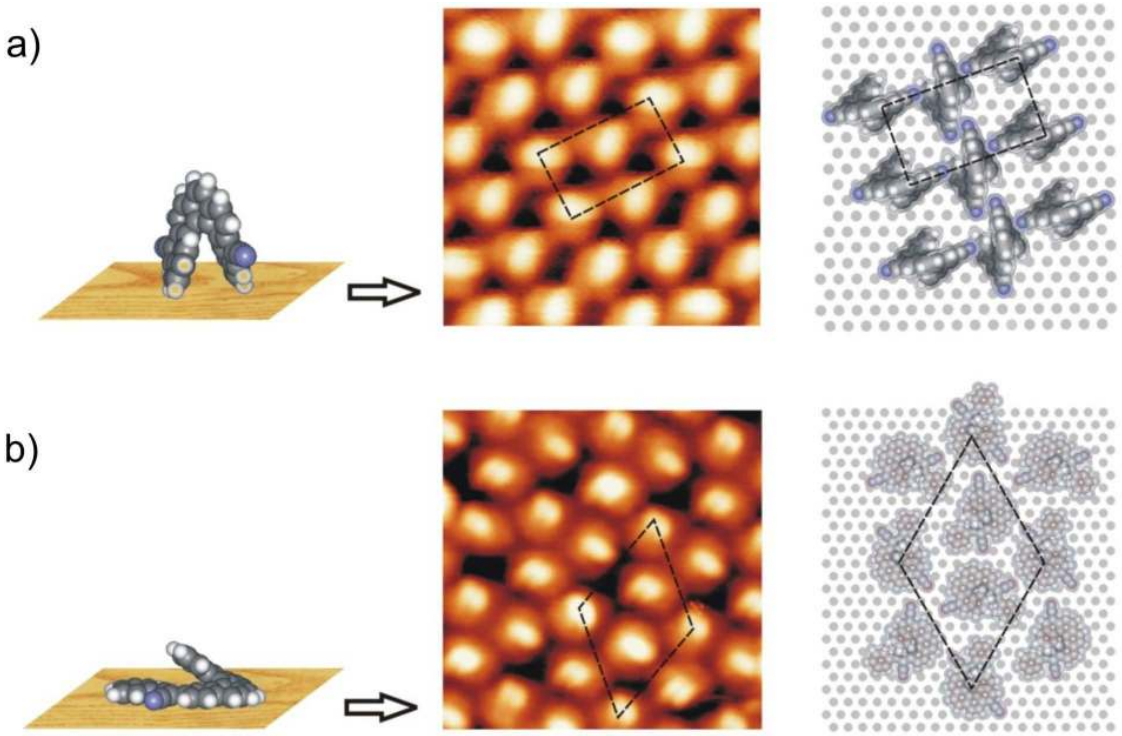

Figure A1.6. The STM images of a) the dimeric packing (5x5 nm^2, 2 V, 20 pA, 77 K) and b) the trimeric packing (7.6x7.6 nm^2, 2 V, 20 pA, 77 K) with their corresponding molecular models. With an upright standing adsorption geometry, pure helicene molecules form a close-packed dimeric arrangement at high coverage. The impurities reveal flat lying adsorption geometry and form a close-packed trimeric arrangement at high coverage.

As already known from the experimental results of the pure helicenes, there is a chiral recognition mechanism between the molecules and the enantiomers segregate into homochiral domains. The same result is also observed for the trimeric arrangement. As seen in figure A1.7, the impurities aggregate into mirror image domains upon adsorption on Cu(111) surface at high coverage.

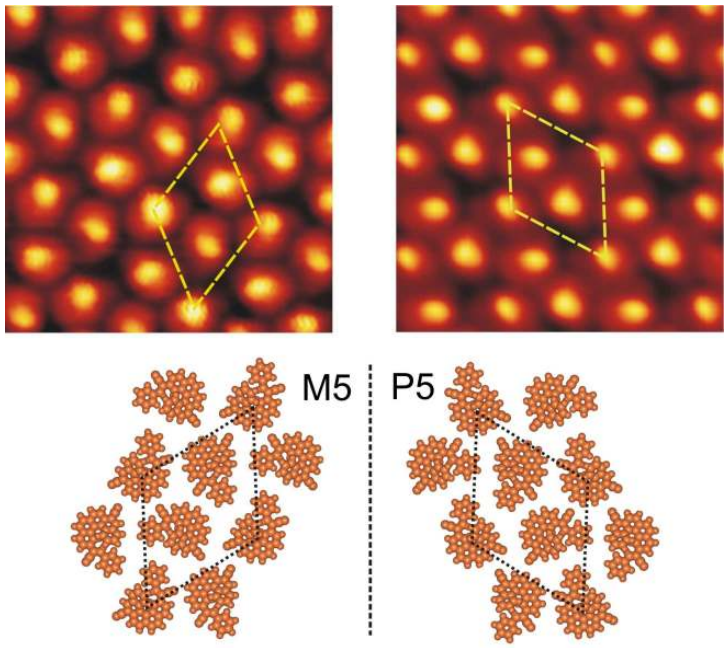

Figure A1.7. Mirror domains of the trimeric pattern formed by **M5** and **P5**.

References A1

[1] N. Wintjes, Hornung J, Lobo-Checa J, et al., Chemistry-A European Journal 15**,** 11139-11150 (**2009).**

[2] M. Böhringer, W.D. Schneider, R. Berndt, Angew. Chem. Int. Ed. 39**,** 792-+ (**2000).**

Appendix 2

The concept of heat induced interlinking of functional units from preorganized molecular building blocks studied in chapter 3 is here applied to a longer unit formed by three phenyl rings to which two Boc protecting groups at para positions of the molecular core are attached. The molecule structure is shown in figure A2.1 and hereafter it will be called as molecule **6**.

Experimental results of molecule **6** on a Cu(111) surface are presented in two parts. This is due to the different molecular evaporator stations of the UHV system employed in the molecule deposition. In **part 1**, the molecules were deposited onto the sample from a resistively heated tantalum crucible whereas in **part 2** they were deposited from glass-crucibles. The different design of the crucibles (different heating systems), interestingly, reveals different molecular patterns, which are described in the following.

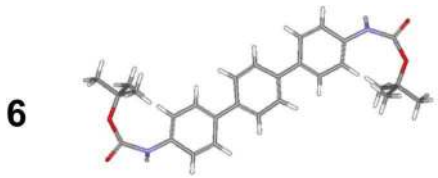

A2.1. Molecular structure of **6** which composes of 3 phenyl rings to which two Boc groups are attached at para positions.

Part 1

At room temperature, molecule **6** forms four different self-assembled structures. Figure A2.2 displays all phases together with their zoomed views on the right side. In these images with submolecular resolution, molecular backbones and the bright lobes representing the Boc groups are visible.

In order to induce coupling reactions between the molecules, the samples are heated at elevated temperatures. However, only a mobile phase is observed on the terraces whereas the step edges are decorated by the molecules up to 155°C. At this temperature, most of the molecules decorating the step edges are found to be intact and arranged in a parallel manner (figure A2.3a) similar to the arrangement in figure A2.2d. Further annealing of the sample at a higher temperature (162°C) induces changes in the molecular structure, i.e., either only one or both of their end groups are lost. Consequently, they are either randomly distributed along the step edges or the ones which

loose both of their end groups form triangular like structures (green triangular in figure A2.3b).

Part 2

Further experiments are conducted on the Cu (111) surface in order to get more insights about the phases obtained at room temperature and the structures found after annealing the sample. This time glass crucibles instead of tantalum crucibles were used to deposit the molecules onto the substrate. Surprisingly, it was not possible to reproduce the same structures in spite off all the attempts. Most of the Boc groups already split off during deposition of the molecules, leading to the formation of disordered structures on the surface. However, some intact molecules were able to form ordered structures aggregated in small molecular islands similar to the arrangement displayed in figure A2.2d. The coexistence of both disordered and ordered molecular structures is shown in figure A2.4 in π-system imaging mode.

In the next step the experiments were repeated at low temperature (77K). At very low molecular coverage (~0.07ML), molecules form single rows where they lie parallel to each other (figure A2.5a). This arrangement resembles the building blocks observed upon deposition of biphenyl **1** at low coverage presented in section 3.1. Upon increasing the coverage of **6** to ~0.45ML, the number of rows increase but no self-assembled large islands is observed. Instead, the rows are distributed randomly over the Cu surface (figure A2.5b). Only at coverages close to a full ML, islands of parallel arrangement between the disordered structures are formed, as observed at room temperature. STM image in A2.5c shows these structures in π-imaging mode.

When the sample is annealed at 156°C, a predominant disordered phase is observed. However, the triangular shaped structures, which are rarely found at the step edges after annealing the sample during room temperature measurements, are observed more often at 77K and they are distributed over the terraces. In figure A2.6a, these trimeric structures are marked in green lines. Upon further annealing the sample (165°C) the number of bright dots representing the Boc groups are reduced and, in addition to the trimeric structures, more linked structures lying in a disordered manner on the surface are seen (figure A2.6b).

All the structures observed after annealing the samples at elevated temperatures might be covalently bound. However, for conclusive statements about the self-assembly mechanism before annealing and the interconnection mechanism after annealing, new methods for molecular sublimation are necessary.

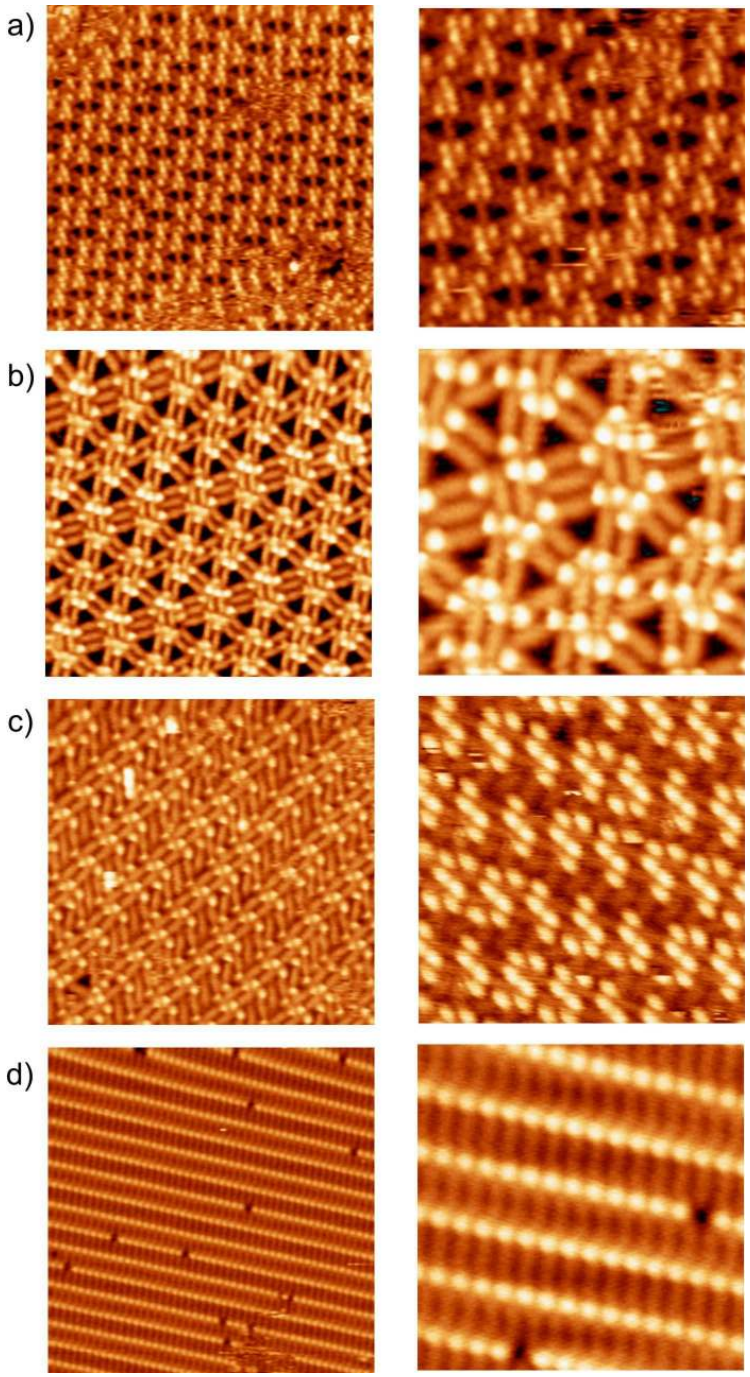

Figure A2.2. STM images of different phases obtained at room temperature. a) 30x30 nm^2, 1.2V, 10pA, RT, and zoomed view: 15x15 nm^2, 1.2 V, 10 pA, RT. b) 22x22 nm^2, 1.3 V, 10 pA, RT, and zoomed view: 10x10 nm^2, 1.2 V, 10 pA, RT. c) 20x20 nm^2, 1.3 V, 20 pA, RT, and zoomed view: 13x13 nm^2, 1.3 V, 20 pA, RT. d) 30x30 nm^2, 1.3 V, 20 pA, RT, and zoomed view: 10x10 nm^2, 1.3 V, 20 pA, RT**.**

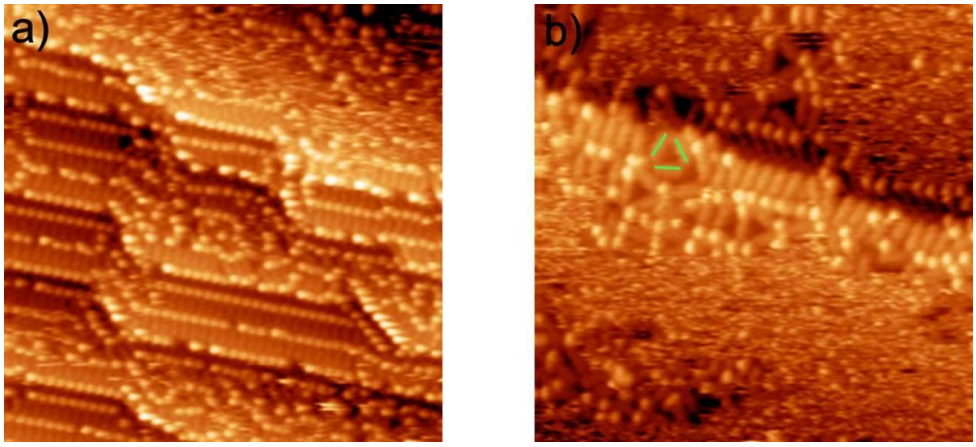

Figure A2.3. STM images of the structures obtained at 152°C. The molecules aggregate at the step edges. a) Intact molecules aggregate in parallel rows at the step edges (30x30 nm^2, -1.4 V, 10 pA, RT). b) At 166°C, the molecules loose their end groups and triangular like structures start to form one of which is marked in green (20x20 nm^2, 1.2 V, 18 pA, RT).

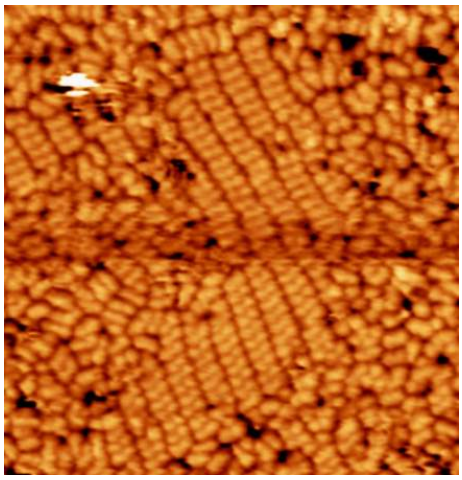

Figure A2.4. STM image of the parallel arrangement surrounded by disordered structures 26.5x27.3 nm^2, -1.6 V, 17 pA, RT).

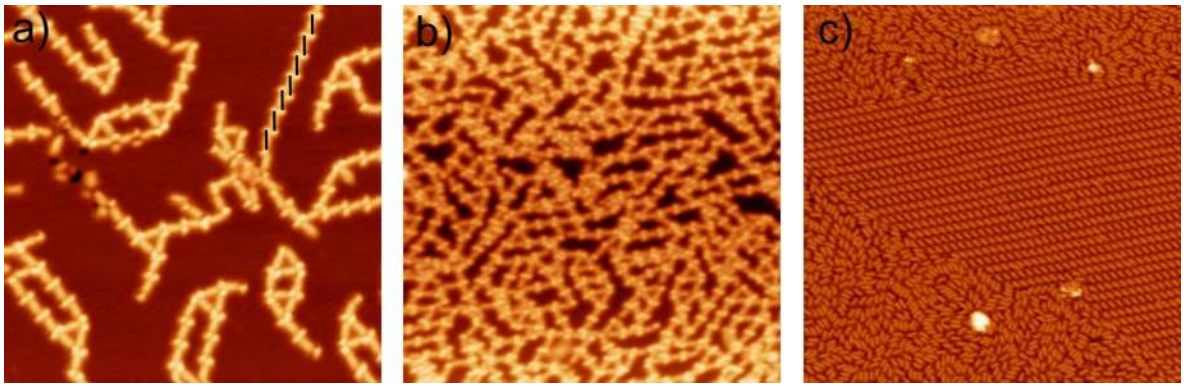

Figure A2.5. STM images of the structures formed at different molecular densities: a) 0.07ML (30x30 nm^2, -1 V, 20 pA, 77K), b) 0.45 ML (40x40 nm^2, -1.1 V, 20 pA, 77K) and, c) 0.95ML (50x50 nm^2, 1.5 V, 20 pA, 77K).

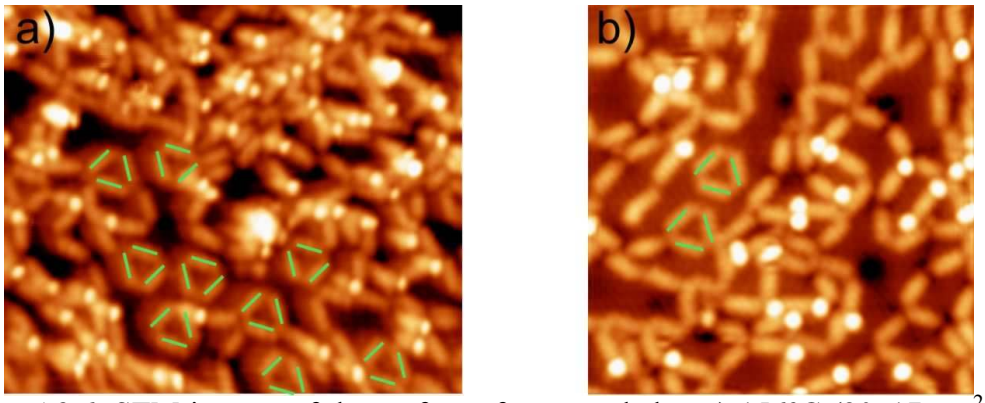

Figure A2.6. STM images of the surface after annealed at a) 156°C (20x17 nm^2, 1.7 V, 20 pA, 77K) and b) at 165°C (15x15 nm^2, 1.4 V, 20 pA, 77K). The trimeric structures are shown in green bars.

Appendix 3

The promising results obtained from the self-assembly of cyano substituted helicenes on surfaces, motivated us to study a new helicene system which could lead to stronger supramolecular interactions and further guide the self-assembly of entire helicene system in a stereoselective manner. For this purpose, hydrogen bonding [7] helicene introduced by *N. Branda et al*.[1] was a promising candidate. The molecular structures of the two enantiomeric forms which will be called as **P7** and **M7** are shown in figure A3.1. Amide groups substituted in the molecules would lead to H-bonding interactions and thus strong surface supramolecular structures. From the extensive studies of Branda and coworkers it is already known that the self-assembly process of racemic mixture of amide helicenes is enantiospecific in solution and diastereoselective in the crystal.

In our study, we investigate the self-assembly behaviour of both racemic and enantiopure amide helicene on a Cu(111) surface.

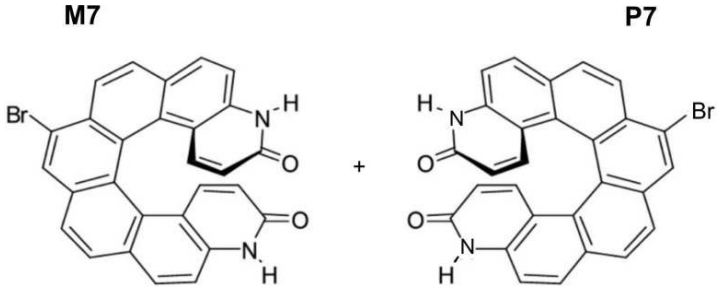

Figure A3.1. Molecular structures of the two enantiomeric forms of amide-[7]-helicene, M and P.

Room temperature measurements of the racemic mixture on Cu(111) reveal two different supramolecular structures which are stable even at very low coverages indicating strong intermolecular interactions. The STM image in figure A3.2a shows the two phases formed at ~0.4 ML. First phase consists of individual straight molecular rows in which the molecules pack into dimers whereas the trimeric structures in the other phase form molecular islands. With increasing coverage, trimeric structures extend into larger islands unlike dimeric rows which are generally found separated over the terraces or attached to the trimeric structures as individual rows. Figure A3.2b shows different domains of extended trimeric structures and a dimeric row grown between these domains at a coverage of ~0.75 ML.

Different appearances of the molecules in two different phases prevent to make conclusive statements about the adsorption geometry of the molecules. Analysis of STM images reveals that each molecule does not appear as a lobe, contrary to the appearance of cyano helicenes (chapter 4). In figure A3.3a, a tentative model of a dimeric row is inserted in the STM image. Here, the molecules are considered to be enantiopure with a "side on" adsorption geometry which would lead to dimers stabilized by H-bonding interactions as observed in solution and in the crystal by Branda et al. On the other hand, the size of three lobes corresponds to the size of a single molecule in the trimeric structure and the molecules look noticeably different compared to their appearance in the dimeric rows. Therefore, low temperature measurements, where the mobility of the molecules is reduced leading to the observation of submolecular features, would further help to conclude about the adsorption geometry of the molecules, discriminate the enantiomers and thus, determine the intermolecular interactions leading to the observed supramolecular structures.

Increasing the coverage step by step results in disordered structures adsorbed randomly between both the ordered dimeric rows and the large trimeric domains. Figure A3.4a displays the structures formed at ~ 0.7 ML of surface coverage.

When the sample is annealed at 200°C, mostly dimeric rows are observed on the surface. Most of the trimeric structures and the disordered phase are transformed into the dimeric rows indicating that the dimeric phase is energetically the most favored one. As can be seen in figure A3.4b, these rows seem to follow three equivalent crystallographic axes of the sixfold symmetric Cu(111) surface.

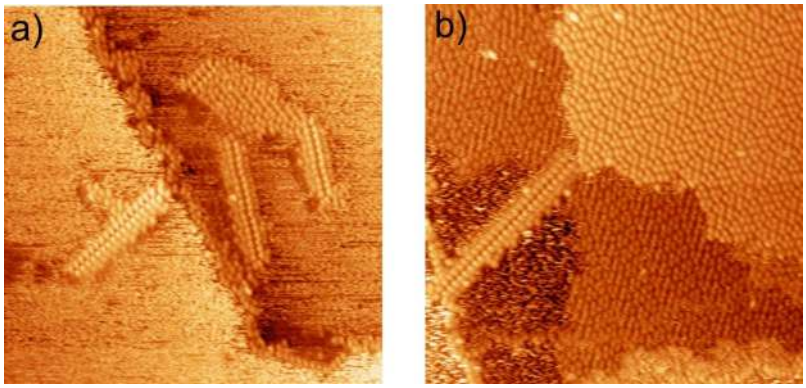

Figure A3.2. STM images showing self-assembled dimeric rows and trimeric islands a) at low coverage (40x40 nm^2, -1.4 V, 20 pA, RT) and b) at higher coverage (38x38 nm^2, -1.3 V, 20 pA, RT).

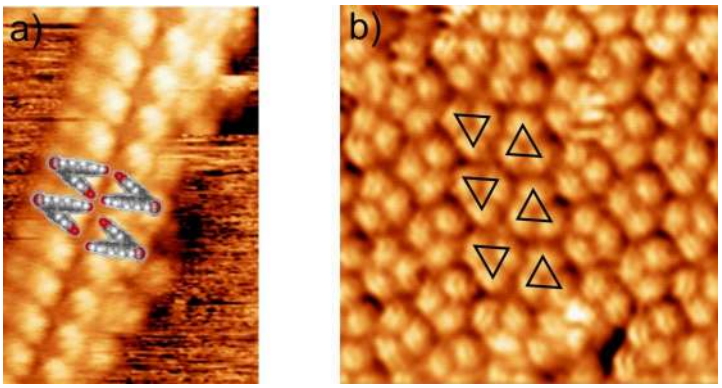

Figure A3.3. a) Zoomed STM image of a dimeric row, in which a few molecules with the same helicity are inserted to show possible H-bonding interactions to form dimers (5.4x8 nm^2, -1.2 V, 20 pA, RT). b) STM image of the trimeric arrangement (8.7x8.7 nm^2, 1 V, 12 pA, RT). The trimers in the neighboring rows are rotated by 180° with respect to each other.

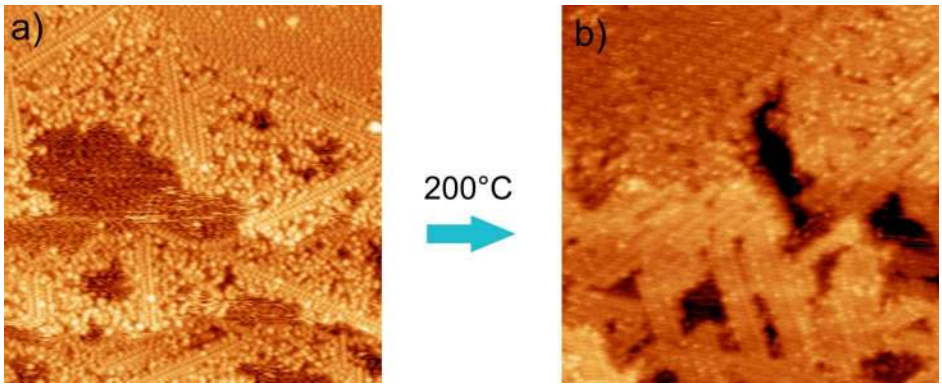

Figure A3.4. a) STM image showing the ordered dimeric rows, trimeric structures and the disordered adsorption of helicenes on Cu(111) as a result of deposition of the molecules in several steps (50x50 nm^2, -1.4 V, 20 pA, RT) b) Structures observed after annealing the sample at 200°C. Irregularly distributed molecules disappear and the number of dimeric rows increases by annealing (46.5x46.5 nm^2, -1.2 V, 20 pA, RT).

A comparison of the molecular structures obtained from the racemic and the enantiopure cases offers an insight into the mechanisms which govern the adsorption and supramolecular self-assembly of the molecules. The observed differences and similarities explain if different structures formed on the surface are due to a chiral recognition between helicenes.

In the following the adsorption of **M7** on Cu(111) is studied and STM results of the racemic and the enantiopure forms are compared.

Deposition of **M7** on Cu(111) results in formation of different supramolecular arrangements depending on the surface coverage. Three different phases obtained at ~0.3ML are presented in the upper part of figure A3.5, whereas in its lower part closeup views of all these structures are displayed. Structure 1 is formed by parallel rows of

bright and dim lobes including holes, and thus shows irregularities. This phase is observed at different coverages.

The existence of dimeric rows (number 2) which have been observed upon deposition of the racemic mixture gives evidence that the dimeric rows in the racemate are exclusively formed by the molecules with the same chirality. This structure has already been proposed in the racemic case (see figure A3.3) and might be the enantiopure H-bonding dimers observed by Branda et al.

The third arrangement is a metastable hexagonal porous network (number 3) which is similar to the porous phase obtained from the enantiopure cyano helicenes (**P4** in section 4.2). As displayed in the subsequent STM images presented in figure A3.6, the number of pores is reduced from eight pores to a single pore indicating the metastability of the network.

Upon increasing the coverage to ~0.45ML, the porous network disappears and a new phase arises parallel to the formation of structures 1 and 2. This new phase is indicated with number 4 in the STM image in figure A3.7 and reveals a hexagonal flower-like structure. However, as in the previous structures, it is not possible to differentiate a single molecule in this structure due to a mismatch of the molecule size and structure compared to the different sized lobes appearing in the STM images.

Further increasing the coverage (~0.75ML) leads to disordered phases. However, similar to the racemic case, all the phases on the surface transforms into the dimeric rows when the sample is annealed at elevated temperatures. In figure A3.8, the surface structure before annealing (a) and after annealing at 150°C (b) and 200°C (c) are displayed.

First STM investigations of amide-helicene at room temperature might be interpreted as follows.

Dimeric rows are energetically the most favoured phase and exclusively formed by the molecules with the same helicity. Since trimeric structures are observed only upon deposition of the racemic mixture, they should be composed of both enantiomers. However, when the sample is annealed at elevated temperatures, the trimeric phase is found to be transformed into the homochiral dimeric rows. The hypothesis of heat induced separation of enantiomers from a racemic phase into a homochiral phase has to be further investigated.

A possible argumentation for different molecular appearances in different supramolecular assemblies can be due to an Ullmann coupling[2] which is a coupling reaction between aryl halides with copper. Probably, when the molecules are deposited on the copper surface, Br atoms react with substrate copper atoms and cleave, which results in coupling of two helicene molecules as displayed in figure A3.9. The holes (etch pits) often observed on the metal surface may confirm that the metal atoms are taken out of the surface. Such a hole is indicated with an arrow in the STM image in figure A3.10.

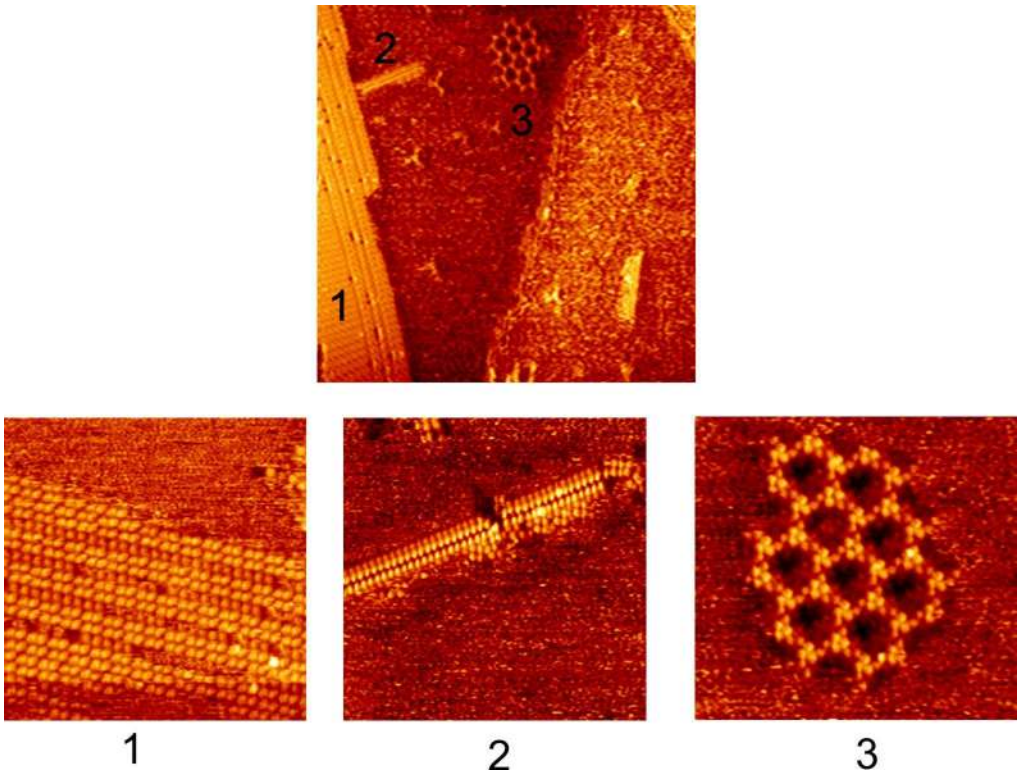

Figure A3.5. STM image of the three different phases formed at low coverage (up) (100x100 nm^2, -1.4 V, 20 pA, RT). Phase 1: parallel rows (20x20 nm^2, -1.3 V, 20 pA, RT). Phase 2: dimeric rows (30x30 nm^2, -1.4 V, 20 pA, RT) and phase 3: porous network (30x30 nm^2, -1.4 V, 20 pA, RT).

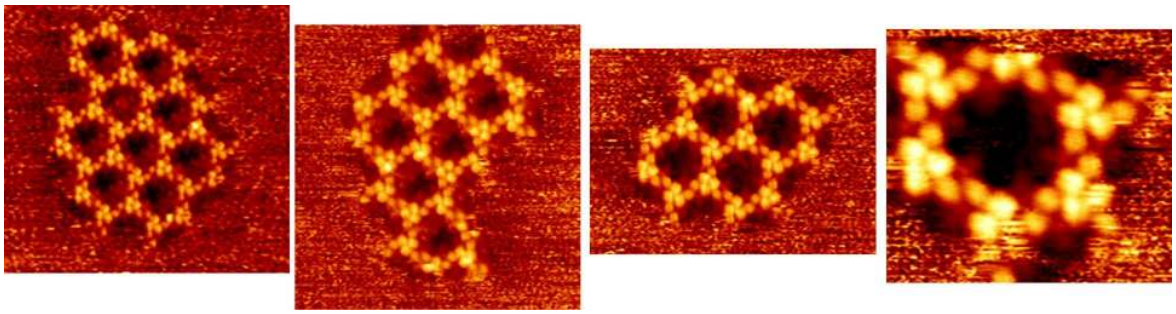

Figure A3.6. Subsequent STM images of the porous network which is reduced in size in time. (all STM images: -1.4 V, 20 pA, RT)

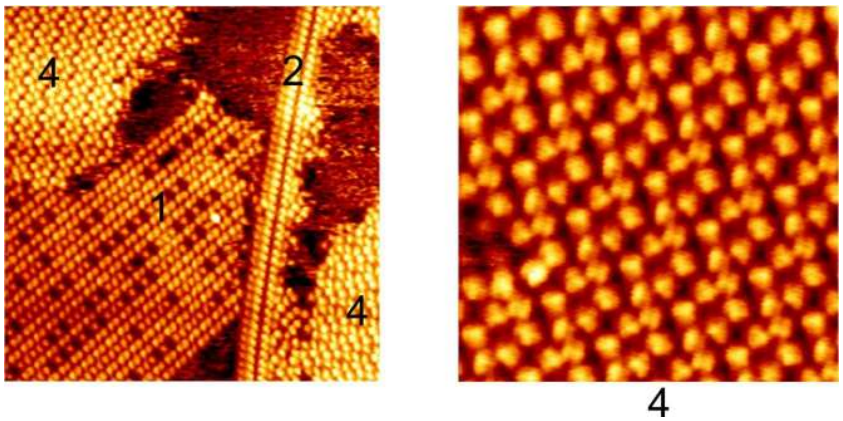

Figure A3.7. STM image of the self-assembled structures of **M7** observed at 4A (left) (30x30 nm^2, -1.2 V, 20 pA, RT). The zoomed view of the new phase (number 4) as shown on the right reveals a hexagonal flower-like structure (10x10 nm^2, -1.2 V, 20 pA, RT).

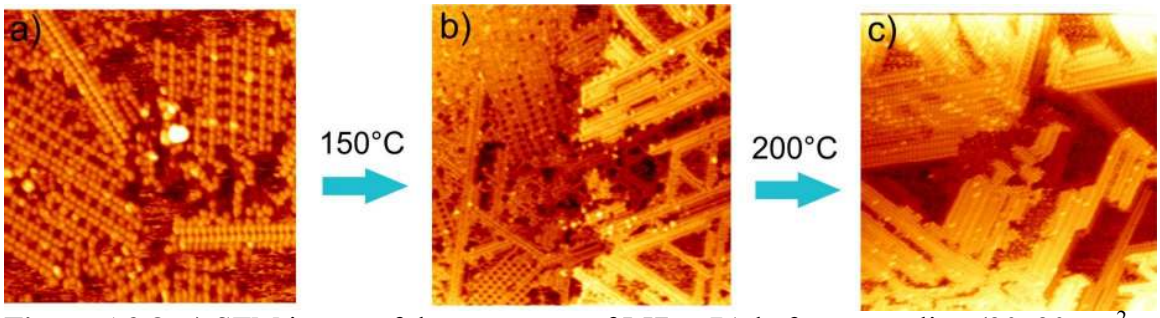

Figure A3.8. a) STM image of the structures of **M7** at 7A before annealing (30x30 nm^2, -1.3 V 20 pA, RT). b) Dimeric rows start to dominate over the others after annealing the sample at 150°C (60x60 nm^2, -1.4 V, 20 pA, RT). c) Only dimeric rows are observed after the sample is annealed at 200°C (50x50 nm^2, -1.3 V, 20 pA, RT).

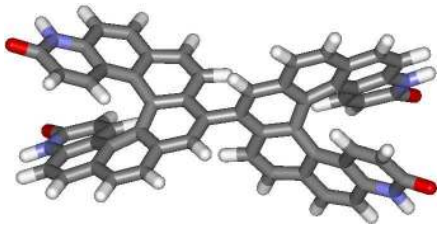

Figure A3.9. Ullmann coupling of two molecules as a result of splitting of Br after reacting with Cu.

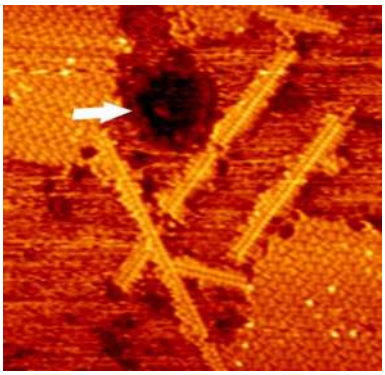

Figure A3.10. An STM image showing an etch pit (48.6x47 nm^2, -1.3 V, 20 pA, RT).

A better molecular resolution by low temperature measurements could lead to the conclusion for the adsorption geometry of the molecules, discrimination of the enantiomers, determining the intermolecular interactions leading to the observed supramolecular structures and finally the phase separation due to a chiral recognition process.

Unfortunately, low temperature measurements did not give the results obtained at room temperature. Deposition of the molecules on Cu(111) surface revealed only clusters. After these results, the bromine atom which may lead to these clusters has been removed synthetically by Michael Schär and this new amide helicene compound will be investigated in future experiments.

References A3

[1] E. Murguly, R. McDonald, N. R. Branda, *Chiral Discrimination in Hydrogen-Bonded [7]Helicenes,* Org. Lett. 2, 3169–3172 **(2000).**

[2] P.E. Fanta, *The Ullmann Synthesis of Biaryls***,** Synthesis-Stuttgart 1**,** 9-21 **(1974).**

Acknowledgements

I would like to thank the following people that helped me to complete this thesis:

- Prof. H. J. Güntherodt, Prof T. Jung and PD. Dr. M. Stöhr for giving me the opportunity to carry out my thesis at the Department of Physics of the University of Basel. I wish to thank Thomas for his helpful discussions and for his effort to help me to finish this thesis. I thank Meike for being my supervisor, for her support and patient explanations during my thesis work and for her help to complete this thesis.
- Prof. M. Mayor and U. Soydaner for the synthesis of the chemical compounds and for fruitful discussions.
- Prof. F. Diederich and M. Schär for synthesizing the chemical compounds and for scientific discussions.
- Dr. D. Passerone, Dr. C. Pignedoli and M. T. Nguyen for supportive theoretical calculations.
- Prof. E. Meyer and the members of Nanolino for nice discussions during our joint meetings.
- All the current and former group members of Nanolab (especially S. Vijaraghavan, S. Scntke and C. Iacovita for their help to correct and finalize this thesis).
- S. Schnell for help in the Nanolab regarding mechanical and technical issues.
- The secretaries of the University of Basel for their kind attitudes and help with the beaurocratical issues.
- S. Özer and I. Kilic for their support and friendship.
- My parents and my sister for their support through the difficult times.

Publications

- S. Boz, M. Stöhr, U. Soydaner, M. Mayor*, "Heat induced coupling of a fluorinated biphenyl derivative on metal surfaces" (manuscript in preparation).*

- S. Boz, M. Stöhr, U. Soydaner, M. Mayor, *Protecting-Group-Controlled Surface Chemistry - Organization and Heat-Induced Coupling of 4,4 '-Di(tert-butoxycarbonylamino)biphenyl on Metal Surfaces* Angew. Chem. Int. Ed. 48, 3179-3183 **(**2009).

- G. Ilicali , W. Rosner , W. Weber, S. Boz, L. Dreeskomfeld, J. Hartwich, J. Kretz, J.R. Luyken, E. Landgraf, F. Hofmann, L. Risch, W. Hansch, *Use of LPCVD TEOS as a direct bonding material for layer transfer: Densified vs. undensified,* IEEE International SOI Conference, Proceedings**,** 44-45 **(**2004).

Conferences

- TNT, Barcelona, Spain, *September* 2009 (Poster)
"Controlling the organization and heat induced coupling of biphenyl derivatives on metal surfaces"

- DPG, Dresden, Germany, *March* 2009 (Oral presentation).
"Controlling the organization and heat induced coupling of biphenyl derivatives on metal surfaces"

- DPG, Berlin, Germany, *February* 2008 (Oral presentation).
"Protection group controlled surface chemistry – organization and heat induced coupling of 4,4'-di(tert.butoxycarbonyl-amino)biphenyl on metal surfaces"

- SPS, Geneva, Switzerland, *March* 2008 (Oral presentation)
"Protection group controlled surface chemistry – organization and heat induced coupling of 4,4'-di(tert.butoxycarbonyl-amino)biphenyl on metal surfaces"

- SAOG, Fribourg, Switzerland, *January 2007* (Oral presentation)
"An Addressable Supramolecular Multi-Stable Rotary Device"

- DPG, Regensburg, Germany, *March 2007* (Oral presentation).
"Creation of open networks from perylene derivates"

- TNT, San Sebastian, Spain, *September 2007* (passive participation)

- ICNT, Basel ,Switzerland, *July* 2006 (passive participation)

Curriculum Vitae

Personal Data

Name	Serpil Boz
Date of birth	Istanbul, 28.07.1978
Nationality	Turkish

Education

1996-2000	BS in Physics, Physics and Mathematics Faculty, Istanbul, Turkey
2001-2002	Foreign Language School, Foreign Languages Department, Istanbul Technical University, Istanbul, Turkey
2000-2001	MS in Educational Science, Institute of Natural Sciences, Istanbul University, Istanbul, Turkey
2002-2005	MS in Physics, Physics Department, Royal Institute of Technology (KTH), Stockholm, Sweden
	Thesis work in Corporate Research Nano Devices, Infineon Technologies, Munich, Germany.
	Title: Nano-Scaled Silicon-on-Insulator Devices by Scanning Spreading Resistance Microscopy
Since June 2006	PhD in Experimental Physics, Institute of Physics, University of Basel, Switzerland